

**ELECTRICAL MEASUREMENTS OF THALLIUM, BISMUTH AND
PLATINUM CONTACTS TO SELENIUM**

by

William Robert Clark

*A thesis submitted to the Faculty of Graduate Studies
and Research in partial fulfillment of the requirements
for the degree of Master of Engineering*

Department of Electrical Engineering

McGill University

Montreal Canada

December, 1990

ACKNOWLEDGEMENTS

The author wishes to express his sincere gratitude to his supervisor, Dr. C.H. Champness for the tremendous education and patient guidance he has given to me throughout this study. Furthermore, thanks are given to Dr. I.S. Shih for his assistance and valuable suggestions. Thanks are also due to Mr. G.P. Rodrigue for his tireless efforts and good humour in keeping the equipment in the laboratory running. The author also wishes to thank Mr. J. Foldvari, Mr. A. Limoges and Mr. B. Dicsó for providing the mechanical packaging mounts for the samples, as well as, other mechanical apparatus in this study. The author would also like to express his appreciation to J. Mui for his photographic work.

The author is also especially grateful to his parents, his first and best teachers and of course to the rest of his family and friends for their implicit and, hence, very powerful encouragement during this study.

Acknowledgements are also due to the Natural Sciences and Engineering Research Council of Canada for its financial support of this work.

The selenium used in this study was kindly supplied by Noranda Inc., C.C.R. Division.

ABSTRACT

Electrical studies have been made on Se-metal contact diodes, where the metal was either Te, Bi or Pt and the Se was a polycrystalline layer. The structures, primarily of the form Al-Bi-Se-metal were fabricated by depositing thin films of the elements involved with evaporation techniques. All the diodes prepared showed rectification, which was strongest for the Te samples and weakest for the Pt samples. Measurements made on the diodes included current-voltage, as well as, capacitance and resistance as a function of bias and frequency. In addition, preliminary photoelectric measurements were carried out for the first time on the Se-metal devices to determine the Schottky barrier heights. At low frequencies, an anomalous non-Faraday inductive effect was observed in many of the samples and in Se-Te devices in particular. In these samples, the effect appeared to be correlated to the presence of the semiconducting compound SeTe, which was detected by x-ray diffraction in the samples after several days of storage. With Pt counterelectrode samples, inverse rectification was observed, due possibly to the formation of an ohmic counterelectrode contact but a rectifying back contact. From current versus voltage and capacitance versus voltage measurements, it was found that, despite the presence of interface states, the Schottky barrier heights determined for freshly made samples decreased with increase of metal work function.

RÉSUMÉ

Des études ont été faites sur des diodes à contact Se-métal, afin d'en déterminer les propriétés électriques. Le métal utilisé était alternativement du Tl, Bi ou Pt alors que le Se est constitué d'une couche polycrystalline. Les structures - principalement de forme Al-Bi-Se-métal - furent fabriquées par dépôt de couches minces de ces éléments, utilisant des techniques d'évaporation. Toutes les diodes ainsi préparées ont montré des propriétés de rectification, qui furent les plus fortes pour les échantillons de Tl, et les plus faibles pour ceux de Pt. Les mesures effectuées sur ces diodes incluent les relations courant-tension, ainsi que la capacité et la résistance en fonction de la tension et de la fréquence. De plus, des études photoélectriques préliminaires furent entreprises pour la première fois dans le but de mesurer la hauteur des barrières Schottky. A basses fréquences, un effet inductif anormal non-Faraday fut observé dans de nombreux échantillons, et dans les échantillons Se-Tl en particulier. Cet effet semble être lié à la présence du composant de semiconducteur SeTl . Cette présence fut déterminée par diffractions aux rayons-x sur les échantillons, après quelque jours de remisage. Une rectification inverse fut observée sur des échantillons de contre-electrode Pt. Ceci est probablement dû à la formation d'un contact de contre-electrode ohmique mais un contact-arrière qui rectifie. D'après des mesures de courant en fonction de la tension et de la capacité en fonction de la tension, on trouva que malgré la présence d'états interfaces, la hauteur des barrières Schottky pour des échantillons soigneusement préparés décroît avec accroissement de la fonction de travail du métal.

TABLE OF CONTENTS

ACKNOWLEDGEMENTS	i
ABSTRACT	ii
RESUME	iii
1. INTRODUCTION	1
2. THEORETICAL CONSIDERATIONS	5
2.1 Introduction	5
2.2 Inductive Effect in Semiconductor Junctions	5
2.3 Barrier Heights in Schottky Junctions	9
2.3.1 <i>Current versus Voltage Method</i>	10
2.3.2 <i>Capacitance versus Voltage Method</i>	11
2.3.3 <i>Photoelectric Method</i>	13
3. SAMPLE PREPARATION	15
3.1 Introduction	15
3.2 Al Stud Preparation	16
3.3 Back-contact Deposition	16
3.4 Selenium Deposition	18
3.5 Counterelectrode Deposition	20
3.6 Electrical Connections and Mounting	21

3.7 Comparison of the Preparation Procedure with that of Pan [2]	21
4. MEASUREMENT TECHNIQUES	31
4.1 Introduction	31
4.2 Current versus Voltage Measurements	31
4.3 Capacitance and Resistance versus Voltage Measurements	32
4.4 Photoelectric Measurements	35
4.5 Materials Analyses	39
5. RESULTS ON Se-Te CONTACTS	47
5.1 Introduction	47
5.2 Electrical Characteristics of Freshly Prepared Se-Te Diodes	48
5.2.1 <i>Capacitance versus Voltage Characteristics</i>	48
5.2.2 <i>Capacitance versus Frequency Characteristics</i>	49
5.2.3 <i>Resistance versus Voltage Characteristics</i>	50
5.2.4 <i>Current Density versus Voltage Characteristics</i>	52
5.3 Aging Effects on the Electrical Characteristics	54
5.3.1 <i>C_p versus Voltage Characteristics at Different Times</i>	55
5.3.2 <i>C_p versus Frequency Characteristics at Different Times</i>	58
5.3.3 <i>R_p versus Voltage Characteristics at Different Times</i>	59
5.3.4 <i>j versus Voltage Characteristics at Different Times</i>	59
5.3.5 <i>Mott-Schottky Plots at Different Storage Times</i>	60
5.3.6 <i>Material Analysis Studies</i>	61

5.4 Discussion	63
6. RESULTS ON Bi AND Pt CONTACTS TO Se	87
6.1 Introduction	87
6.2 Characteristics of Se-Bi and Se-Pt Structures with Bi and Pt Back-contacts	88
6.2.1 <i>Samples with Bi as the Back-contact</i>	88
6.2.2 <i>Samples with Pt as the Back-contact</i>	91
6.3 C_p versus Voltage and Frequency Characteristics	93
6.3.1 <i>Characteristics for Bi Back-contact Samples</i>	93
6.3.2 <i>Characteristics of Pt Back-contact Samples</i>	96
6.4 Evidence for Aging in Bi-Se-Bi Samples	99
6.5 Discussion	100
7. BARRIER HEIGHTS OF Se-METAL CONTACTS	126
7.1 Introduction	126
7.2 Barrier Heights from j-V Measurements	126
7.3 Barrier Heights from Capacitance Measurements	127
7.4 Barrier Heights from Photoelectric Threshold Measurements	130
7.5 Discussion	131
8. GENERAL DISCUSSION	146

9. CONCLUSIONS AND FURTHER WORK	157
9.1 Main Conclusions	
9.2 Further Work and Recommendations	158
9.2.1 <i>Negative Capacitance Studies</i>	
9.2.2 <i>C_p-V Minima Studies</i>	159
9.2.3 <i>Bi and Pt Contact Studies</i>	160
9.2.4 <i>Barrier Height Studies</i>	161
 BIBLIOGRAPHY	 163
 APPENDIX	 166

1. INTRODUCTION

Despite being in existence for well over 100 years, the metal-semiconductor diode continues to be a very challenging subject to study. Crystalline selenium is an excellent semiconductor to use in such research because it has the highest reported work function of all the elements [1] and it is always p-type, so that any metal in contact with it should, in principle, give a Schottky barrier. Most Schottky junctions are dominated by Fermi level pinning at the interface because of surface states. This is particularly true for the semiconductors Si and GaAs, where the barrier heights of such Schottky diodes do not vary systematically with metal work function. In Se metal contacts, however, the barrier heights do decrease with metal work function, indicating that Fermi level pinning in these cases is not very important, despite the fact that a high concentration of interface states must be present. Thus, while selenium has many undetermined electronic conduction parameters, it is still an excellent material to study the different effects of metals used for the Schottky contacts.

In the present work studies were carried out on Se-metal contacts that were made with polycrystalline Se and the three metals Te, Bi and Pt. These metals were chosen because they cover a reasonable range of work function values, so that the dependence between the barrier height and the work function can easily be seen. The samples had a structure mainly of the form Al-Bi-Se-metal and were fabricated by successively depositing the elements involved by evaporation in vacua. Once fabricated, the samples had current versus voltage and capacitance and resistance as a function of bias and frequency measurements made on

them. Some preliminary photoelectric measurements were also carried out on some of the samples with Bi as the counterelectrode metal.

Although the present work was essentially a continuation of previous studies by Pan [2] and Chan [3], it nevertheless, bared some noteworthy differences. In previous studies by Pan [2] and Chan [3] similar samples were fabricated and also had capacitance as a function of bias and frequency measurements on them. However, the frequencies used in those measurements only covered a range between 100 Hz and about 1 MHz. In the present study, the frequencies ranged from as low as 20 Hz to as high as 10 MHz. Some rather extraordinary observations in the capacitance measurements at the lower frequencies were observed in this work that were not previously seen in this laboratory. While, Pan [2] made some materials analysis studies in his research by means of x-ray diffraction studies of films on glass slides, he never performed such analyses on actual samples. The present work did use actual samples in its materials analysis studies and in addition to x-ray diffraction, scanning electron microscopy was also employed. The results from these analyses gave some very revealing information about the actual structures involved. Furthermore, while in previous work [2], [3], Te and Bi contacts to Se were extensively studied, as they were in the present study, no work was done on Pt contacts to Se. The present work, on the other hand, did examine such Pt contacts and, in fact, it was the first time a comprehensive study has been made on Pt contacts to Se. Finally, Pan [2] and Chan [3] determined barrier heights in their samples from current versus voltage and capacitance versus voltage measurements. In the present study, while barrier heights were also determined using these measurements, they were also found from photoelectric measurements for Se-Bi samples. Although the

results from these photoelectric measurements were somewhat preliminary, they, nevertheless, marked the first time barrier heights have been determined using this technique in the present laboratory.

It should be mentioned here that the present work is an empirical study, primarily concerned with obtaining consistent experimental results. Therefore, the conclusions derived from this study were essentially qualitative rather than quantitative. Quantitative analyses, in the form of an examination of a circuit model like the one postulated by Pan [2], were not carried out here because it is the author's belief that the results were not sufficiently complete, especially considering some of the rather extraordinary observations that were made.

The structure of this thesis is as follows. Following this introductory chapter, chapter 2 presents an argument that explains, at least qualitatively, the existence of non-Faraday inductance in semiconductor diodes. Furthermore, the chapter also gives a brief description of how barrier height values were determined from current-voltage, capacitance-voltage and photoelectric measurements. The third chapter describes the manner in which the samples were fabricated and then compares this preparation procedure with that of a previous worker, Pan [2]. In chapter 4, the measurement techniques used in this work are described. Special attention is given to the photoelectric measurements, since these represent the first time such a technique has been employed in this laboratory to determine barrier heights. Chapter 5 is the first chapter that presents actual results and is mainly concerned with the capacitance characteristics of samples with Te counterelectrodes. It also presents the results of detailed studies on how the capacitance results changed with sample storage time along

1 with how the structure itself changed from a materials analysis point of view. In chapter 6, the electrical characteristics of samples made with Bi and Pt contacts to the Se are presented with the focus primarily on the ohmic character of some of these contacts. Chapter 7 presents the results of the barrier height determinations by the three measurement techniques for the three different metal contacts. While a brief discussion is given at the end of each of chapters 5, 6 and 7, chapter 8 gives a more comprehensive discussion of all the results of this work. Finally, chapter 9 presents some conclusions and also suggests further studies to answer the many questions still unanswered, as well as, those which were raised by this work.

2. THEORETICAL CONSIDERATIONS

2.1 Introduction

In later chapters of this thesis it will be seen that many of the samples displayed a very interesting low frequency inductive effect. This effect showed up primarily as negative capacitance values in the capacitance versus voltage characteristics. Such an effect in semiconductor diodes was investigated by other researchers [4], [5], [6], [7], [8] and this chapter presents a brief theoretical basis of such inductances.

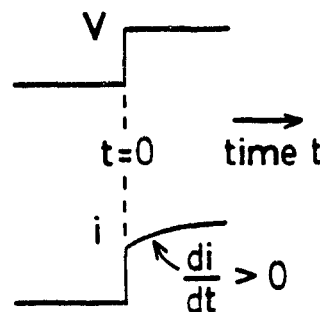
When working with metal-semiconductor Schottky contacts, it is usual to characterize them with a parameter known as the barrier height. This parameter was measured by various methods in this work and this chapter also presents some of the theoretical background behind these barrier height determinations.

2.2 Inductive Effect in Semiconductor Junctions

At high frequencies, junction diodes can show normal Faraday inductance, usually arising from the leads of the device. It has also been observed, however, that a low frequency inductive effect can also occur in junction diodes. Such an effect was observed in pn junctions by Kanai [4] and was attributed to conductivity modulation. Misawa [5] presented a detailed theoretical discussion of the effect as did Melchior and Strutt [6]. The latter observed low frequency inductances as well in germanium pn junctions. Green and

Shewchun [7] discussed further the theoretical aspects of the effect and suggested that it ought to be more prevalent in a Schottky junction than in a regular pn junction because of the lower minority storage and hence, also lower diffusion capacitance. Recently, low frequency inductance observations were reported for NiSi_2 -Si Schottky junctions by Werner, Levi, Tung, Anzlowar and Pinto [8] and they explained the inductive behaviour as being the result of high level injection.

An explanation of how the inductive effect comes about in diodes is as follows. Consider a p^+n junction, short on the n side. Since it is one sided, the electron contribution to the total current can be neglected to a first approximation. Now, if a large forward bias voltage step is applied to the device, as shown here,



high level injection of holes from the p^+ region into the n-side will take place. These injected holes are so numerous that they reduce the total resistance of the device. However, this does not happen instantaneously, since it takes some time for the holes to travel the length of the n-side, W . The flow of these injected carriers is mainly due to drift in an electric field E , whereas, under low level injection, the injected carriers would flow by

I diffusion alone. Thus, the time taken for a hole to cross the n-region is about $W/(\mu_p E)$, where μ_p is the hole mobility. Therefore, in this time the current rises (i.e. $di/dt > 0$), even though the voltage across the device is constant. When the current in a device rises, while the voltage across it remains constant, the device is behaving as if it had an inductance value of $V/(di/dt)$. Hence, for large forward bias values, where injection is strong, the small signal impedance of a diode has an inductive component. Thus, while minority carrier injection at a low level gives rise to the well-known diffusion capacitance component, high-level injection leads to an inductive component.

An explanation of this inductive effect from a more theoretical point of view was first given by Kanai [4] and a summary of his treatment is now presented. He considered a pn junction, short on the n-side, biased in the forward direction at a dc voltage V . When this voltage was sufficiently large, the number of injected holes in the narrow n-region was also large, so that it was assumed that the current flowed not only by diffusion but by drift as well, for both the holes and electrons [9]. Thus, according to Kanai, the ac current due to an additional small signal ac voltage $v \exp(j\omega t)$ is given by

$$i = \frac{\Delta P}{W} q (\mu_p + \mu_n) E \quad , \quad (1)$$

where q is the absolute value of the electronic charge, μ_p and μ_n are the hole and electron mobilities respectively in the n-region, W is the distance an injected hole can travel before recombining (the smaller of either a diffusion length or the width of the n-region), E is the electric field strength in the n-region (assumed to be a constant independent of position) and ΔP is the total number (not concentration) of injected holes in the n-region, which is

also a sinusoidal function with frequency ω . This last quantity, according to Kanai [4], can be given by the expression

$$\Delta P = C \left(\frac{qp_n}{kT} \right) \exp\left(\frac{qV}{kT}\right) v \exp(j\omega t) \frac{b\tau}{(1+j\omega\tau)} [1 - \exp(-\Gamma/\tau - j\omega\tau)] , \quad (2)$$

where in his notation C is the diode cross sectional area, p_n is the hole density in the n-region, k is Boltzmann's constant, T is the absolute temperature, b is the injected hole drift velocity (equal to $\mu_p E$), τ is the injected hole lifetime and Γ is the time required for an injected hole to cross the n-region. Kanai discussed two cases when determining the impedance of the n-region under high level injection. The first one was when the n-region was so wide that $\Gamma \gg \tau$ and W was taken as being equal to $b\tau$. In this case the impedance, Z , was given by an equation of the form

$$Z = \frac{ve^{j\omega t}}{i} - A(1+j\omega\tau) , \quad (3)$$

where

$$A = \frac{1}{C \left(\frac{qp_n}{kT} \right) e^{\frac{qV}{kT}} q(\mu_p + \mu_n) E} . \quad (4)$$

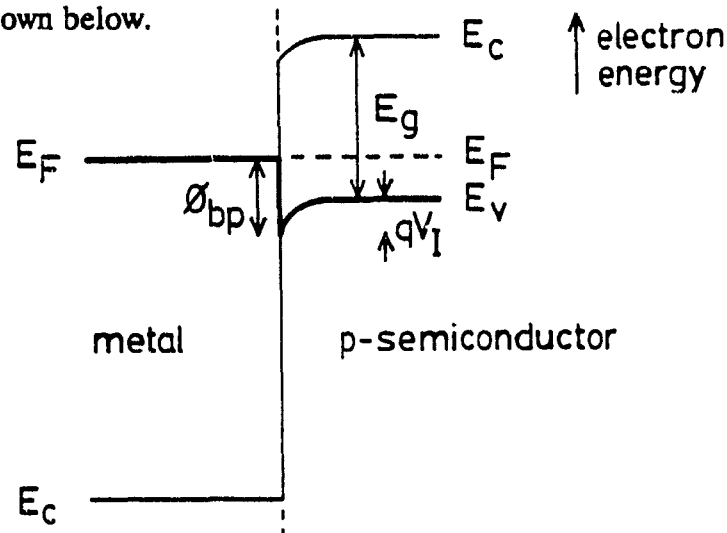
The second case was when the n-region was short so that $\tau \gg \Gamma$ and W was taken as being equal to $b\Gamma$. Furthermore, the frequency of the applied voltage signal was so low that $\omega\Gamma \ll 1$. Under these conditions the impedance was determined to be of the form

$$Z = A(1+j\omega\Gamma/2) . \quad (5)$$

Notice that in both cases, (3) and (5), the impedance had a positive imaginary term, indicating that it was inductive. Thus, it is seen, at least qualitatively, that a forward biased junction diode can, in theory, display inductive behaviour. It should be stressed, however, that under low level injection the minority carriers flow predominantly by diffusion resulting in an impedance which is capacitive. Furthermore, the treatment by Kanai was only approximate and more detailed quantitative treatments have been given by other workers in references [5] to [7].

2.3 Barrier Heights in Schottky Junctions

The energy band diagram of a Schottky contact between a metal and a p-type semiconductor is shown below.



Here ϕ_{bp} is the barrier height, E_g is the semiconductor gap energy, E_F is the energy of the Fermi level, E_v is the energy at the top of the valence band in the semiconductor, E_c is the energy at the bottom of the conduction band in the semiconductor and qV_I is the built-in

potential. According to Rhoderick [10] there are basically three different methods that are used to measure the barrier height value: these are current versus voltage measurements at room temperature and with variation of temperature, capacitance versus voltage measurements and finally, photoelectric measurements. Barrier heights for samples in this thesis were determined using all three methods. However, the current-voltage measurements were made at room temperature only. The way in which the barrier heights were determined with the three methods is now described.

2.3.1 Current versus Voltage Method

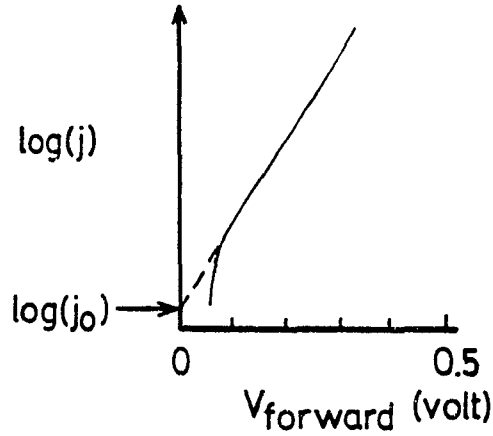
According to the thermionic emission theory [9] [10], the current density, j , through a Schottky diode under a bias, V , is given by the expression

$$J = j_o \left(e^{\frac{qV}{kT}} - 1 \right) \quad (6)$$

Here

$$j_o = A^* T^2 e^{-\frac{\phi_{bp}}{kT}}, \quad (7)$$

where A^* is Richardson's constant, taken as $120 \text{ amp cm}^{-2} \text{ K}^{-1}$ in this work and T , the absolute temperature, is taken as 295 K. Thus, a $\log(j)$ versus V plot for positive voltages would look similar to the curve shown below,

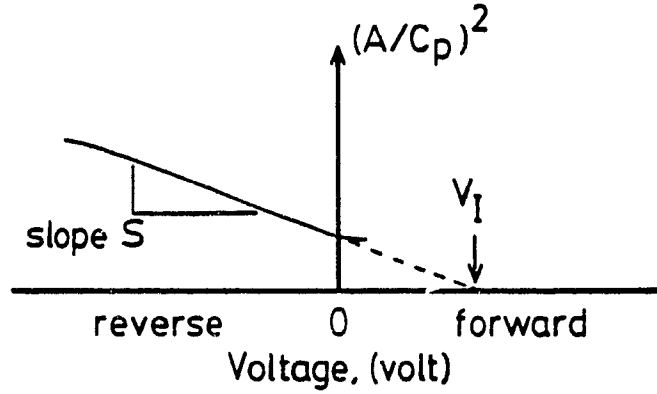


where it is seen that for voltages above about $3kT/q$ (about 0.08 volt) the characteristic is a straight line. The extrapolated intercept of this straight line region on to the $\log(j)$ axis is just $\log(j_0)$. Therefore, from this intercept and using equation (7) the barrier height of the junction is determined as

$$\phi_{bp} = kT \ln\left(\frac{A^* T^2}{j_0}\right) \quad (8)$$

2.3.2 Capacitance versus Voltage Method

The method of determining the barrier height of the junction by capacitance measurements is very well documented in the literature [9] [10]. This method uses capacitance versus voltage data for reverse voltages (i.e. $V < 0$) plotted in the form of a Mott-Schottky plot $((A/C_p)^2 \text{ versus } V$, where A in this case is the diode area and C_p is the parallel incremental capacitance of the diode) as illustrated below.



From the slope, S , of such a curve the impurity doping concentration N_A , in the p-semiconductor is determined with the equation

$$N_A = \frac{2}{q\epsilon_r\epsilon_o S} \quad (9)$$

Here ϵ_r is the relative dielectric constant of the semiconductor (taken as 7.8 for selenium in this work) and ϵ_o is the permittivity of free space. Assuming that the free carrier concentration, p , in the p-semiconductor is equal to the doping concentration, N_A , the energy difference between the Fermi level and the top of the valence band in the bulk of the semiconductor is determined with the equation

$$E_F - E_V = kT \ln\left(\frac{N_V}{N_A}\right) \quad (10)$$

where N_V is the valence band edge density of states, taken in this study to be $2.5 \times 10^{19} \text{cm}^{-3}$. The voltage intercept of the curve corresponds, simply, to the built-in potential V_I . Thus, the barrier height is determined as

$$\Phi_{bp} = qV_I + (E_F - E_V) \quad (11)$$

2.3.3 Photoelectric Method

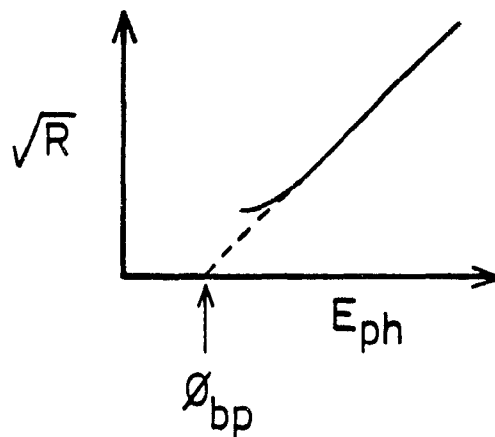
Barrier height values are also determined from photoelectric measurements or more specifically, from relative photoresponse versus photon energy measurements. In this case, photons of energy $E_{ph} = h\nu$, where ν is the frequency of the light, excite holes (electrons for a metal on n-semiconductor junction) from the metal over the barrier and into the p-semiconductor. The resultant photovoltaic e.m.f. causes a photocurrent, I_{ph} , to flow in an external circuit. According to Fowler [11], the ratio, R , of the photocurrent to the number of photons absorbed is given by the relation

$$R \propto \left(\frac{T^2}{E_s - E_{ph}} \right) \left[\frac{x^2}{2} + \frac{\pi^2}{6} - (e^{-x} - \frac{e^{-2x}}{4} + \frac{e^{-3x}}{9} - \dots) \right] \quad (12)$$

for $x \geq 0$, where $x = (E_{ph} - \phi_{bp})/(kT)$ and E_s is the sum of the barrier height and the Fermi energy measured from the bottom of the conduction band of the metal. For values of $E_s \gg E_{ph}$, and $x > 3$, this equation reduces to

$$R \propto (E_{ph} - \phi_{bp})^2, \quad (13)$$

so that a plot of $(R)^{1/2}$ against photon energy E_{ph} in this energy range gives a straight line with an intercept on the energy axis at the barrier height value ϕ_{bp} as shown below.



Note that, the vertical scale here is actually in arbitrary units in accordance with the fact that in practice R is a relative quantity. Nevertheless, the units of this scale do not, of course, have any effect on the intercept value.

3. SAMPLE PREPARATION

3.1 Introduction

In this work the samples prepared for study consisted mostly of the form Al-Bi-Se-counter-electrode-In as indicated in Fig.3.1. Table I shows the fabrication details for these samples numbered consecutively from WC24 to WC66. Among other things, the fabrication deposition times, temperatures, as well as, film thicknesses are listed for diodes with counter-electrodes of thallium, bismuth, platinum and in one case aluminum. A structure was prepared by first evaporating a Bi back-contact film on to an Al stud. In several samples, however, a Pt film was deposited instead of Bi. Next, a layer of crystalline Se was put down on top of the back contact film by evaporation. This step was followed by the evaporation of the counter-electrode metal on to selected areas of the Se layer using a mask similar to the one illustrated in Fig.3.2. Electrical contact films of In or Wood's alloy (50% bismuth, 25% lead, 12.5% tin and 12.5% cadmium) were then deposited on to the counter-electrodes by using another mask. Finally, the sample was mounted in a Teflon holder and thin copper wires were soldered to the In (or Wood's alloy) areas to make electrical connection to the device. More details on this preparation procedure are given in the remainder of this chapter.

3.2 Al Stud Preparation

Aluminum studs with a cylindrical shape, about 2 cm in diameter and 1 cm in length, were used as the substrates for all the samples of this work. To prepare a stud for deposition, its working face was first mechanically polished with 600 grit alumina powder. The stud was then rinsed with tap water, then with methyl alcohol and set aside to dry. Once dry, the stud was immersed in boiling acetone for about 20 minutes. This ensured that the working face was free of any organic films, which may have been resistant to the etchant in the next step. Next, the stud was immersed into an ultrasonic bath for 15 minutes containing an Al etching solution. This consisted of either a saturated solution of NaOH or a solution of Na_2CO_3 (25 grams/litre) and $\text{Na}_3\text{PO}_4 \cdot 12\text{H}_2\text{O}$ (62 grams/litre). A black residue usually remained on the stud but was easily removed by immersion in HNO_3 . The etching step roughened the working face, so that the adhesion was enhanced between the stud face and the subsequently deposited back-contact film. The stud was then rinsed with deionized water, then alcohol and set aside to dry. This step was followed by a final cleaning in boiling acetone for 20 minutes. The stud at this point was ready to be mounted in the vacuum chamber for back-contact deposition.

3.3 Back-contact Deposition

As noted earlier, both Bi and Pt were used as the back-contact metals. Their deposition procedures are now described.

The Bi back-contact deposition was carried out by evaporating several Bi pellets (99.999% pure) from a molybdenum boat in a Cooke Vacuum Products model CV301FR vacuum coater pumped to a base pressure of about 10^{-6} Torr. The apparatus is illustrated in the diagram in Fig.3.3. In each run, deposition of the Bi was carried out on 4 studs at a time mounted on a stainless steel holder. Between 1 and 5 pellets were used in the evaporation, depending on how thick a Bi film was desired. The deposition time was typically about 2 minutes and was controlled with a shutter between the boat and substrate holder. The distance between the boat and substrates was 6 cm in all cases. The resulting Bi film was uniform, usually brownish-grey in color and about $3\text{ }\mu\text{m}$ thick.

Where Bi was not used as the back-contact metal, Pt was employed. Since Pt has such a high melting point ($1769\text{ }^{\circ}\text{C}$) and because it tends to alloy with refractory metals, thicker films, like those used at the back contact, were found to be more efficiently deposited by dc sputtering than evaporation. This sputtering was done in a 12 inch Edwards model E306A coating system, as shown in the diagram in Fig.3.4. The target was a disk of Pt (99.99% pure) about 1.2 cm in diameter and 1 mm thick. The substrate-to-target distance was 4 cm. The plasma discharge was in an Ar atmosphere at a pressure of 30 millitorr. The dc voltage and current used were 3 kV and 4 mA respectively. The sputtering time was typically around 120 minutes and was controlled by opening and closing a shutter situated between the target and the substrate. Under these conditions, the Pt films were quite uniform and estimated to be about $1\text{ }\mu\text{m}$ thick, as observed with an optical microscope.

3.4 Selenium Deposition

The selenium deposition was done by evaporation from a crucible in a 12 inch Edwards model E12E3 vacuum system, pumped to a base pressure below 10^{-6} Torr. This apparatus is shown in the diagram in Fig.3.5. The crucible was made of stainless steel and was heated with a tungsten coil. An aluminum oxide cup, electrically insulated the crucible from the coil heater. The crucible temperature (T_{cr}) during deposition was typically about 230 °C (about 13 degrees higher than the melting point of selenium) and was monitored using a J-type thermocouple fitted into a small hole in the rim of the stainless-steel crucible. The substrates (4 of them at a time) were held on a graphite holder with the back-contact film surface about 8 cm above the crucible. Prior to raising the substrates to the temperature for the deposition stage, they were heated to 220 °C and held there for 45 minutes. By doing this, the substrates were thermally etched and, at the same time, outgassed along with the graphite holder. This was expected to reduce the amount of contaminants present during the subsequent selenium growth stage. The temperature of the substrates was controlled by means of a 33 watt heating element connected to an Omega temperature controller with a J-type thermocouple in thermal contact with the graphite holder. It was found by experiment that, for the temperature range of interest here (30 °C to 220 °C), the temperature of the substrates themselves were within 4 °C of that of the holder. Thus, the substrates and the holder were at essentially the same temperature. Immediately prior to the actual deposition, the substrate temperature was lowered from 220 °C to 130 °C and held there for the entire deposition. This temperature ensured good crystallinity of the Se film. The deposition time

was usually between about 60 and 120 minutes and was controlled by opening and closing a shutter located between the crucible and the substrates. Note that the shutter was not opened until the molten selenium in the crucible had stopped bubbling (usually about 30 minutes). This bubbling was most likely due to the escape of dissolved gases from the selenium. After the deposition was completed, the substrates were brought to room temperature slowly, avoiding the peeling of the film off the Al substrate. Fig.3.6 shows two SEM photographs of a selenium film cross-section. One photograph is of the back-scattered electron image and clearly shows the selenium and bismuth back-contact layers. The other photograph is a secondary electron image and displays the crystalline grains of the selenium.

While selenium doped with 60 ppm Cl was used almost exclusively in this work, one film of undoped selenium was also deposited. It was noted that, it was much easier to deposit doped selenium than undoped selenium, suggesting that the deposition of crystalline selenium was influenced greatly by the doping level. It was also observed that, occasionally a Se film was black in color instead of the usual grey. This black appearance was found to be due to the presence of many "spikes", as shown magnified in the SEM photograph of Fig.3.7. These apparently consisted of filamentary growths of selenium nucleated at many points over the entire selenium surface. Such "spikes" were undesirable from a consistency stand point and so were avoided by closely controlling the deposition process. The exact cause (or causes) of their appearance is still unknown. However, it is speculated that they come about if the sample is not adequately cleaned.

3.5 Counterelectrode Deposition

As mentioned previously, the counterelectrode metals were mainly Tl, Bi and Pt. All three were deposited by evaporation in a high vacuum system (base pressure less than 10^{-6} Torr) in order to ensure a clean contact to the Se. Furthermore, measures were taken to keep the substrate temperature low to minimize the formation of selenides. Moreover, the metals used here were at least 99.999% pure. The procedures for these depositions are given in more detail in the subsequent paragraphs.

The thallium deposition process was carried out in a Cooke Vacuum Products model CV301FR vacuum coater, where 1 or 2 pellets were loaded into a molybdenum boat. The set-up used is illustrated in Fig.3.8. Excessive heating of the sample was avoided by mounting the substrate in a large thermal mass holder and also by using short deposition times, typically between 20 and 40 seconds as indicated in Table I. The deposition time was controlled with a shutter, as previously described. The surface of the sample was located 6 cm above the boat for all the Tl depositions and the boat current was typically 25 amperes.

Deposition of bismuth counterelectrodes was carried out in the same vacuum system that was used in the Tl deposition. The conditions for this evaporation were essentially the same as those used for the Tl deposition except that the boat current was slightly lower, at about 20 amperes, reflecting the fact that Bi has a melting point of 271 °C, 32 degrees lower than that for Tl (303 °C).

Platinum was deposited also by evaporation. However, it was carried out in an Edwards model E306A vacuum coater. The set-up for this deposition is shown in the diagram in

Fig.3.9. In this case, three riders of Pt wire were evaporated from a tungsten filament. Since Pt has such a high melting point, a heat shield was employed to prevent excessive sample heating during the deposition. It was also found that a large portion of the Pt appeared to alloy with the filament and so, to get a reasonable film thickness, a filament-to-sample separation of only 2 cm was used. The deposition time was typically about 20 seconds and was also controlled by a shutter. It was estimated that Pt films made under these conditions were about 30 nm thick.

3.6 Electrical Connections and Mounting

Following the counterelectrode deposition, a film of In with its low melting point (156 °C) or Wood's alloy (melting point 71°C) was deposited. The sample was then mounted in a Teflon holder and thin copper wires were soldered to the In or Wood's alloy film to make electrical connection. Excessive heating was once again avoided by using low melting point Wood's alloy as the solder material. In the thallium samples, the counterelectrode was usually completely covered by the indium layer to inhibit atmospheric attack on the Te, as reported by Pan [2] and Champness and Pan [12].

3.7 Comparison of the Preparation Procedure with that of Pan [2]

In this study, several sample fabrication parameters were different from those of Pan [2] in an effort to improve the sample performance. The most significant differences are now

discussed in the subsequent paragraphs.

Firstly, the Al studs in this work were chemically etched, whereas those of Pan were manually abraded. It is believed that the etching provided more control over the roughness of the Al surface than the abrasive method and hence, more consistency could be obtained. It was noted that the adhesion of the deposited film to the etched surface was not noticeably inferior to that for the abraded surface.

Next, the crucible temperature was between 220 °C and 240 °C in the present case, while it was higher for that of Pan at between 240°C and 260°C. This corresponded to a lower selenium vapour incidence rate at the substrate surface for the present work and so it was expected that the selenium film was of better quality here than in Pan's case.

Furthermore, Pan did not report having a high temperature thermal etch and outgassing step for the substrates just prior to the selenium deposition. It is believed that such a step was very important in achieving good, consistent results.

In addition, a molybdenum boat was used in the thallium and bismuth depositions in this study as opposed to a boat made of tantalum, as was the case of Pan [2]. This was done because it was found that less alloying with the boat occurred with molybdenum than tantalum.

Moreover, in the present work special measures were taken to prevent excessive heating of the sample, particularly after the counterelectrode was deposited. No such measures were mentioned in the work of Pan beyond the low melting point Wood's alloy solder that was used. It is well known that heating of structures, like those studied in these investigations, has pronounced effects.

Finally, most of the samples in this work had an electrical contact film of indium rather than Wood's alloy. From experience in the present work, it was found that a sufficient layer of indium could be deposited more efficiently than an equivalent layer of Wood's alloy. Furthermore, the soldering step to the indium film, which was carried out with Wood's alloy solder, was much easier to perform because of better wetting. Hence, both of these features with the indium film resulted in reduced inadvertent heating of the sample.

TABLE I Sample Fabrication Data

Struct	Sample number	Se deposition						Back cont depos		Counterelectrode dep		Contact deposition		
		Crucib temp (°C)	Substr temp (°C)	Dep time (min)	Se thick (μm)	Texture	Adhes	metal	thick (μm)	metal	dep time (seconds)	metal	dep time (seconds)	vac sys used
Bi-Se-Te	WC35	220	140	80	10	smooth	fair	Bi	-	Te	20	W a (c)	75	E6(d)
	WC36	-	150	2	26	rough	v good	Bi	-	Te	20	W a	75	E6
	WC37	230	130	60	7	smooth	good	Bi	3	Te	45	W a	120	E6
	WC38	230	120	60	27	bumpy	fair	Bi	3	Te	35	In	90	Cooke(e)
	WC39	230	130	120, 310(a)	22, 35	smooth	good	Bi	3	Te	40	In	45	Cooke
	WC40	230	130	120, 310(a)	22, 35	smooth	good	Bi	3	Te	90	In	30	Cooke
	WC41	230	130	180	15	smooth	fair	Bi	<<1	Te	35	In	45	Cooke
	WC43	230	130	135	10	smooth	good	Bi	<<1	Te	30	In	35	Cooke
	WC44	230	130	220	25	smooth	good	Bi	3	Te	30	In	45	Cooke
	WC45	230	130	220	25	smooth	good	Bi	3	Te	30	In	45	Cooke
	WC46(b)	220	130	120	7	smooth	good	Bi	4	Te	30	In	30	Cooke
	WC48	220	130	80	10	smooth	good	Bi	10	Te	30	In	60	Cooke
	WC49	240	130	90	25	smooth	good	Bi	3	Te	30	In	60	Cooke
	WC52	240	130	90	25	bumpy	good	Bi	3	Te	30	In	45	Cooke
	WC53	240	130	90	25	bumpy	good	Bi	3	Te	30	In	45	Cooke
	WC54	240	130	90	25	bumpy	good	Bi	3	Te	30	In	45	Cooke
	WC61	230	130	90	40	smooth	good	Bi	2	Te	30	In	30	Cooke
	WC62	230	130	90	40	smooth	good	Bi	2	Te	60	In	30	Cooke
Bi-Se-Bi	WC24	240	130	90	10	smooth	fair	Bi	0.5	Bi	60	W a	120	E6
	WC26	240	130	100	9	smooth	fair	Bi	4	Bi	120	W a	90	E6
	WC27	240	130	75	8	smooth	good	Bi	<<1	Bi	-	W a	-	E6
	WC32	230	140	68	12	smooth	good	Bi	1	Bi	105	W a	75	Cooke
	WC33	220	140	80	10	smooth	fair	Bi	2	Bi	30	W a	120	E6
	WC34	240	140	65	20	smooth	fair	Bi	2	Bi	20	W a	240	E6
	WC42	220	130	135	10	smooth	good	Bi	<<1	Bi	30	In	45	Cooke
	WC50	240	130	90	27	smooth	good	Bi	3	Bi	20	In	45	Cooke
	WC51	240	130	90	27	smooth	good	Bi	3	Bi	20	In	45	Cooke
	WC55	240	130	90	27	smooth	good	Bi	3	Bi	20	In	45	Cooke
	WC57	240	130	90	30	rough	excel	Bi	2	Bi	10	In	45	Cooke
	WC60	230	130	90	40	smooth	good	Bi	2	Bi	10	In	45	Cooke
	WC61	230	130	90	40	smooth	good	Bi	2	Bi	10	In	45	Cooke
Pt-Se-Bi	WC30	235	140	90	20	smooth	good	Pt	<<1	Bi	90	W a	60	E6
	WC56	240	130	90	30	rough	excel	Pt	2	Bi	20	In	45	Cooke
	WC58	230	130	60	23	bumpy	v good	Pt	1	Bi	8	In	45	Cooke
	WC59	230	130	60	23	bumpy	v good	Pt	1	Bi	30	In	30	Cooke
Bi-Se-Pt	WC25	240	130	90	10	smooth	good	Bi	<<1	Pt	15	W a	120	E6
	WC28	240	130	75	9	smooth	good	Bi	3	Pt	20	W a	240	E6
	WC29	240	140	75	9	smooth	good	Bi	<<1	Pt	30	W a	300	E6
	WC64	230	130	90	40	smooth	good	Bi	2	Pt	20	In	45	Cooke
	WC65	230	130	90	40	smooth	good	Bi	2	Pt	20	In	45	Cooke
Pt-Se-Pt	WC31	235	140	90	20	smooth	good	Pt	1	Pt	20	W a	60	E6
	WC66	230	130	80	20	bumpy	good	Pt(f)	1	Pt	20	In	45	Cooke
Bi-Se-Al	WC47	220	130	80	10	smooth	good	Bi	10	Al	30	In	60	Cooke

a Two areas of the substrate were subject to two different deposition times. Hence, the areas had different film thicknesses

b The Se deposited for WC46 was undoped

c W a refers to Wood's alloy (50% Bi, 25% Pb, 12.5% Sn and 12.5% Cd) that was used as the electrical contact film

d E6 means an Edwards model 6E4 vacuum system was used

e Cooke means a Cooke Vacuum Products model CV3011R vacuum system was used

f The Pt back contact for this sample was made by first sputtering a Pt layer about 1 μm thick on to the substrate and then evaporating over it another thinner Pt film of 99.999% purity

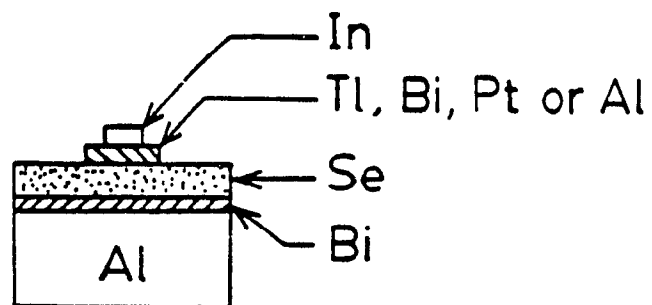


Fig3.1. Schematic showing cross-sectional view of the sample structure used in this study.

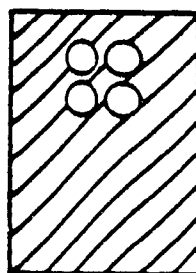


Fig3.2. Schematic of metal mask used for counterelectrode deposition.

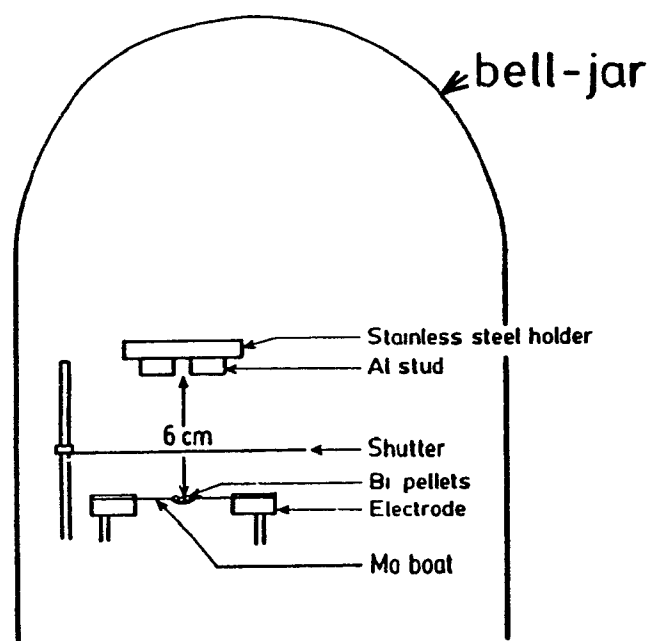


Fig.3.3. Schematic illustrating Bi back-contact evaporation apparatus.

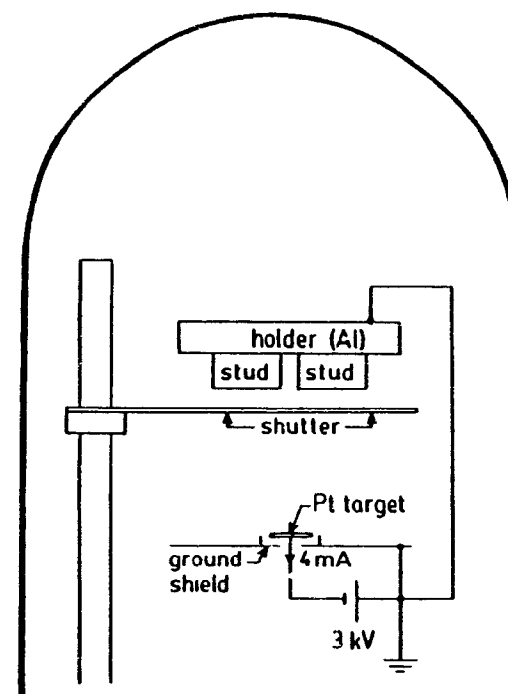


Fig.3.4. Schematic for Pt back-contact sputtering set-up.

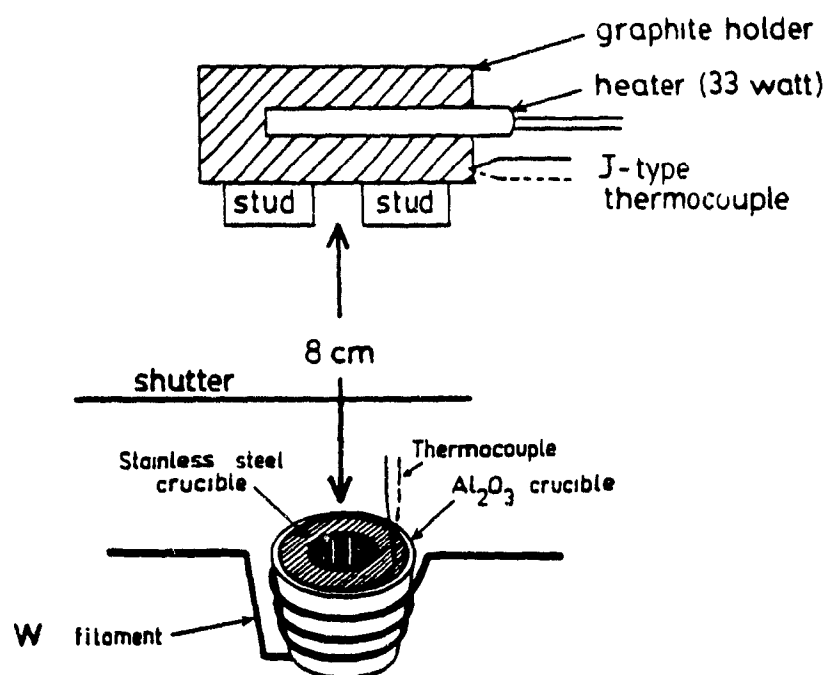


Fig3.5. Schematic showing Se evaporation set-up.

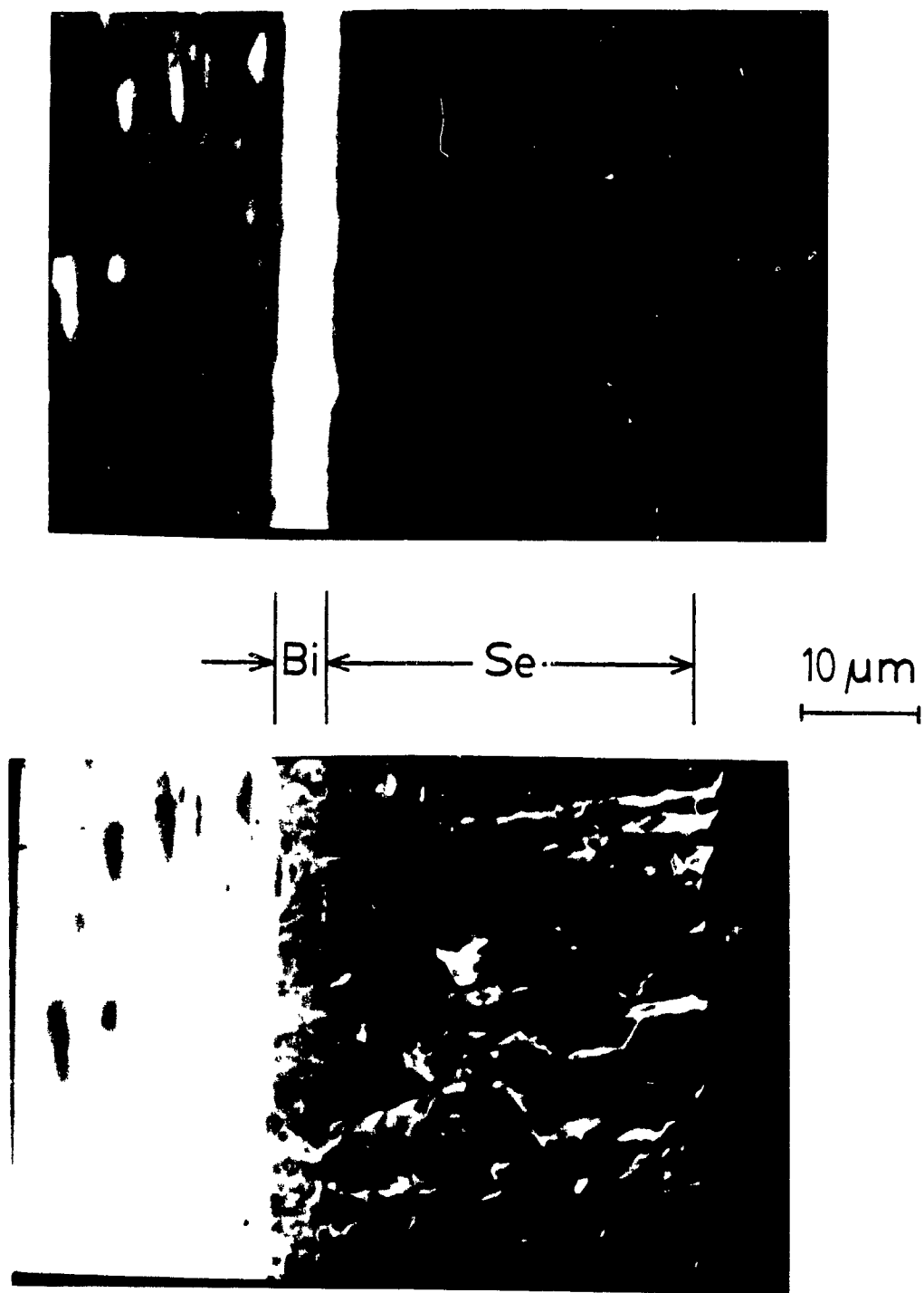
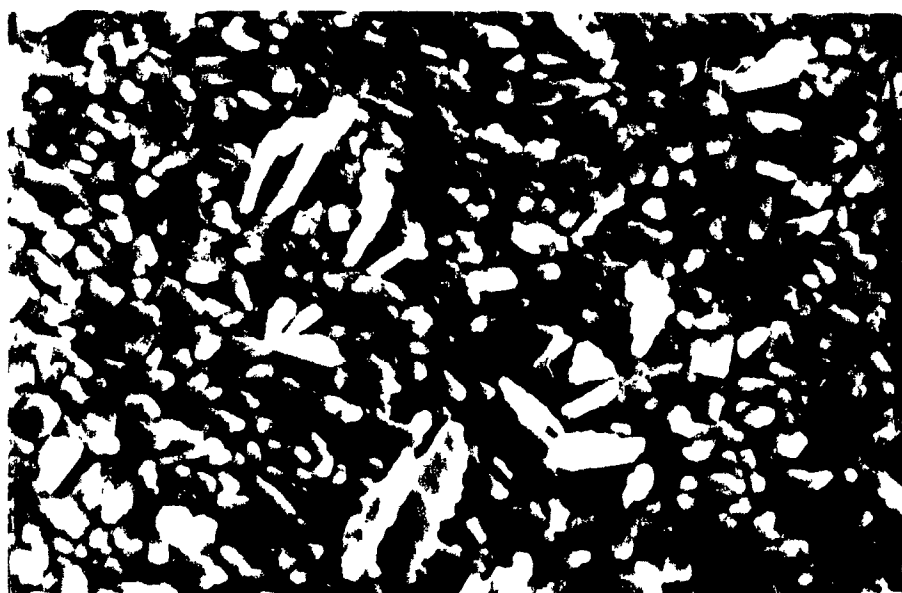


Fig.3.6. SEM images of the cross-section of a Se layer on a Bi layer. The top photograph is of the back-scattered electron image. The bottom photograph is of the secondary electron image. Both photographs are of the same area.



10 μm


A horizontal scale bar with vertical end caps, indicating a length of 10 micrometers.

Fig.3.7. SEM image of the surface of a so-called "black" Se film

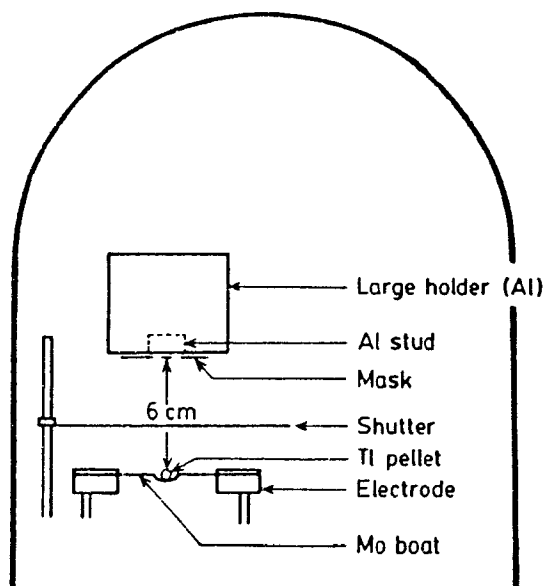


Fig.3.8. Schematic of Tl counterelectrode evaporation set-up.

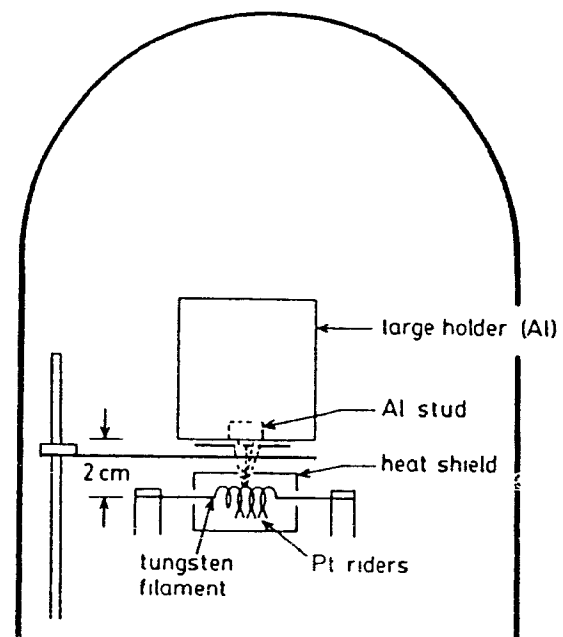


Fig.3.9. Schematic illustrating set-up used for Pt front-contact evaporation.

4. MEASUREMENT TECHNIQUES

4.1 Introduction

The methods used to measure the samples described in the previous chapter are now presented in the present chapter. These include static dark current-voltage measurements, incremental parallel capacitance and resistance against voltage and frequency measurements and photoelectric response as a function of wavelength measurements. The results of these measurements are presented in later chapters. All of the samples had current versus voltage measurements made on them and about 90% of the samples had incremental parallel capacitance and resistance versus voltage measurements. Photoresponse as a function of wavelength was measured for several Bi-Se-Bi samples and these characteristics represent the first time this laboratory has reported the results of such measurements. In addition to the electrical measurements that were made, several Se-Te samples were also examined from a materials analysis stand-point using x-ray diffractometry (XRD) and scanning electron microscopy (SEM). Details of these measurements are now presented

4.2 Current versus Voltage Measurements

The manner in which the static dark current-voltage (I-V) measurements were made was essentially the same as that described by previous workers [2] [3]. A schematic of the measurement apparatus used is shown in Fig 4.1. In these measurements, the current-density (j) values were obtained by simply dividing the current values by the cross-sectional area of

the diode, which was either 0.143 or 0.78 cm². It should be noted that, throughout the present work the current-voltage measurements for the bias direction where the back-contact was positive (normally forward bias direction for the samples), were always made before those where the back-contact was negatively biased. Furthermore, the bias was always scanned in an increasing direction starting at 0 volt and ending at 1.0 volt for either polarity. It was observed that some of the readings, especially those for the Se-Te samples in the forward bias, required a relatively long time (about one minute) to stabilize after the bias was changed and so the bias in these measurements was increased at a relatively slow rate.

4.3 Capacitance and Resistance versus Voltage Measurements

The incremental parallel capacitance, C_p , and resistance, R_p , of the samples were also measured against voltage at a number of frequencies between 20 Hz and 10 MHz using two different measurement set-ups, as shown in the diagrams of Figs. 4.2 and 4.3. For frequencies between 20 Hz and 100 kHz, the sample was measured with a General Radio model 1689 Digibridge, shown schematically in Fig.4.2(a). Here, a Farnell model L30B stabilized power supply, connected to the external bias adaptor of the instrument, provided the dc bias across the sample. A Hewlett-Packard 3478A multimeter was connected to the supply to measure this dc bias. A schematic illustrating the measurement technique used by the Digibridge is shown in Fig.4.2(b). From this figure, it is seen that two differential amplifiers with identical gains, along with some filtering circuitry (not shown), measured the ac voltage, e_1 , across the sample and also the ac voltage, e_2 , across a small sensing resistor,

R_s , in series with the sample. The voltage across this series resistor, e_s , corresponded to the current that passed through the sample. From the magnitudes and relative phases of these two voltages, the Digibridge calculated the impedance or admittance of the sample and hence, the values of C_p and R_p were also calculated. Note that, with such a design only the impedance of the sample was measured; the impedance of the voltage sources and multimeter did not affect this measurement. It is also apparent from the diagram, however, that the applied dc bias does not appear entirely across the sample. A portion of this applied voltage also appears across the series resistor, R_s , as well as the output resistances of the voltage sources. Though a precise value for these resistances was not obtainable from the specifications of the instruments, it was, nevertheless, found that the dc bias across most of the samples, while mounted in the Digibridge, was within 2% of that across the output terminals of the Farnell supply, even when the samples were biased in the forward direction. A few samples, though, particularly several Se-Bi and Se-Pt structures with a relatively large area, did show a greater difference between the voltage values at the supply and the sample when the device was biased in the low resistance direction. In these special cases, the voltage across the sample was measured directly with an HP3478A multimeter. This meter was connected only briefly, just to obtain the voltage reading and was not connected while the capacitance and resistance of the sample were actually measured. In fact, however, the capacitance and resistance values of the sample were observed to be the same with or without the multimeter connected, indicating that the admittance of the multimeter was negligible compared with that of the samples. For the frequencies between 400 kHz and 10 MHz, a Hewlett-Packard model HP4192A LF impedance analyzer was used to measure the

sample (Fig.4.3). The dc bias across the sample in this case was provided by a voltage source internal to the instrument. With this arrangement it was quite common to see that the actual voltage across the sample was more than 10% below that indicated by the HP4192A instrument. Therefore, as was done for the special cases with the Digibridge set-up, the bias across the sample was obtained by measuring it directly with a Hewlett-Packard 3478A multimeter connected across the terminals of the sample. Again, this meter was connected only briefly at a time and not connected while the capacitance and resistance of the sample were actually measured. It was found, nevertheless, that the capacitance and resistance values of the sample were the same with or without the multimeter connected.

The basic measurement procedure for both measurement arrangements was as follows. For a given measurement frequency, the dc voltage applied to the sample was increased in steps, usually of 0.1 volt, from -1 volt, where the back-contact was negatively biased, to +1 volt, where the back-contact voltage was positive. At each step the C_p and R_p values of the sample were recorded. Such a scan was repeated for a number of frequencies beginning with 20 Hz and finishing with 10 MHz. The Digibridge and HP4192A used a 0.02 volt ac signal for the measurements in all cases, which was small enough to resolve singularities but large enough for sufficient sensitivity. It should also be mentioned that, prior to each measurement session, the Digibridge was calibrated with a short circuit, for $R_p = 0$ and an open circuit, for $C_p = 0$. This calibration was done with a #14 AWG copper wire connected across the measuring terminals to act as the short circuit, while the terminals (about 3 cm apart) were left unconnected to act as the open circuit. The calibration was performed with the Farnell supply and 3478A multimeter connected to eliminate any influence their

impedances may have had on the measurement readings due to leakage. Such a calibration procedure, however, was not possible with the HP4192A, as this instrument was calibrated once only at the factory. During the low frequency measurements with the Digibridge, it was occasionally seen that the readings were somewhat unstable. This instability was overcome, however, by programming the instrument to take an average over many measurement values, typically ten. Such an averaging feature was also not possible with the HP4192A, though, this instrument was used only at higher frequencies, above 400 kHz, where the readings were stable anyway. It was also seen with the HP4192A that, a sample would display normal Faraday inductive behaviour at the higher frequencies, above 1 MHz. This effect was found to be somewhat reduced by keeping the leads of the sample short (about 2 cm long at each terminal of the device).

In these measurements it was often the case that the "automatic" features of the instruments, such as automatic scaling, actually hindered the reliability of the readings. Therefore, these measurements were performed with as much direct control from the operator as possible.

4.4 Photoelectric Measurements

Measurements of relative photoresponse, R , versus wavelength, λ , (or photon energy E_{ph}) were also made on several Se-Bi samples for near infrared wavelengths between $0.8 \mu\text{m}$ and $2 \mu\text{m}$ (E_{ph} between about 1.5 and 0.6 eV). A schematic of the basic measuring arrangement used is shown in Fig.4.4. Basically, monochromatic radiation of known relative photon flux,

Φ_{in} , from a monochromator was incident on the thin film counterelectrode metal, Bi, (approximately 30 nm thick) of the sample. The resultant photocurrent, I_{ph} , arising from the photovoltaic effect in the device, was measured by passing it through a small shunt resistance, R_{sh} , across which the voltage, V_{ph} , was measured. The relative photoresponse, R , was calculated by dividing this photocurrent by the relative photon flux of the incident beam, Φ_{in} . This was done for a number of wavelengths, thus obtaining an R versus λ characteristic. More details of the measurement set-up and procedure are given in the paragraphs which follow.

In the photoresponse measurements, it was very important to have a large I_{ph} value. Therefore, in the sample fabrication process, measures were taken to make a sample which would produce a large photocurrent. Firstly, a relatively large Bi counterelectrode area of 0.78 cm^2 was deposited, while the area of the electrical contact film was made relatively small (only about 0.05 cm^2) thus, providing a large effective light collection area. Secondly, the counterelectrode films were deposited to a thickness estimated to be about 30 nm, since it was found that samples with this thickness had the highest photocurrents.

The monochromatic beam mentioned above was provided by a Perkin-Elmer model 13U spectrophotometer, the optics of which are shown schematically in Fig.4.5. The light source was a Nernst glower, built in to the instrument, through which a constant current flowed, thus giving a constant light output intensity. This source emitted radiation of wavelengths mainly between $1 \mu\text{m}$ and $8 \mu\text{m}$. The light from the Nernst glower was passed through a single pass Littrow type monochromator to produce the monochromatic beam. This monochromator used a prism (labelled P in the figure) made either of rock-salt (NaCl) or

of fused silica (SiO_2). It was found that the NaCl prism performed better than the SiO_2 prism for wavelengths between about 1.2 and 2.0 μm (E_{ph} between 1.0 and 0.6 eV), while the SiO_2 prism was the better of the two for wavelengths between about 0.8 and 1.1 μm (E_{ph} between 1.1 and 1.5 eV). The entrance and exit slits of the monochromator (labelled S1 and S2 respectively) determined both the flux, Φ_{in} , and the wavelength interval, $\Delta\lambda$, of the monochromatic beam incident on the sample. Fig.4.6 shows a plot of measured values of $\Delta\lambda$ and Φ_{in} against slit-width for a wavelength of 1.55 μm using a SiO_2 prism. Shown also, are I_{ph} values measured for several slit widths for sample WC57. It is seen that both $\Delta\lambda$ and I_{ph} show a linear dependence on slit width, while the Φ_{in} variation is more curved. In fact, the log-log plot, shown in Fig.4.7, shows that Φ_{in} varies as the square of the slit width. Such a dependence is expected for a two slit Littrow type monochromator. In any case, it is apparent from the plot in Fig.4.6 that, while increasing the slit width increased the photocurrent, it also increased the $\Delta\lambda$ value of the beam as well. Therefore, a trade-off between the photocurrent and the wavelength interval was made and the slit widths used were usually between 0.3 and 0.6 mm, resulting in photocurrents of the order of several nanoamperes. These widths corresponded to a $\Delta\lambda$ value always less than 10% of the wavelengths.

As mentioned earlier, the photocurrent of a sample was measured by passing the current through a small resistance shunt, R_{sh} and measuring the resultant voltage, V_{ph} . Since the photocurrent was small and the noise level large, this voltage had to be measured with the special apparatus shown schematically in Fig.4.8. In this arrangement the light beam was chopped at 13 Hz with a light chopper situated between the Nernst glower and the

monochromator optics. A finely tuned lock-in amplifier (Princeton Applied Research model 124A) was then used to measure the resultant 13 Hz voltage signal, V_{ph} , across the shunt and hence, the photocurrent, I_{ph} , of the sample. This lock-in amplifier was locked on to the frequency of the chopper by means of an EG&G SGD 100A detector placed in the chopped white beam. It should be mentioned that, while a large resistance shunt would have produced large voltages to measure, in fact, the shunt used was quite small at only 10 ohms. Such a small resistance was used for two reasons: (1) It was important that the shunt resistance was much smaller than the resistance of the sample (effectively short circuiting the sample) so that, essentially all of the photocurrent passed through the shunt and hence, was measured. (2) By using a small shunt resistance a small noise (Johnson noise) level was maintained at the lock-in amplifier input terminals.

To obtain the relative photoresponse value, both the photocurrent, I_{ph} , as well as the relative incident photon intensity, Φ_{in} , were required. This Φ_{in} value was obtained by diverting the incident beam with a mirror (labelled M11 in Fig.4.5) on to a thermopile detector (labelled T in Fig.4.5) built in to the spectrophotometer. A meter, also built in to the spectrophotometer, connected to the detector, indicated the relative incident power of the beam. By dividing this power reading by the photon energy, $h\nu$, of the beam, the value Φ_{in} was obtained.

The basic procedure for making these photoresponse measurements was as follows. First, the sample was positioned so that the monochromatic beam from a parabolic mirror, M14 in Fig.4.5, was focused on to the counterelectrode of the sample. The angle of this mirror was then finely adjusted, by means of two screws, so that the beam on the counterelectrode

was directed away from the contact metal area. This ensured that the photocurrent was entirely due to the effect of the counterelectrode metal and not the indium contact metal. For obvious reasons the wavelength of the beam used for this alignment step was in the visible range. A measurement scan was usually started at this point. The wavelength was selected by changing the angle of the Littrow mirror (M9 in Fig.4.5) with a rotatable graduated drum on the side of the monochromator housing. The scale on the drum was previously calibrated to correspond to the wavelengths of the monochromatic beam. A scan was always made in the direction of increasing wavelength and typically ran from about 0.8 μm to 2.0 μm . At each wavelength selected, usually at 0.05 μm steps, the monochromatic beam was directed first on to the sample for the photocurrent measurement and then reflected with a mirror (M11 in Fig.4.5) on to the thermopile detector for the relative incident intensity measurement.

4.5 Materials Analyses

In addition to the electrical measurements that were made in this work, materials analysis measurements were also made using facilities in the Metallurgical Engineering and Geology departments. These included x-ray diffraction (XRD) measurements made with a Rigaku Rotaflex diffractometer, as well as, x-ray fluorescence (XRF) measurements made with a JEOL model JSM-840 scanning electron microscope (SEM). The XRD measurements, which used copper $K\alpha_1$ radiation, provided information on the materials that were present in the samples, while the XRF studies with the SEM showed the arrangement of these materials

relative to one another. The SEM used an electron-beam energy of 20 kV in this work.

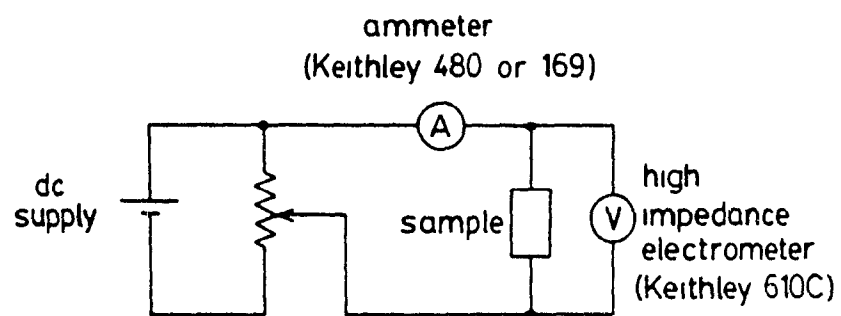
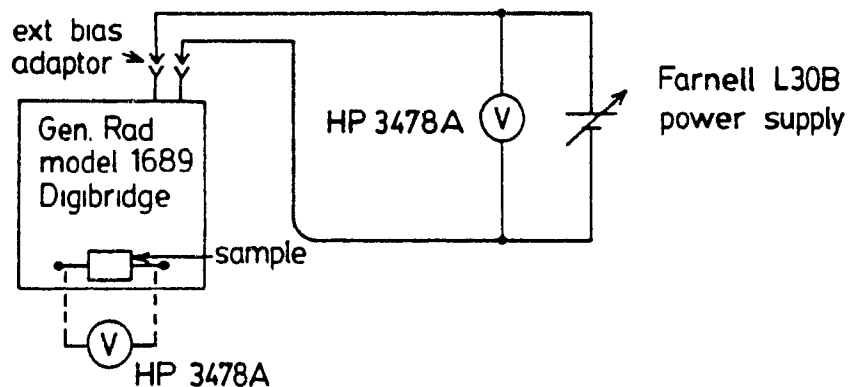


Fig.4.1. Schematic of current-voltage measurement apparatus.

a)



b)

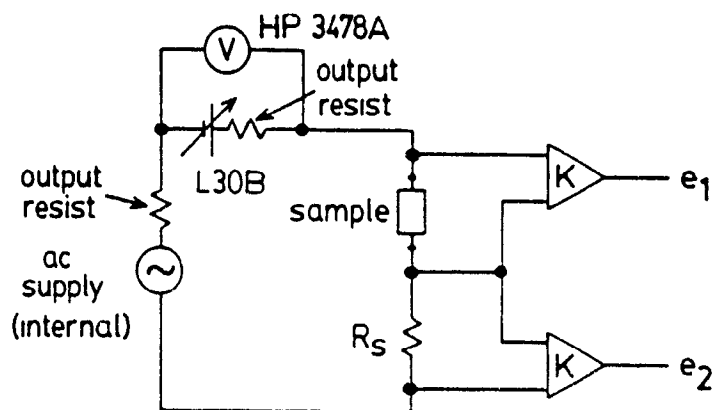


Fig.4.2. a) Arrangement used in making incremental capacitance and resistance measurements with the General Radio model 1689 Digibridge for frequencies between 20 Hz and 100 kHz. The broken lines from the HP3478A meter to the sample indicate a temporary connection. b) Diagram illustrating measurement principle used by Digibridge instrument.

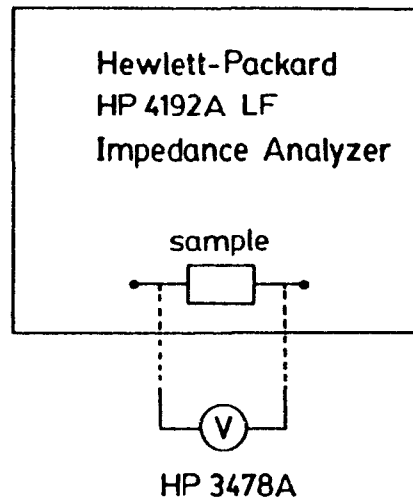


Fig.4.3. Diagram of arrangement used to measure incremental capacitance and resistance with the Hewlett-Packard HP4192A LF Impedance Analyzer for frequencies between 400 kHz and 10 MHz. The broken lines between the sample and the HP3478A meter indicate temporary connection.

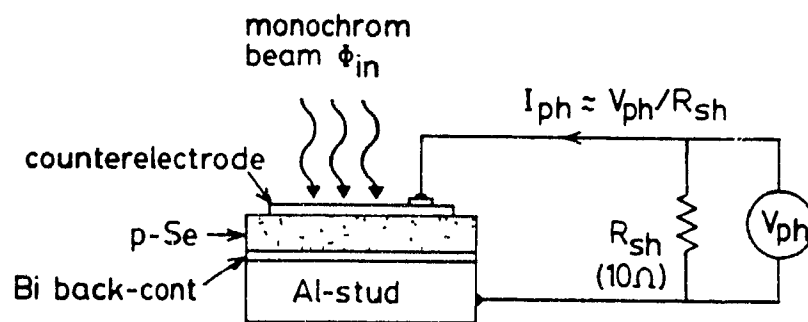


Fig.4.4. Illustration of basic photoelectric measurement arrangement.

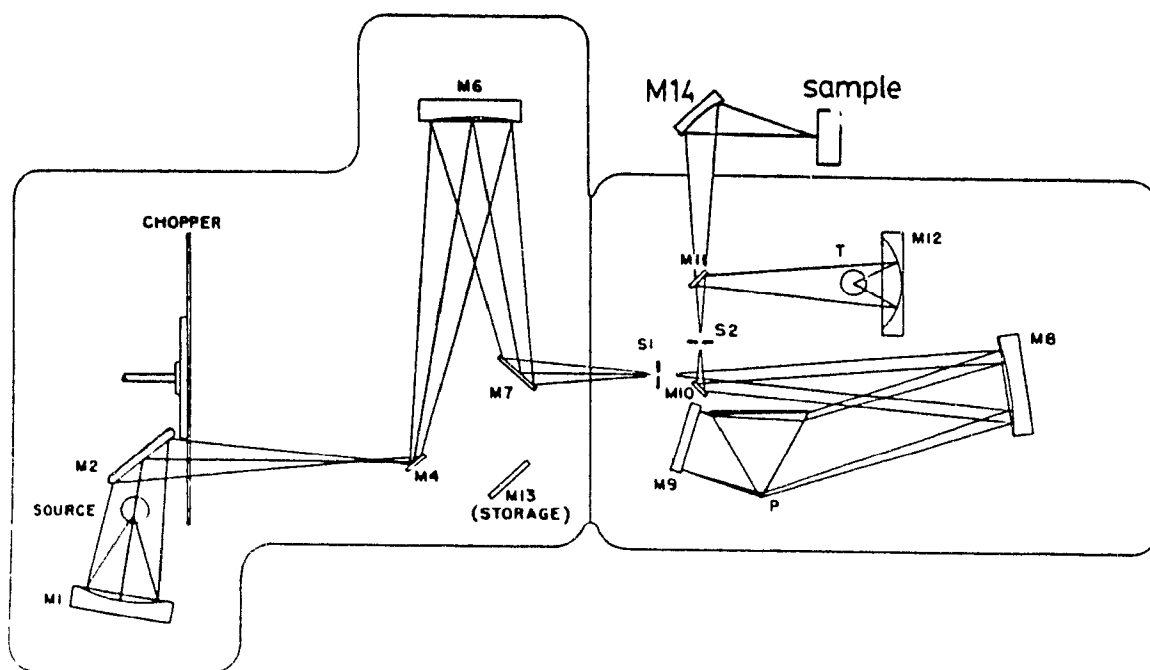


Fig.4.5. Schematic of Perkin-Elmer model 13U spectrophotometer optics as arranged for use in this study.

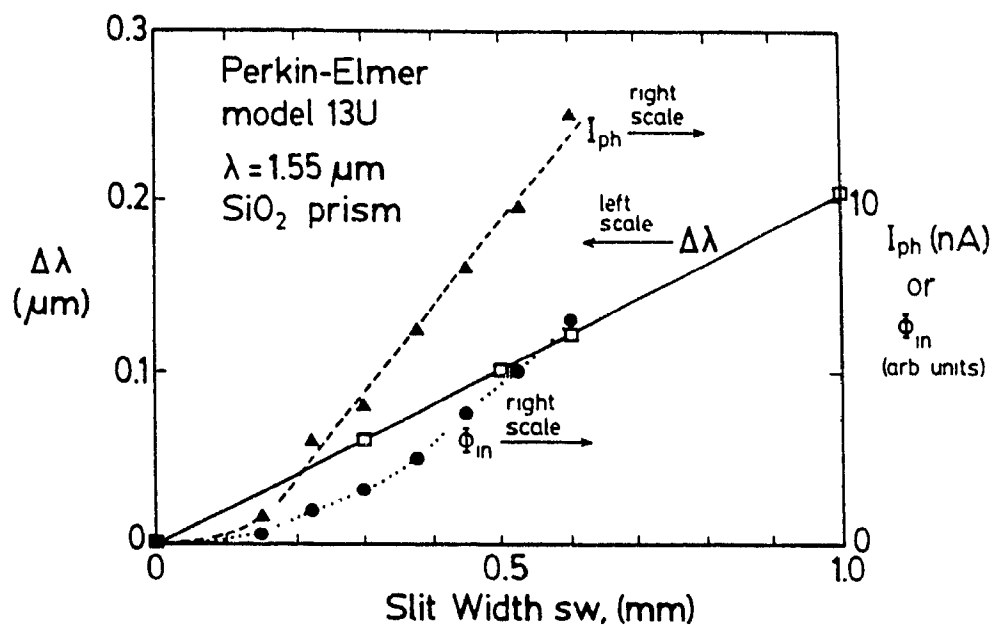


Fig.4.6. Plot of wavelength interval $\Delta\lambda$ (left vertical scale), against monochromator slit width for a wavelength of $1.55 \mu\text{m}$ with an SiO_2 prism. Plotted also against slit width are the (right vertical scale) relative photon intensity, ϕ_{in} , of the incident beam and the photocurrent, I_{ph} , measured for sample WC57.

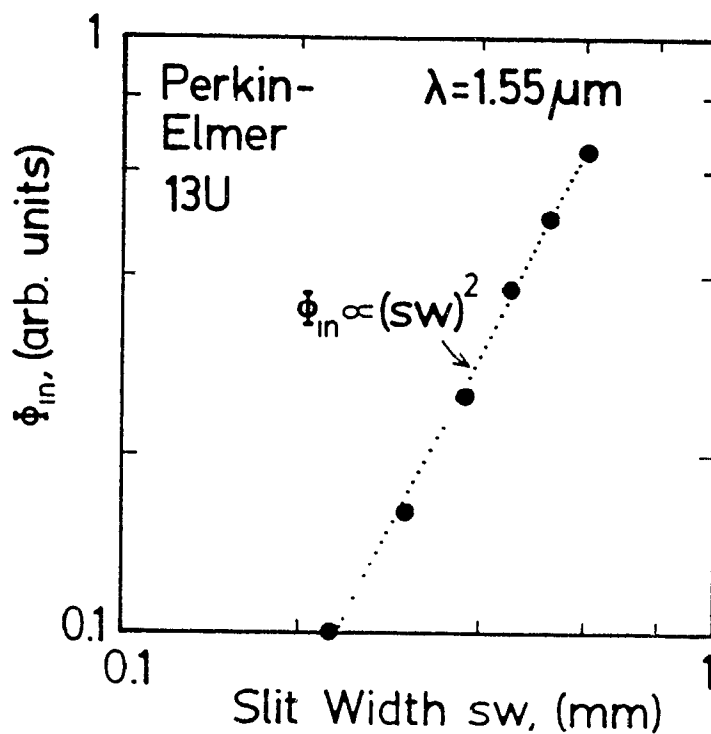


Fig.4.7. Plot of relative photon intensity of incident beam, ϕ_{in} , against monochromator slit width on log-log scales. Shown also is a square dependency curve (dotted line).

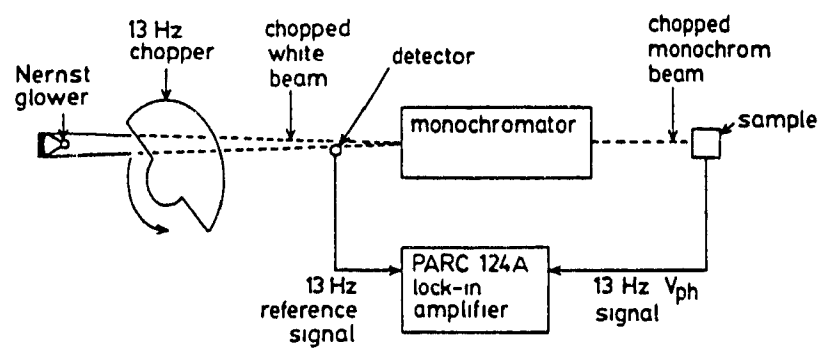


Fig.4.8. Schematic of arrangement used to make photoelectric measurements.

5. RESULTS ON Se-Te CONTACTS

5.1 Introduction

The Se-Te contact is especially interesting to study because of its excellent forward-to-reverse rectification, when freshly made and also because it has a forward ideality factor very near unity, as is expected for a Schottky junction. Pan [2] and Chan [3] observed furthermore, an interesting minimum in the incremental capacitance versus voltage (C_p -V) characteristics in the forward direction for such diodes, and explained this, phenomenologically, with an equivalent extra capacitor arising internally in the device. In this work, similar minima were observed, but unlike the previous studies, some C_p -V curves actually turned to negative C_p values. This negative C_p effect was seen in several types of structures. However, it was strongest and most consistent in the Se-Te samples of this work. Accordingly, this chapter is mainly concerned with the description of incremental capacitance and resistance measurement results for the Se-Te diodes listed in Table I, along with their static dark current-density versus voltage (j-V) characteristics. Another very interesting feature of Se-Te diodes is that, their rectification properties degrade quite considerably with storage time, as reported previously by Pan [2], Champness and Pan [12] and Chan [3]. Further work on this degradation makes up a very important part of this chapter. The chapter is divided essentially into two parts. The first part presents electrical characteristics for freshly made Se-Te samples, while the second part describes results of some aging studies.

It should be noted that, all of the Se-Tl samples studied here had Bi as the back-contact, as indicated in Table I.

5.2 Electrical Characteristics of Freshly Prepared Se-Tl Diodes

This section will present the electrical characteristics of freshly made Se-Tl samples. By freshly made is meant that the Tl film was deposited and the sample completed on the same day that the measurements were taken, referred to in the thesis as "day-0" measurements.

5.2.1 Capacitance versus Voltage Characteristics

Figs. 5.1 to 5.4 show plots of incremental capacitance C_p , against voltage for forward and reverse bias voltages for three Se-Tl samples, WC39, WC46 and WC61. It is apparent that, all the curves decline monotonically as the reverse voltage increases. However, they show somewhat more complex behaviour in the forward direction, where, as can be seen, all the figures show a minimum between 0.2 and 0.4 volt for the lower frequencies (i.e. below 1 kHz). This minimum for sample WC46 at 20 Hz, and WC61 at 20 and 100 Hz, actually extends to negative C_p values. This is indicated in the separate lower portion of the plots in Figs. 5.3 and 5.4 (needed, since the vertical scale is logarithmic). While the 0.2 volt dip for sample WC39, areas 2 and 3, is strong at 20 Hz, it does not go to negative values. The curves for this sample exhibit negative capacitance, however, at higher voltage. Interestingly,

samples WC46 and 61 show curves with two minima. The 100 Hz curve for WC46 displays such a feature with the second minimum occurring at 0.6 volt. The trait is also observed in the 20 and 100 Hz characteristics of WC61, where the second minimum appears between 0.7 and 0.8 volt. The two figures for WC39, corresponding to areas 2 and 3, do not show such a double minimum. They do exhibit a similarity to each other, despite the fact that area 2 had a Se film thickness some 60% greater than that of area 3. The main difference is only that the 100 Hz curve for area 3 turns negative at a bias slightly less than 1 volt, whereas that for area 2 remains positive up to this voltage.

The properties described above were quite representative for most of the Se-Tl diodes prepared in this work. Out of the 16 samples that had C_p -V measurements on them, 14 showed negative C_p values, 15 had at least one minimum and 9 had a double minimum at either 20 or 100 Hz or both. All these singularities occurred only with forward bias at low frequencies. Two samples that did not show negative C_p values on day-0 were WC38 and WC45. Their day-0 C_p curves are shown in Figs. 5.13 and 5.15 and are discussed further in section 5.3.1.

5.2.2 Capacitance versus Frequency Characteristics

The C_p versus frequency characteristics for samples WC40, 44 and 46 are shown in Figs 5.5, 5.6 and 5.7 respectively for frequencies ranging from 20 Hz to between 10^6 and 10^7 Hz at bias voltages from -1 volt (reverse) to +1 volt (forward). It is seen that while there are variations from one figure to another, there are several common features. The -1 and 0 volt

curves are relatively flat between 20 and 10^5 Hz. All the curves fall off somewhat for frequencies between 10^5 and 10^7 Hz. Furthermore, each sample shows a negative C_p region for frequencies below about 100 Hz in one or more of the forward bias curves. Note that these curves always display a rise in C_p with frequency at the lower frequencies. Another common feature is that all of the curves appear to converge together at higher frequencies near 10^6 Hz. It is interesting to note that the forward bias curves of WC40 and 44 exhibit a tendency to a plateau at a frequency around 10^6 Hz. This tendency appears to be more pronounced at larger forward potentials. Note also that in all three figures, some of the curves cross below the others as the frequency rises. This occurs mainly at the larger forward voltages between 0.5 and 1 volt. The 1 volt curve for WC46 is somewhat unusual, in that it shows high C_p values at low frequency (20 Hz) and decreases rapidly up to 1 kHz. It should be pointed out, however, that this sample was different from the others, as it was made with undoped selenium.

In this work, 14 of the 16 Se-Te samples measured displayed characteristics like those just described. However, two samples, WC38 and WC45, showed somewhat different characteristics which are discussed separately in section 5.3.2. These samples did not show any negative C_p values as mentioned in the previous section. Nor did they show any rise in C_p with frequency. The day-0 curves for WC38 are displayed in Fig.5.21.

5.2.3 Resistance versus Voltage Characteristics

The incremental resistance R_p , plotted versus voltage for WC44 and 61 between -1

(reverse) and 1 volt (forward) is shown in Figs. 5.8 and 5.9 respectively. As is seen, the figures are quite similar to each other. In each, the curves for the different frequencies show a large spread in the reverse direction but a relatively narrow one in the forward, where a convergence is apparent for the frequencies between 20 and 10^4 Hz. Furthermore, the resistance variation from reverse to forward decreases greatly as the frequency increases. Note also that R_p generally decreases monotonically with frequency for any given voltage. Such a variation is more apparent in Fig. 5.10, where R_p is plotted against frequency for sample WC38 at several bias voltages. Here it is seen that the curves converge together at higher frequencies, as they fall at a rate close to $1/\text{frequency}$. There are, however, two slight differences between the plots of Figs. 5.8 and 5.9 that are worth mentioning. Firstly, the WC61 curves show a minimum at a forward voltage of about 0.5 volt, whereas the WC44 variations do not. Secondly, there is a maximum in the 20 Hz curve at -0.2 volt for WC61 but none for WC44 at this frequency. Nevertheless, the characteristics of these two samples are representative of all the Se-Te samples measured in this work. More specifically, 10 out of 16 samples showed characteristics similar to those of WC61, while the remaining six had curves resembling those of WC44.

It is important to note at this point, that the R_p -V characteristics were seen to be relatively free of the type of the singularities exhibited by the C_p characteristics, discussed previously. In particular, no singularity in the R_p -V characteristics was observed between 0.2 and 0.3 volt for samples WC44 and 61, even though their C_p -V curves showed a pronounced minimum at these voltages. This was the case for all the samples studied.

5.2.4 Current Density versus Voltage Characteristics

Figs. 5.11, 5.12 and 5.13 show plots of current density j , against voltage V , for some of the Se-Te diodes in this work. Fig. 5.11 shows how the j - V curves compare with each other for all the samples made with doped selenium. It is seen in the figure that there is, in general, some consistency from sample to sample (more so than previous workers). In fact, it is seen in Fig. 5.11 that about 80% of the samples show characteristics with an excellent forward-to-reverse rectification ratio of around four to five and a half orders of magnitude at 1 volt. Furthermore, all but two of the samples have forward curves that show ideality factors between 1.0 and 1.1 at voltages from 0.1 to 0.2 volt. (The ideality factor is defined assuming a dependence of the form $j = j_0 \exp[qV/(nkT)]$, where n is the ideality factor and the remaining quantities are as defined in chapter 2.) It was observed in this work that the ideality factor was larger, in general, for samples with larger reverse current densities. Consistency is further observed in that about 80% of the forward curves lie within a range of a factor of three at 1 volt. This range is bounded by the WC45 (top) and WC43 (bottom) forward curves. Moreover, almost 90% of the reverse curves fall within a range covering only one and half orders of magnitude at 1 volt. This range is between the reverse curves of WC37 (top) and WC44 (bottom). The characteristics for WC36, on the other hand, are somewhat different, in that the sample displays an abnormally low forward current density and an unusually high reverse current density, so that its forward-to-reverse rectification ratio is only one and a half orders of magnitude. Furthermore, the sample has an ideality factor more than two. It should be pointed out, however, that this sample was made in an

atypical manner, in that its selenium layer was deposited by a "quick evaporation" technique, which is described earlier in section 4.4.

Fig.5.12 displays the j - V curves for two diodes, areas 2 and 3, of sample WC39 on log-linear scales. Despite a difference in the selenium thickness of some 60% between the areas, the characteristics for the two diodes are seen to be almost identical. The forward-to-reverse rectification ratio for both diodes is seen to be some five orders of magnitude at 1 volt. Both forward curves also have essentially equal ideality factors near unity for voltages between 0.1 and 0.2 volt. An unusual feature of this sample is an inflection in the forward characteristic at about 0.8 volt, which implies a minimum in the incremental resistance at this voltage. No such minimum was observed, however, in the R_p - V measurements (not shown). The forward characteristics are shown again, each on log-log scales in the two insets, where a steep dependence on voltage is apparent. More specifically, if a dependence of the form $j \propto V^p$ is assumed, then p is found to be between 3 and 4.

The forward and reverse j - V characteristics for WC44 and WC46 are shown in Fig.5.13 on log-linear scales. Sample WC44 was made with selenium doped with 60 ppm $C\ell$ and its characteristic is representative of most of the Se- $T\ell$ samples in this work. WC46 on the other hand, was made with undoped selenium. It is seen that, while both the forward current densities have almost equal values at 1 volt, the samples display, otherwise, very different characteristics. Firstly, the forward j -values for WC46 are seen to be substantially higher than those for WC44 for voltages below about 0.9 volt. Furthermore, the straight line region of the forward curves between 0.1 and 0.2 volt gives an ideality factor of about 1.0 for WC44 and 1.3 for WC46. It is also seen that the reverse curve for WC46 is some two orders of

magnitude larger than that for WC44. Hence, the forward-to-reverse rectification ratio is only about three orders of magnitude for WC46 at 1 volt, while it is about five and a half orders for the WC44 characteristic. The forward characteristics alone are shown again on two log-log scales in the insets. From these, it is found that the WC44 curve is similar to that of sample WC39. In contrast, the curve for WC46 is in general not so steep, and is not straight. Interestingly, however, the WC46 curve tends toward a linear dependency ($p=1$) as the bias climbs to 1 volt. Even though these curves on log-log scales are different from each other, they are nevertheless, representative of all the Se-Tl samples in this work. In fact, 11 out of 18 samples had forward $\log(j)$ - $\log(V)$ curves similar to that of WC44, while the remaining 7 had curves resembling that of WC46.

Like the R_p - V characteristics described earlier, the j - V curves did not appear to show any strong singularities that correspond to those observed in the capacitance characteristics. For example, the forward j - V curves of WC39 in Fig.5.12 do not show any anomalies at 0.2 volt in the forward direction, while the C_p - V characteristics for this sample exhibit a pronounced minimum here, as shown in Figs. 5.1 and 5.2. It is seen in these figures that an inflection occurs in the forward j - V curves for this sample at about the same voltage that the 20 Hz C_p - V curves turn negative. However, such an apparent correlation was not seen in virtually any of the other samples.

5.3 Aging Effects on the Electrical Characteristics

It was demonstrated in the previous section that while the Se-Tl samples in this work had

prominent singularities in their C_p plots, their other characteristics were quite well behaved. However, this applied entirely to electrical measurements made on day-0. This section now presents results on the aging of the structures with storage time, where the electrical characteristics were measured at different times for several samples stored in air. In this work, the history of two samples, WC38 and WC45, was followed which, initially did not show negative C_p values. The history of samples which did show negative values initially, is not presented here. However, their histories were, nevertheless, similar, except their characteristics appeared to be advanced by several days. The results of some material analysis studies on the Se/Tl interface are also presented here.

5.3.1 C_p versus Voltage Characteristics at Different Times

As was mentioned previously in section 5.2.1, two of the Se-Tl samples showed no negative C_p values on day-0. These were samples WC38 and WC45. Figs. 5.14 and 5.16 display respectively their C_p -V characteristics. Though the curves in these plots are seen to be entirely in the positive C_p domain, they are not without singularities. At least one minimum is observed in each of the curves for frequencies between 20 Hz and 10 kHz. It is usual, however, for such minima to be present in the day-0 characteristics, as was discussed in section 5.2.1. What is uncommon in this work, is that these curves are entirely positive.

In Fig.5.15, the C_p -V characteristics are shown for sample WC38, on day-375, meaning that the measurements were made 375 days after the thallium film was deposited and the

sample fabrication completed. Comparing these curves with the day-0 curves in Fig.5.14, it is clear that the characteristics for WC38 changed dramatically with time. The most striking difference between the two figures is in the 20, 100 and 1000 Hz curves. These curves on day-375 are seen to show strong negative C_p values in the forward bias region, while the day-0 curves actually show strong positive C_p values at the same voltages. It is also seen in Fig.5.15 that the 10 kHz curve has essentially no minimum, while that in Fig.5.14 does have a minimum. The 20, 100 and 1000 Hz curves on day-375 show a minimum located between 0.4 and 0.5 volt in the forward direction. However, these curves for day-0 have their minimum between 0.2 and 0.3 volt. Interesting also, is that the 1 MHz curve for day-375 shows a broad minimum at 0.2 volt, while the day-0 counterpart displays none. It is clear that the electrical characteristics for this sample have changed over time, and that negative C_p values have emerged as the sample has aged.

A more complete study of the effects of aging on C_p -V characteristics is now presented for sample WC45. Figs. 5.16 to 5.21 display the C_p versus voltage plots for this sample at six different times from day-0 to day-101. It is apparent from these figures that the curves in the forward direction change considerably over time, whereas, in the reverse direction there is relatively little variation from day to day. From Figs. 5.16 to 5.18, it is observed that the presence of negative C_p values grows in the first ten days after fabrication. The day-0 curves in Fig.5.16 are seen to be entirely in the positive C_p domain. In Fig.5.17, however, the day-2 curves for 20 and 100 Hz show a narrow region of negative C_p values around 0.3 volt, where there is a pronounced minimum. As is seen in Fig.5.18, after 10 days the sample shows very prominent negative C_p values for the 20 and 100 Hz curves from 0.2 up to at least 1.0 volt

in the forward direction. Even the 1 kHz curve dips to negative C_p values at around 0.4 volt. In Figs. 5.19 to 5.21, a change in the trend is seen, whereby the negative C_p effect declines with time from day-10 to day-101. Though the day-21 curves for 20 and 100 Hz in Fig. 5.19 are still strongly negative beyond 0.2 volt, they do not have negative values as large as those for day-10. Moreover, the 1 kHz curve does not show any negative values at all from day-21 onwards. The day-46 curve for 20 Hz in Fig. 5.20 has, in general, even smaller negative values than for day-21. Furthermore, while the 100 Hz curve for day-21 is negative at forward voltages above 0.2 volt, that for day-46 is negative for bias values only above 0.7 volt. By day-101 the 20 Hz curve, as shown in Fig. 5.21, actually displays oscillations between positive and negative values in the forward direction; this exhibits yet a further overall decline in the negative C_p effect. This oscillation is especially interesting, in that it seems to be more apparent for day-46 and day-101, when the sample is older. Note that the day-101 20 Hz curve apparently has at least two minima, one at 0.1 volt and the other at 0.3 volt. The minimum at 0.1 volt was not observed at any earlier storage time for this sample, nor for any other Se-Te sample in this work. It is of further interest to note that the day-2 plot for WC45 has a strong resemblance to the day-0 plot for WC61 in Fig. 5.4. Among other similarities, both sets of curves show a very sharp minimum at 0.3 volt in the forward direction for 20 and 100 Hz. Furthermore, both show a second minimum in the 20 Hz curve at about 0.8 volt. Two other plots showing interesting likenesses are those for WC38 on day-375 and WC45 on day-10 in Figs. 5.15 and 5.18 respectively. Their resemblances include the fact that they both display very strong negative C_p values in the forward direction for the 20 and 100 Hz curves. Furthermore, the two plots have 1 kHz curves that dip into the negative

C_p domain around half a volt in the forward direction.

5.3.2 C_p versus Frequency Characteristics at Different Times

The C_p -frequency plots for sample WC38 on day-0 and day-375 are displayed in Figs. 5.22 and 5.23 respectively. It is seen that there are considerable differences between the figures, especially for the 0.5 and 1 volt forward curves at frequencies lower than 10^4 Hz. These curves on day-0 are entirely positive and decrease monotonically with increase in frequency. On the other hand, on day-375 they display prominent negative C_p values at frequencies less than about 10^3 Hz, and also, show a rise with frequency between 10^3 and 10^4 Hz. However, despite these differences, the figures still display some similarities to each other. For instance, the curves in each are seen to converge together at higher frequencies near 10^6 Hz. Another likeness is that the -1 volt (reverse) and 0 volt curves for both times decrease very gradually with frequency between 10^3 and about 10^4 Hz. They then fall off more rapidly at higher frequencies. It is of interest to note that the day-375 characteristics resemble those presented previously in section 5.2.2 for samples WC40, 44 and 46 in Figs. 5.5, 5.6 and 5.7 respectively. Thus, the day-375 curves are not out of the ordinary. However, since the day-0 curves for WC38 do not show any negative C_p values, nor any increase with increase of frequency, these curves are considered unusual for this work.

5.3.3 R_p versus Voltage Characteristics at Different Times

The R_p versus voltage plots are shown for sample WC38 on day-0 and day-375 in Fig 5.24 and for WC45 on day-0 and day-101 in Fig.5.25. It is seen that these characteristics are quite similar to those already presented in section 5.2.3 and therefore are not out of the ordinary. It is also seen that the characteristics change somewhat with time for each sample. The resistance values for WC38 are observed to decrease slightly from day-0 to day-375 at all the biases indicated. Those for WC45 show a decrease with time for the reverse voltages but an increase with time for the forward voltages. It is also seen that the day-0 curves for WC45 show a minimum at 0.5 volt, whereas the day-101 curves show no minimum. Furthermore, the day-0 curves show a stronger tendency to converge together in the forward region than do the day-101 curves. It is important to note that, while the samples show changes in their R_p -V characteristics over time, they still do not show any pronounced singularities. This is despite the emergence of negative C_p values and sharp minima in the C_p characteristics of these samples over the same time period, as shown in Figs. 5.14 to 5.21.

5.3.4 j versus Voltage Characteristics at Different Times

In Fig.5.26 the forward and reverse j -V characteristics for sample WC45 are shown at six different times from day-0 to day-101. It is seen, in general, that the forward j values decrease with storage time, while the reverse curves show an overall increase with time. This results in a reduction of the 1 volt forward to reverse rectification ratio from about 5

orders of magnitude on day-0 to about 3 orders of magnitude on day-101. Over this same period, the forward ideality factor evaluated between 0.1 and 0.2 volt increases from about 1.2 to 1.7. It is important to note here that, like the R_p -V characteristics, all of these curves are quite well behaved. The C_p characteristics for this sample, on the other hand, show the development of considerable singularities and negative C_p values over the same time period.

5.3.5 Mott-Schottky Plots at Different Storage Times

The Mott-Schottky plots $((A/C_p)^2$ versus voltage, where A is the diode area) for sample WC45 on day-0 and day-101 are shown in Figs. 5.27 and 5.28 respectively. It is clear from these two figures that changes occurred in the reverse voltage region over the 101 day period. Firstly, it is seen that the extrapolated intercept values on the voltage axis changed with storage time. The 20 and 100 Hz curves show a decline in this value from 0.55 volt on day-0 to around 0.36 volt on day-101. The 1 kHz intercept also shows a decrease with time, though somewhat smaller, from 0.58 volt to 0.48 volt. The 10 and 100 kHz curves show intercepts that have actually risen with time, from 0.58 and 0.64 volt respectively on day-0, to 0.65 and 0.90 volt respectively on day-101. It is also seen that the intercepts for the different frequencies on day-0 are relatively close together, within 0.1 volt of each other, while those for day-101 are more spread out, covering a 0.55 volt range. Note, however, that both figures display a rise in intercept value with frequency. Another variation is an increase in the average slope by about a factor of two over the 101 day storage period. Furthermore,

the day-0 curves are much closer together than the day-101 curves. The curves for day-0 are within about $2 \times 10^{14} \text{ cm}^4/\text{F}^2$ of each other, while those for day-101 are spread over a range about 8 times larger. Note, however, that in each figure, the highest curve is that for 100 kHz, while the lowest is that for 20 Hz. In summary then, it is seen from these figures that the intercept values decrease with storage time for the 20, 100 and 1000 Hz curves, they increase with time for the 10 and 100 kHz curves, and the slopes of the straight line portions of the curves increase over the 101 day period.

5.3.6 Material Analysis Studies

In this part of the study, several samples were examined by x-ray diffraction (XRD) analysis and by scanning electron microscopy (SEM). This study was made to get a better understanding of the Se/Tl interface and to attempt to correlate the findings with the electrical characteristics.

In Fig.5.29, XRD scans are shown for sample WC61 on day-1 and day-10. From these, it is seen that the semiconducting compound TlSe is present on day-10, where all of the expected TlSe peaks are present. However, no peaks for this compound are detectable on day-1. It is also seen that the presence of Tl metal is very weak, in that there is only one peak for Tl present on day-1 and no peaks at all for day-10. Both scans, however, show peaks for Se, though they are not as prominent in the day-10 scan as they are for day-1. Several peaks for Tl_2CO_3 are also observed in both scans. This compound forms as a result of a reaction between the Tl and the atmosphere, as was reported previously [2] [12]. More

extensive results confirming its formation with storage time are shown in Fig.5.30. This figure shows two XRD scans of a Tl film deposited on a glass slide; one scan when the film was fresh; the other, after about six months of storage time in air. The vertical line segments indicate where Tl and Tl_2CO_3 peaks are expected. It is seen that the day-0 scan displays a strong presence of Tl, but no clear peaks for the carbonate. On the other hand, the day-200 scan shows no sign of Tl but a very strong presence of Tl_2CO_3 . Thus, it is clear from these studies that the Tl films in this work were converted into TlSe (a semiconductor) and Tl_2CO_3 (an insulator) with storage time. In both of these XRD figures there are some peaks which remain unexplained. However, their analysis is beyond the focus of this work and is left to be studied at a later date.

SEM photographs of the cross-section of two samples, WC49 and WC54, are shown in Fig.5.31 for day-0. The photographs are of the back-scattered electron image and show different layers of material in each sample as identified by x-ray fluorescence analysis (see appendix). It is seen that the Tl, Se and Bi layers are very well defined for WC54. While these layers are also present for WC49, there appears to be an extra layer between those for Tl and Se. From x-ray fluorescence analysis (see appendix), this intermediate layer is found to be a mixture of Se and Tl, possibly TlSe. Thus, it seems that some Tl has diffused into the Se layer. Shown also in this figure, are the 100 Hz C_p -V curves for both samples on day-0. It is of interest to note at this point, that the curve for WC49 shows negative C_p values, while the values for WC54 remain entirely positive, suggesting that the negative C_p effect is associated with the diffusion of the Tl. The 20 Hz curves (not shown) for the two samples are somewhat more complex, but nevertheless, confirm the overall

trend. Another interesting observation is that the diffusion of Tl into the Se appears to have been much faster for WC49 than for WC54, despite the fact that the fabrication parameters were nominally the same for the two samples. Thus, it would seem that the Tl diffuses more readily in some samples than in others. It was also observed from SEM studies of samples at different storage times, that the extent of the Tl diffusion changes very little with storage time after fabrication, suggesting that the greater part of the diffusion took place during the fabrication process.

5.4 Discussion

The most interesting result in this chapter was the observation of negative capacitance in Se-Tl structures in the forward direction at low frequencies. This occurred for the most part at the capacitance minimum near 0.2 volt. At this voltage, however, no singularity was observed in the j -V or R_p -V characteristics. While most of the freshly made samples showed the negative capacitances, there were two exceptions, which had capacitance characteristics that were entirely positive. These samples were therefore labeled as "unusual" but after storage in air these samples too showed negative capacitance.

While inductive behaviour can arise in Schottky junctions due to high level injection, as explained in chapter 2, the aging experiments reported on in this chapter suggest that in the present samples, the negative capacitance arose from the formation of the semiconductor TlSe at the Tl/Se interface. This compound resulted from the diffusion of the thallium into the selenium. Thus, the aging process could be as follows. At the beginning the device was

a Schottky junction between the thallium and the selenium - this is provided that, in the thallium deposition step, the sample temperature was not allowed to rise too much, otherwise extensive diffusion would take place before the sample was removed from the deposition chamber. In any case, with storage time, thallium diffused into the selenium and TlSe was formed in a very thin n-type layer. Because this layer was initially smaller than a carrier diffusion length, high level injection occurred with forward bias, which gave rise to inductive behaviour. This inductive or negative capacitance effect became stronger as the TlSe layer grew thicker. However, when the thickness exceeded a diffusion length, the high level injection effect was reduced because of the greater volume of TlSe semiconductor and hence the negative capacitance effect decreased. These stages correspond to what was actually observed with storage time for sample WC45. While the aging was followed in detail for only one sample which had purely positive capacitance when freshly made, the changes with time were similar to those of other samples except that with these the aging was more advanced. It is therefore postulated for most of the samples that much of the aging or formation of TlSe had already started during the fabrication process.

While much work was done previously on Se-Tl diodes, negative capacitance was not specifically reported, although a rise of capacitance with frequency was reported by Pan [2]. Such a rise with frequency, which was also observed in this work, could only come about if there was an inductive component in the reactance [13]. The reason for not seeing the negative capacitance values in previous work was partly due to the fact that the lowest measurement frequency was only 100 Hz, whereas in the present work it was 20 Hz. However, this is not enough to explain the difference, since some samples in the present

work showed negative values at frequencies as high as 1 kHz. Thus, there must have been a difference in the fabrication conditions between the present and past work.

Storage in air also had some interesting effects on the current-density versus voltage characteristics. The forward current-density decreased monotonically with storage time for sample WC45 in a similar manner to that reported by Pan [2]. Pan attributed this decrease to the conversion of the Tl counterelectrode to Tl_2CO_3 , an insulator, which resulted in an overall increase in the resistance of the device. While this carbonate was also observed in several samples of the present work, it is not likely to have formed in sample WC45, since its counterelectrode was completely covered by a protective indium layer. Chan [3], on the other hand, suggested that the decrease in forward current-density was due to the formation of TlSe at the Tl/Se interface, which resulted in an n-type TlSe/p-type Se heterostructure. Thus, the forward current-density decreased because the n-type TlSe had far fewer carriers than Tl metal. The ideality factor and the reverse current density also changed with storage time, in that, they both increased. It is suggested that this effect was also due to the formation of the TlSe layer. The lattice mismatch between the TlSe and the Se [14] resulted in a high density of recombination traps at the interface. As the TlSe grew, the effect of recombination resulted in an increase of the ideality factor and the reverse current-density [9] [10]. The emergence of this recombination may also have contributed to the decline in the negative capacitance effect, as mentioned earlier, since injection of carriers into the TlSe would have been lowered as well.

Chan [3] also suggested that the formation of this TlSe layer had an effect on the Mott-Schottky plots. In this case, he stated that the depletion region extended into the newly

formed TlSe layer, where there was a carrier concentration lower than in the bulk Se. This resulted in Mott-Schottky curves that became steeper as the TlSe layer grew thicker with storage time. In this work, such an effect was also observed in the Mott-Schottky plots for sample WC45.

While there was a large degree of consistency in the j-V characteristics from sample to sample, there were still some notable differences. It is suggested here that these differences were mainly due to different morphologies in the Se layer for each sample. This morphology was determined in part by the deposition rate as well as the doping level in the Se. It is believed from the results of sample WC36 that better rectifiers resulted when they were made with Se films that were deposited at slow rates as opposed to fast rates.

Champness and Pan [15], as well as, Pan himself [2] previously reported a plateau region in the 0 volt C_p -f characteristics for Se-Tl samples at higher frequencies. In this work, however, only a tendency to such a plateau was observed and, even then, only at forward bias voltages. The lack of such a plateau at a 0 volt bias in this work was similar to what was reported by Chan [3]. A circuit model, consisting of a diode in series with a parallel combination of a resistor and capacitor, was proposed by Pan [2] [15] to explain the plateau and if this model is applied here, then the discrepancy seen between the present results and those of Pan may have been due in part to the fact that the incremental resistance at 0 volt for the Se-Tl samples in this study was somewhat lower than in Pan's. A lower resistance would result in a larger cutoff frequency at which the plateau is seen and in this work the plateau may have actually been at a frequency beyond those measured. It is difficult to compare the C_p -f curves for forward bias voltages, however, since Pan's results were

incomplete. In any case, it is expected that a better understanding of these C_p -t characteristics would be obtained from a circuit model similar to that proposed by Pan.

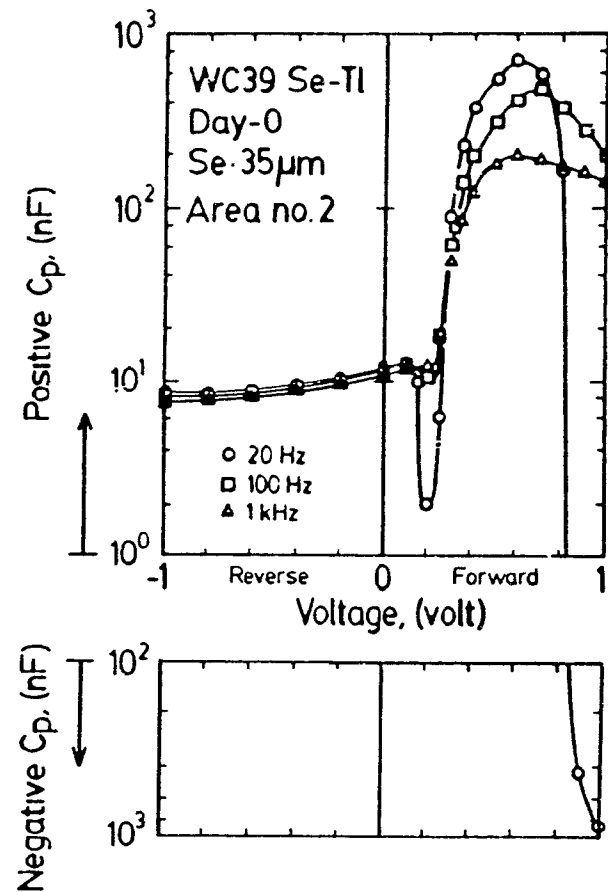


Fig.5.1. Plot of capacitance against voltage for Se-Tl sample WC39 area number 2 for frequencies of 20 Hz, 100 Hz and 1 kHz.

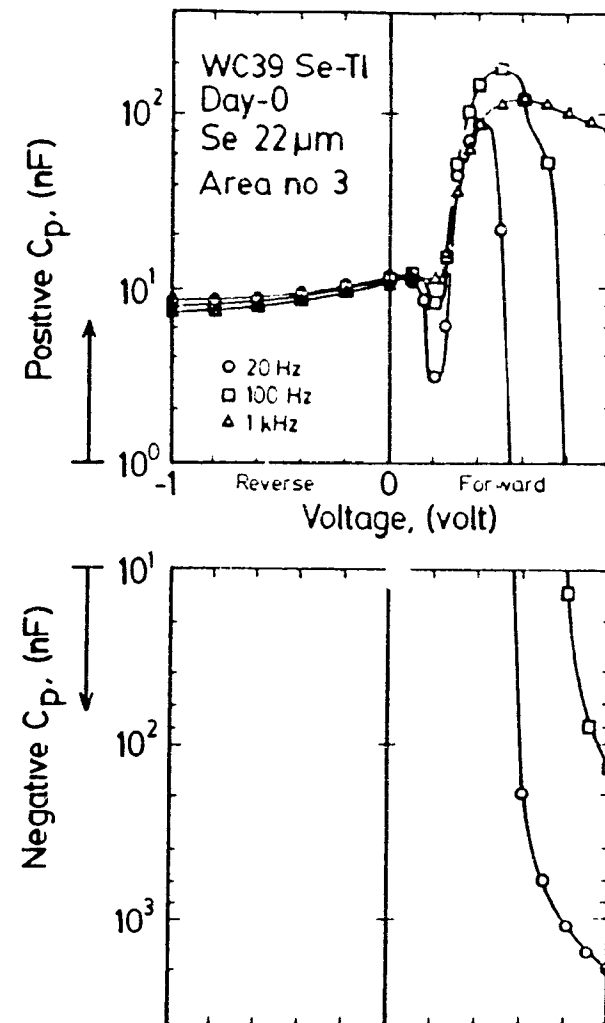


Fig.5.2. Plot of capacitance against voltage for Se-Tl sample WC39 area number 3 for frequencies of 20 Hz, 100 Hz and 1 kHz.

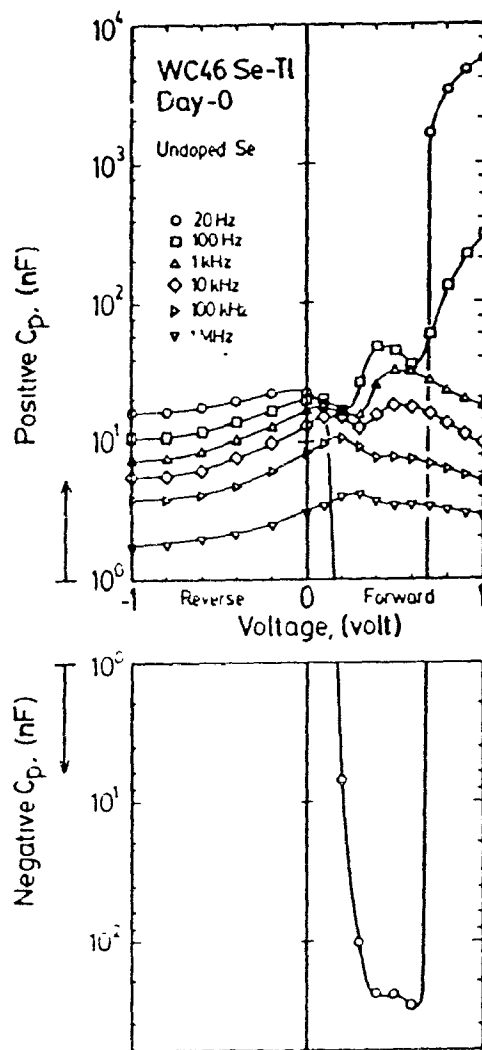


Fig.5.3. Capacitance versus voltage plot for Se-Tl sample WC46 made with undoped Se for frequencies between 20 Hz and 1 MHz.

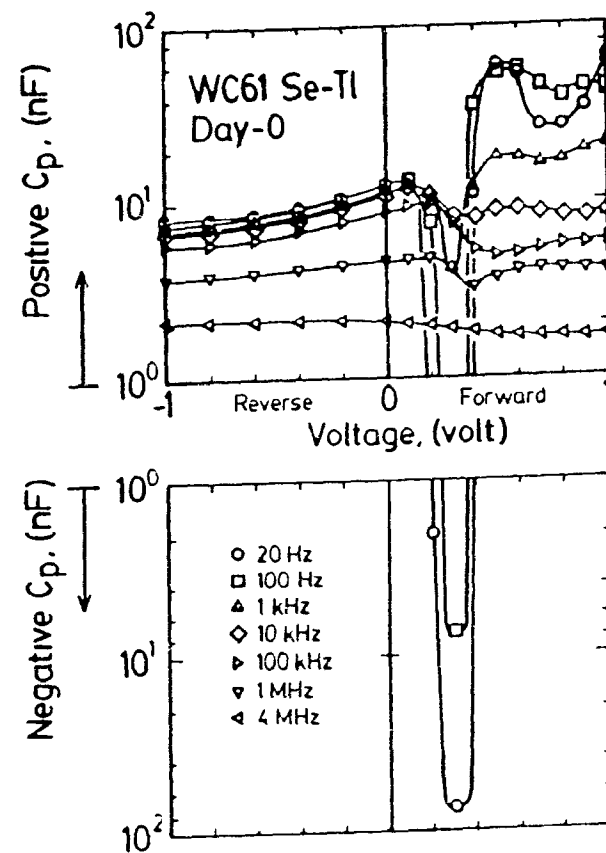


Fig.5.4. Plot of capacitance against bias voltage for Se-Tl sample WC61 at frequencies from 20 Hz to 4 MHz.

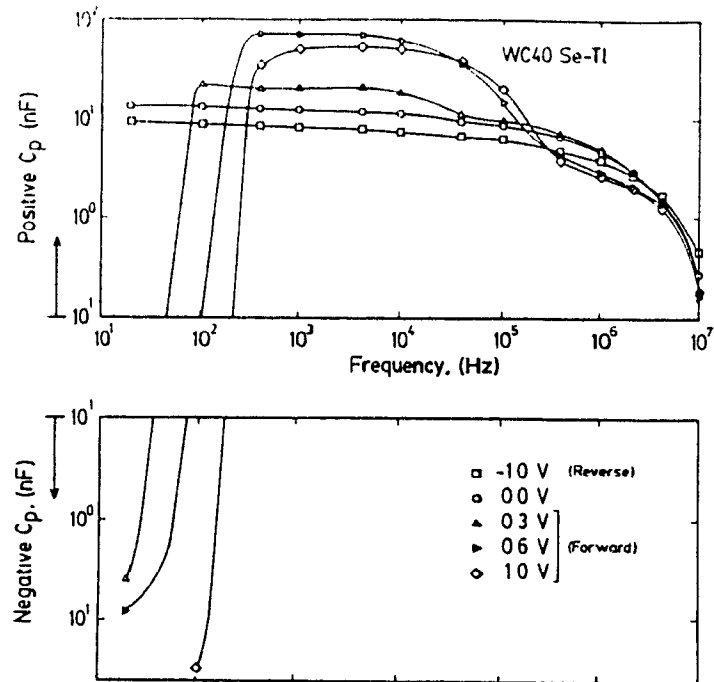


Fig.5.5. Plot of capacitance against frequency for Se-Tl sample WC40 at different bias voltages.

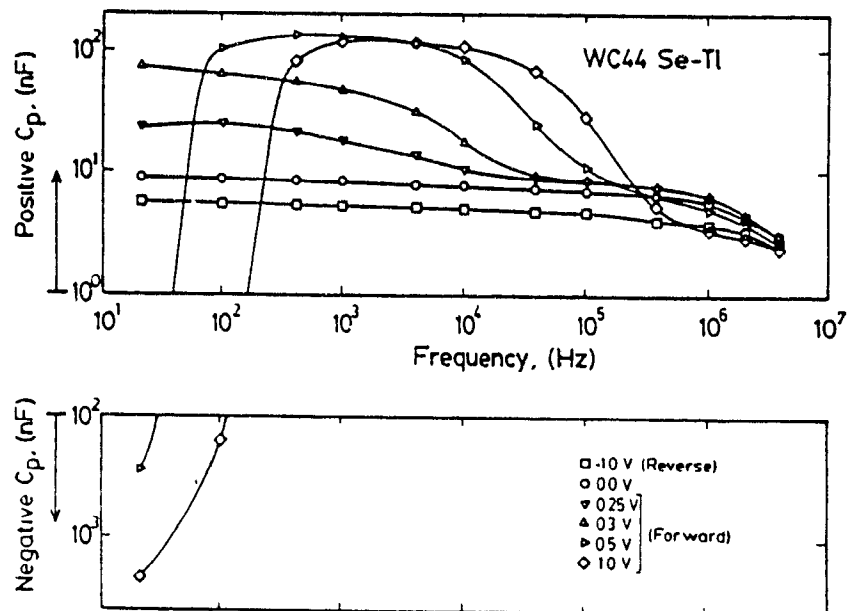


Fig.5.6. Capacitance versus frequency plot for Se-Tl sample WC44 at different bias voltages.

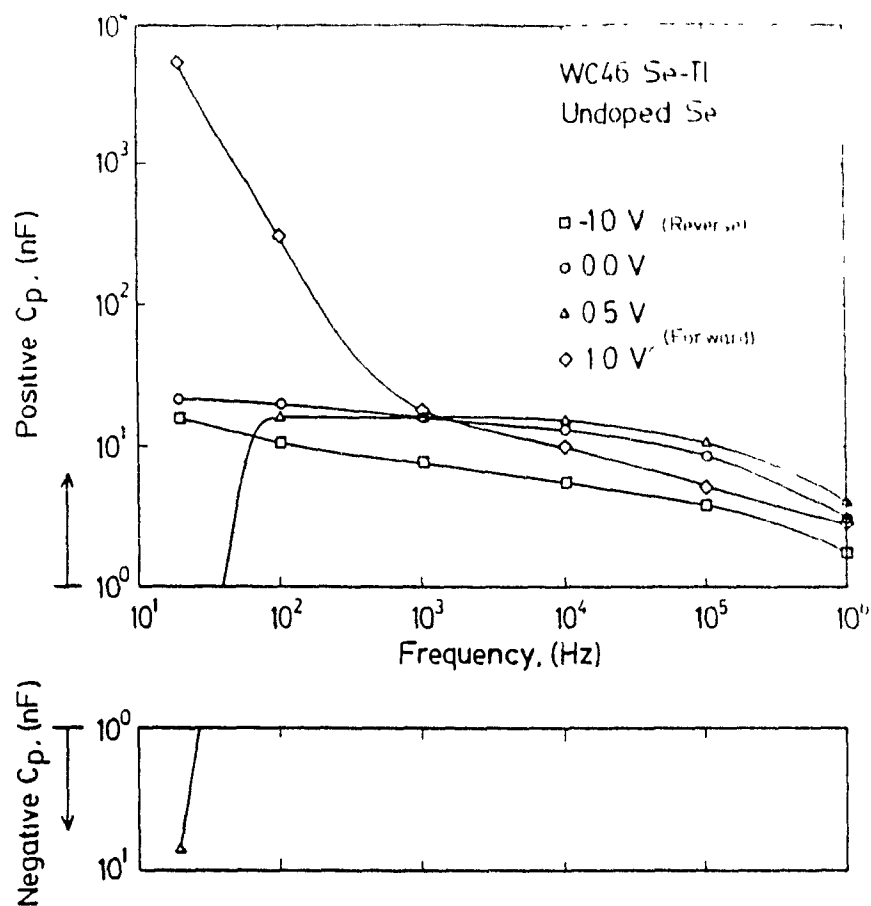


Fig 5.7. Plot of capacitance against frequency for Se-Tl sample WC46 at different bias voltages.

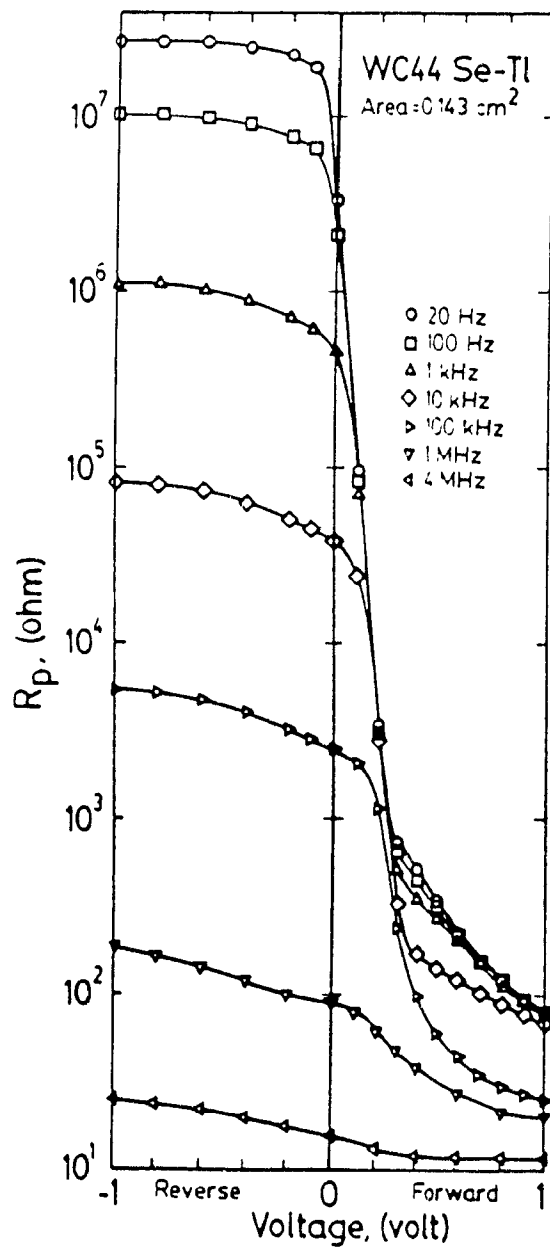


Fig.5.8. Resistance versus voltage plot for Se-Tl sample WC44 at different frequencies.

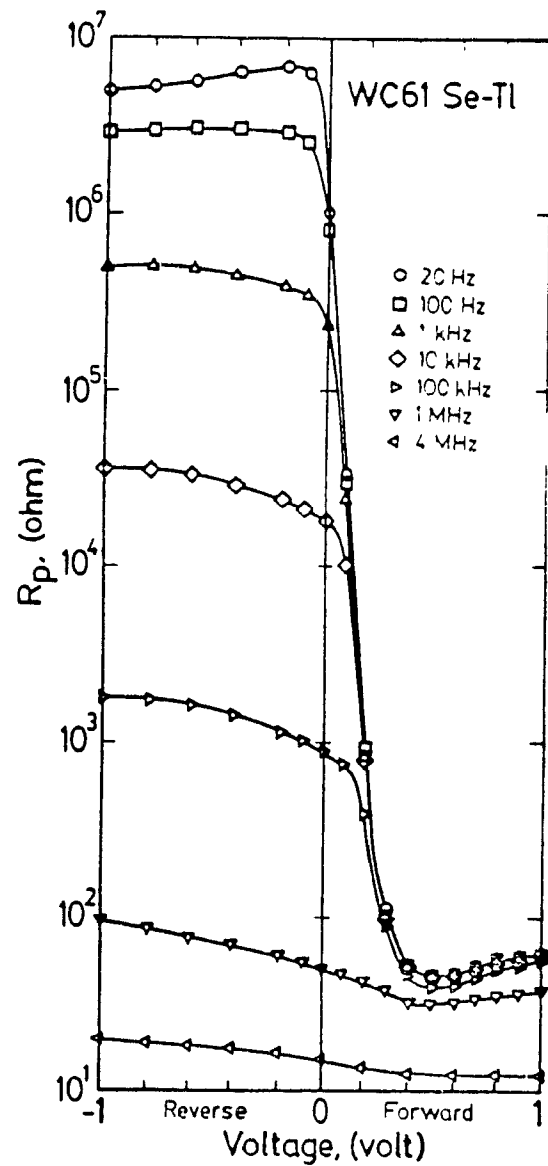


Fig.5.9. Resistance versus voltage plot for Se-Tl sample WC61 at different frequencies.

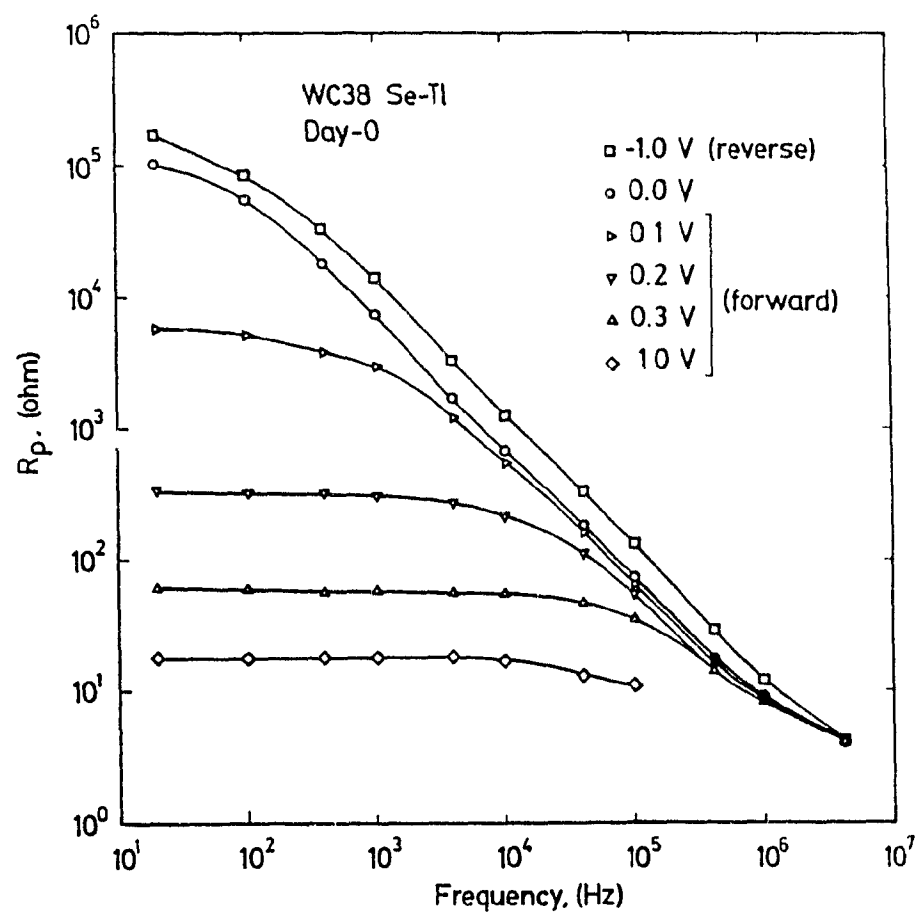


Fig.5.10. Resistance versus frequency plot for Se-Tl sample WC38 at different bias voltages.

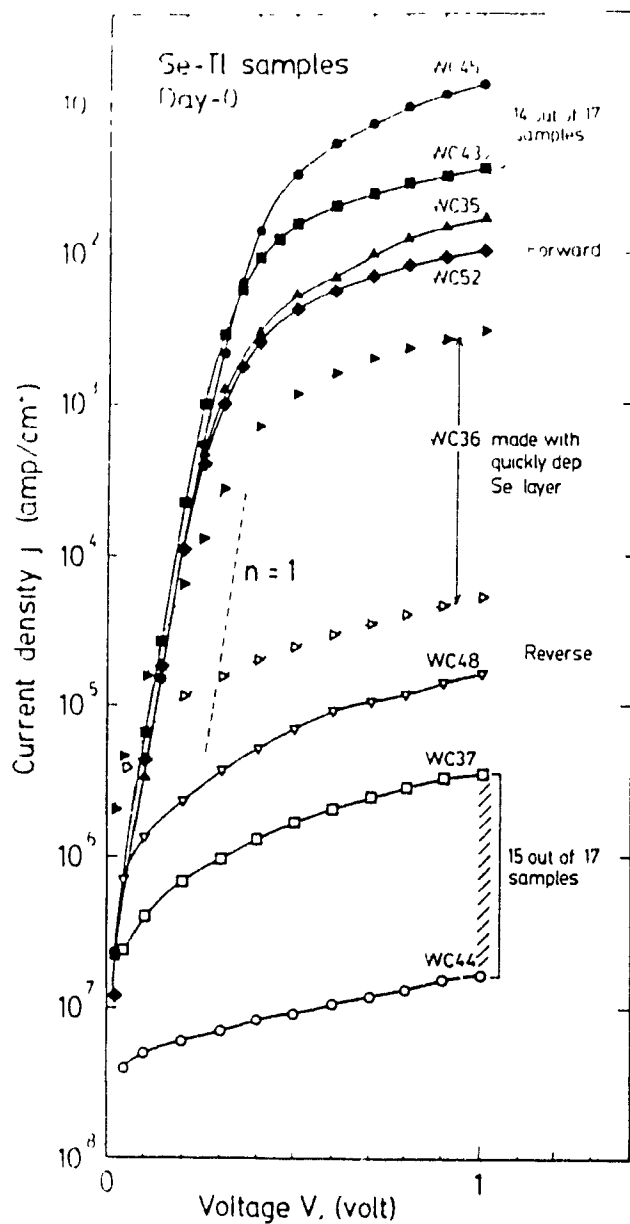


Fig 5.11. Current-density versus voltage plot for many of the Se-Tl samples of this work.

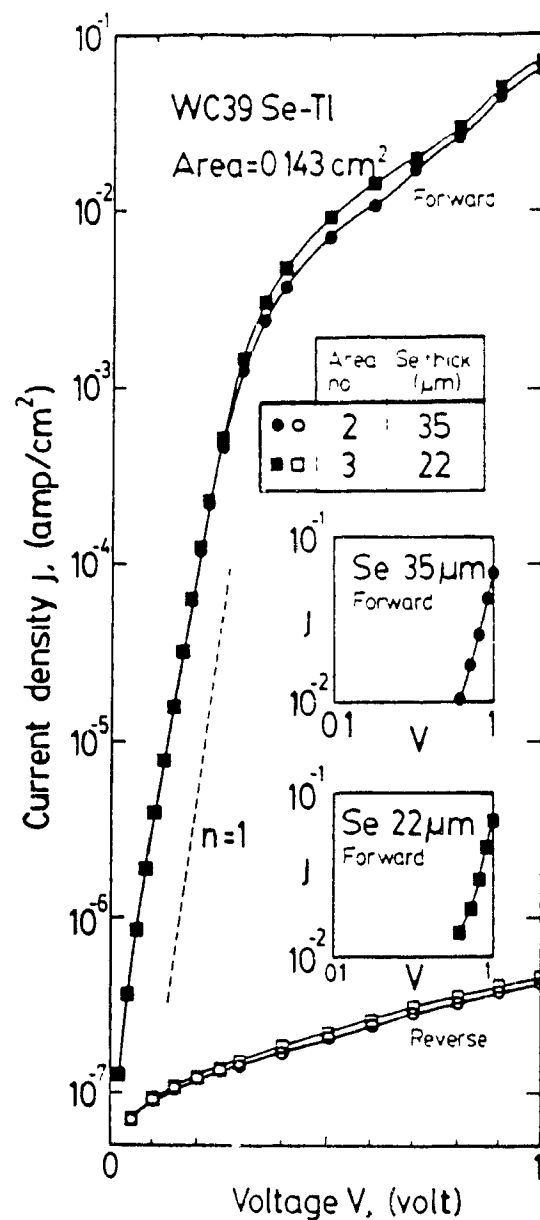


Fig 5.12. Plot of current-density against voltage for Se-Tl sample WC39 areas 2 and 3.

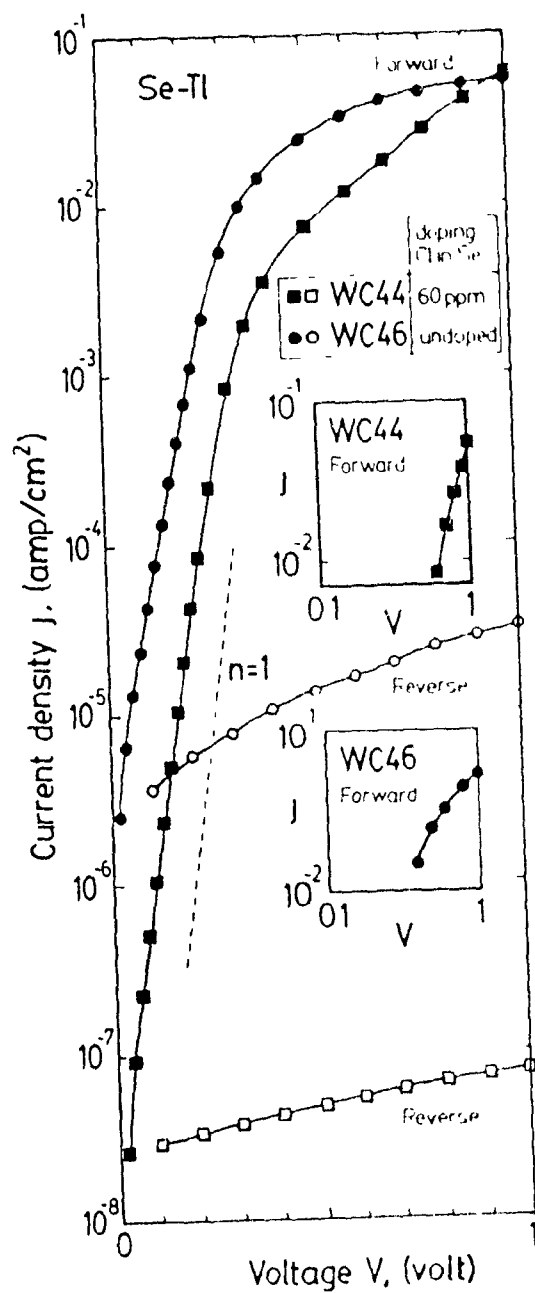


Fig.5.13. Current-density versus voltage plot for Se-Tl samples WC44 and WC46.

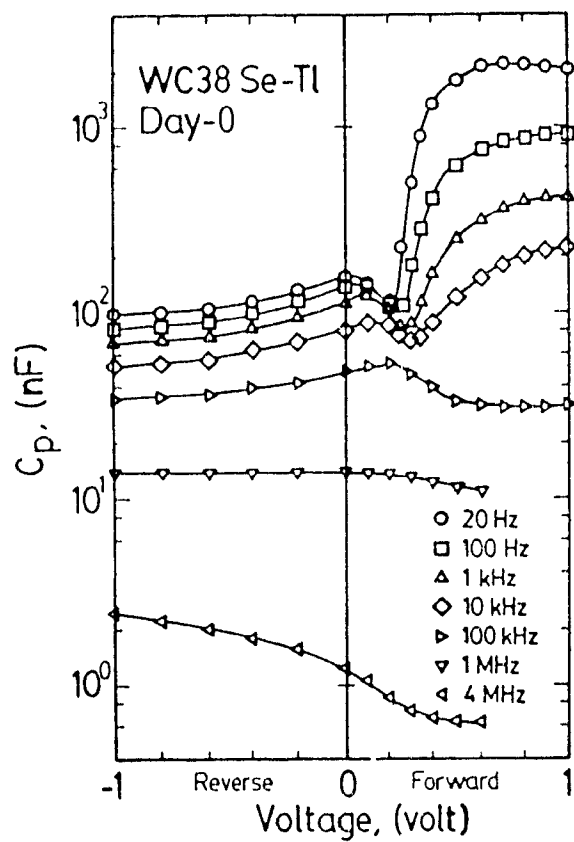


Fig.5.14. Capacitance versus voltage plot for Se-Tl sample WC38 measured on day-0 for different frequencies.

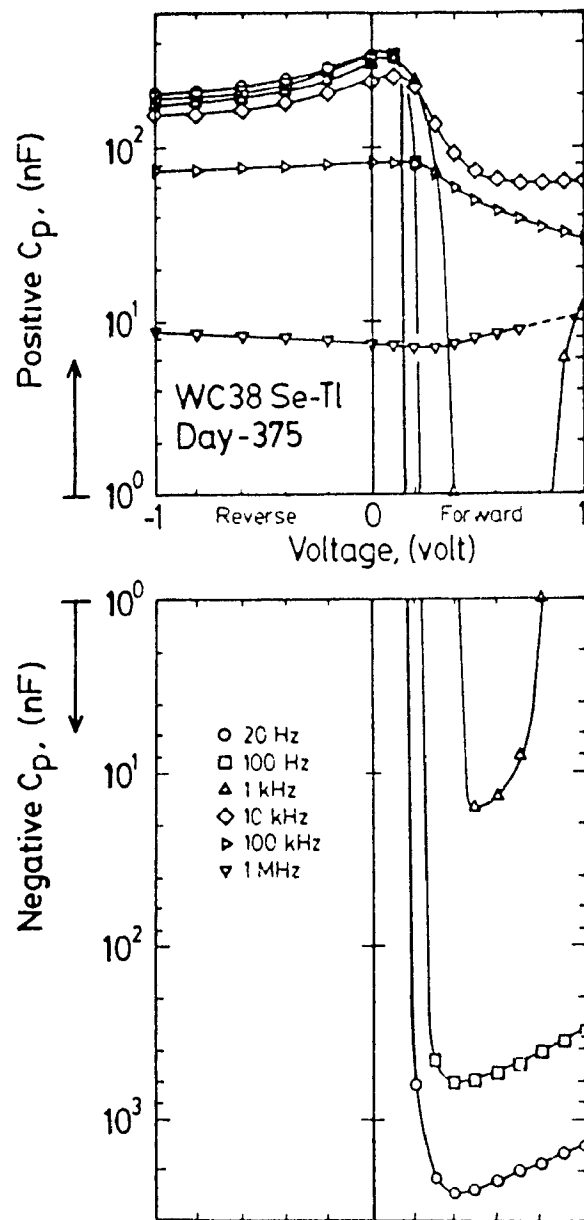


Fig.5.15. Capacitance versus voltage plot for Se-Tl sample WC38 measured on day-375 for different frequencies.

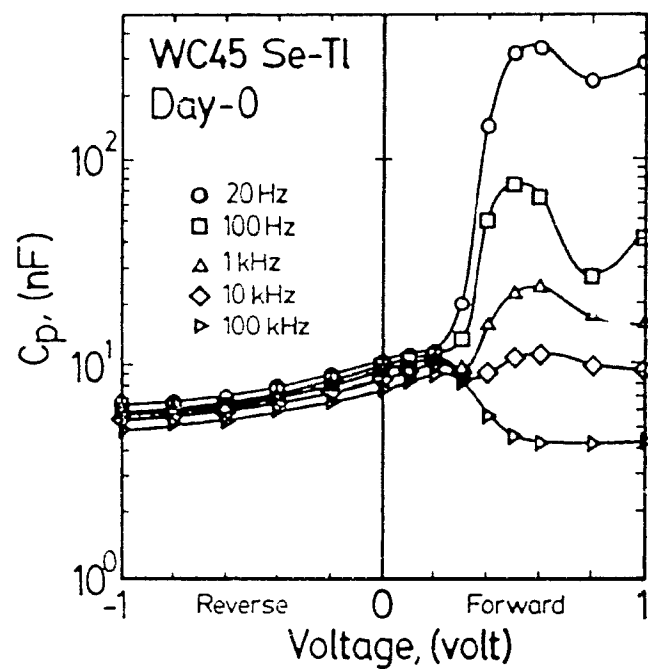


Fig.5.16. Plot of capacitance against voltage for Se-Tl sample WC45 measured on day-0 at different frequencies.

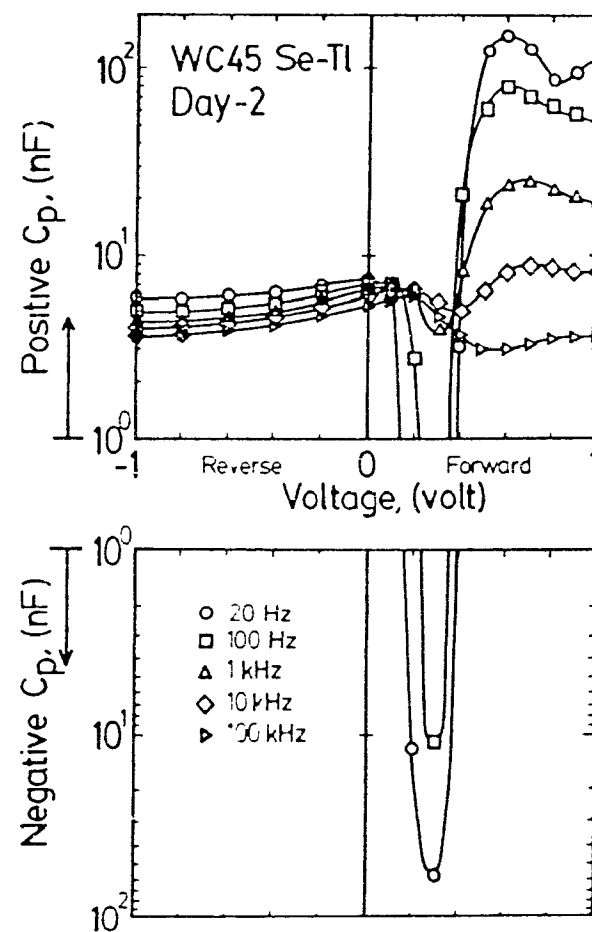


Fig.5.17. Plot of capacitance against voltage for Se-Tl sample WC45 measured on day-2 at different frequencies.

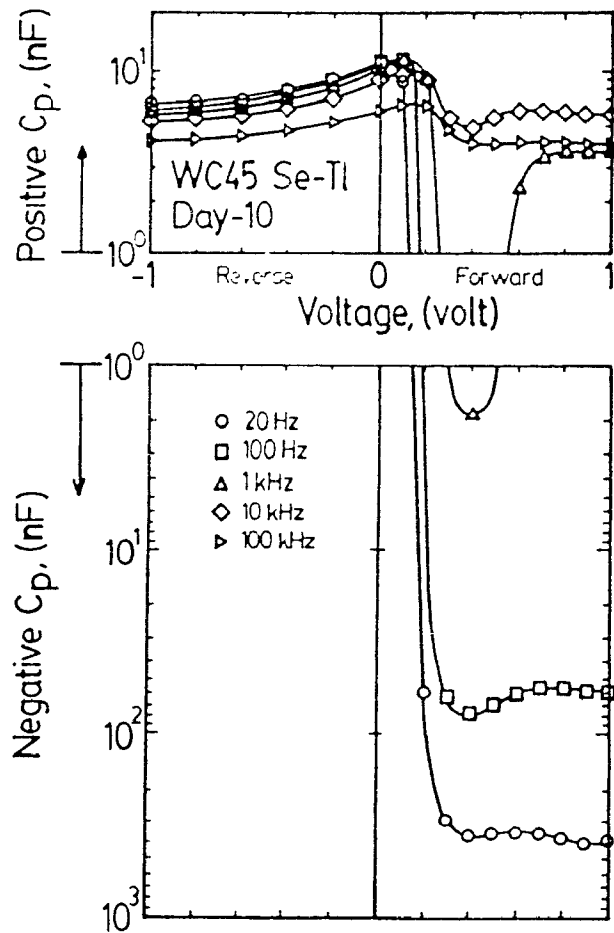


Fig.5.18. Plot of capacitance against voltage for Se-Tl sample WC45 measured on day-10 at different frequencies.

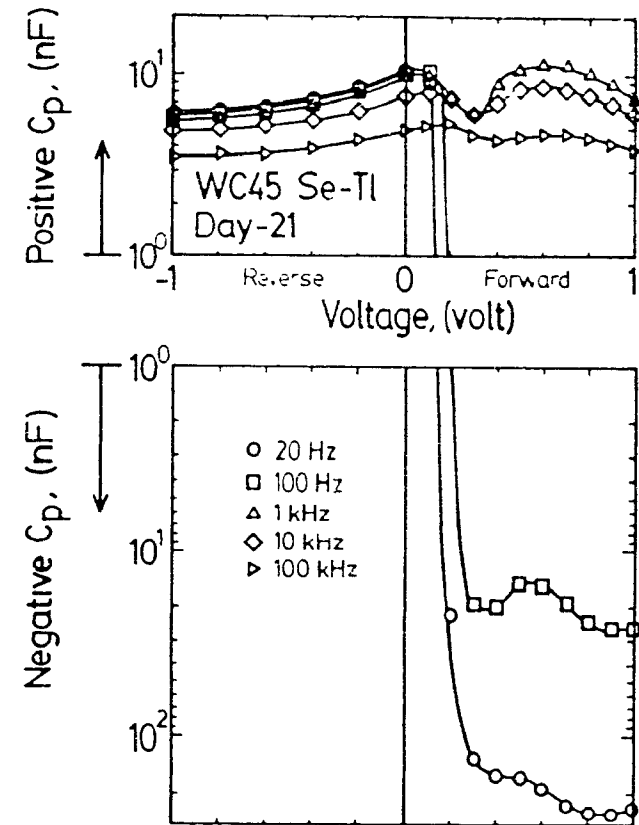


Fig.5.19. Plot of capacitance against voltage for Se-Tl sample WC45 measured on day-21 at different frequencies.

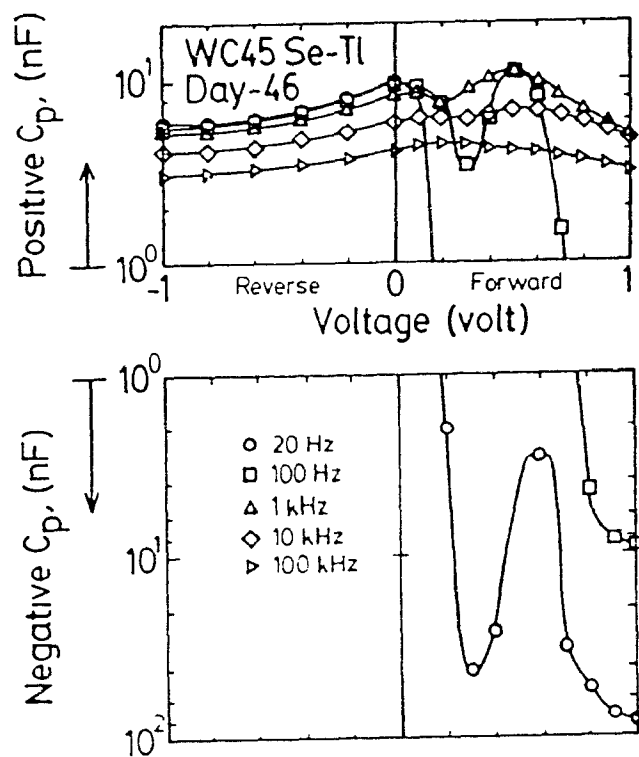


Fig.5.20. Plot of capacitance against voltage for Se-Tl sample WC45 measured on day-46 at different frequencies.

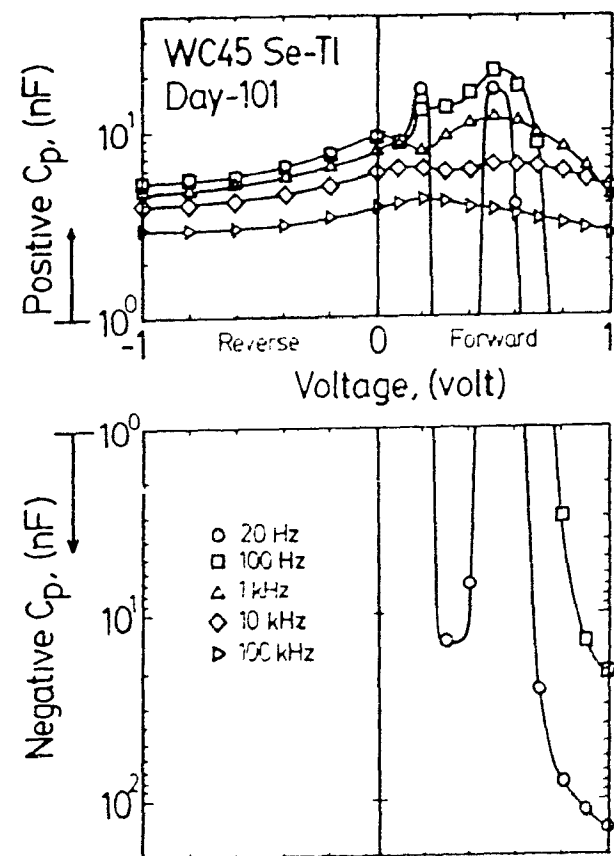


Fig.5.21. Plot of capacitance against voltage for Se-Tl sample WC45 measured on day-101 at different frequencies

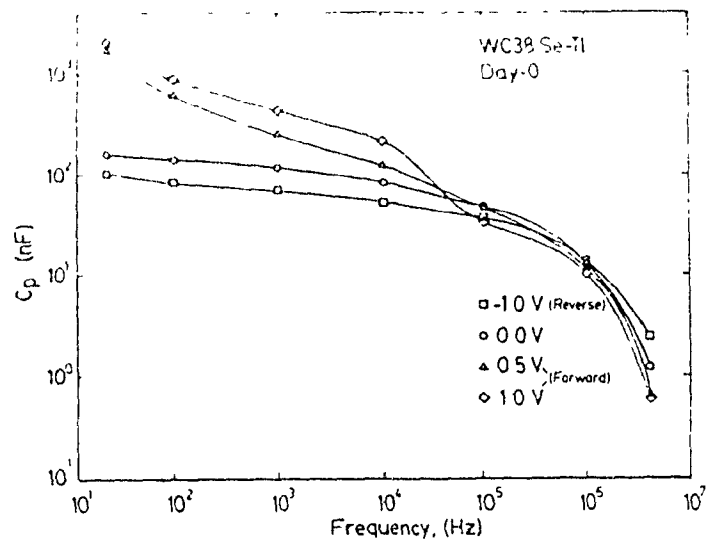


Fig.5.22. Capacitance versus frequency plot for Se-Tl sample WC38 on day-0 for different bias voltages.

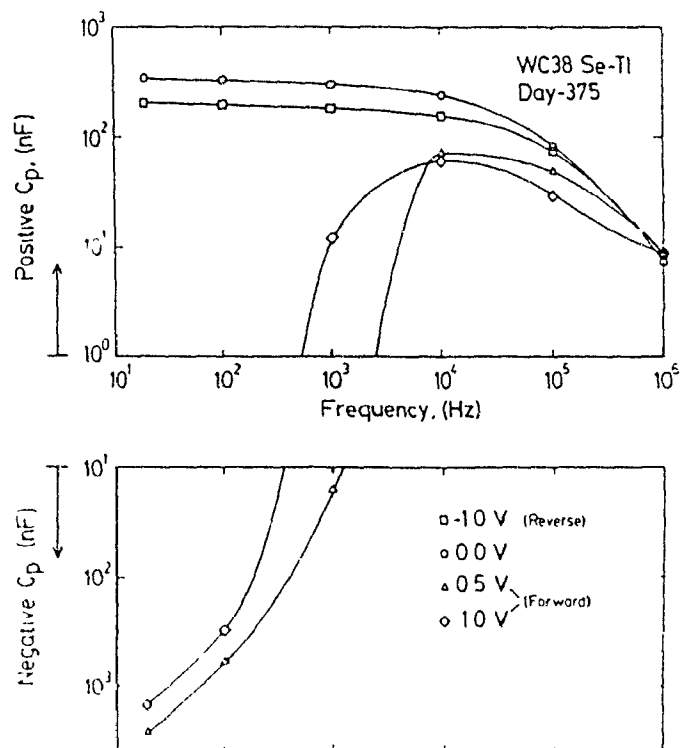


Fig.5.23. Capacitance versus frequency plot for Se-Tl sample WC38 on day-375 for different bias voltages.

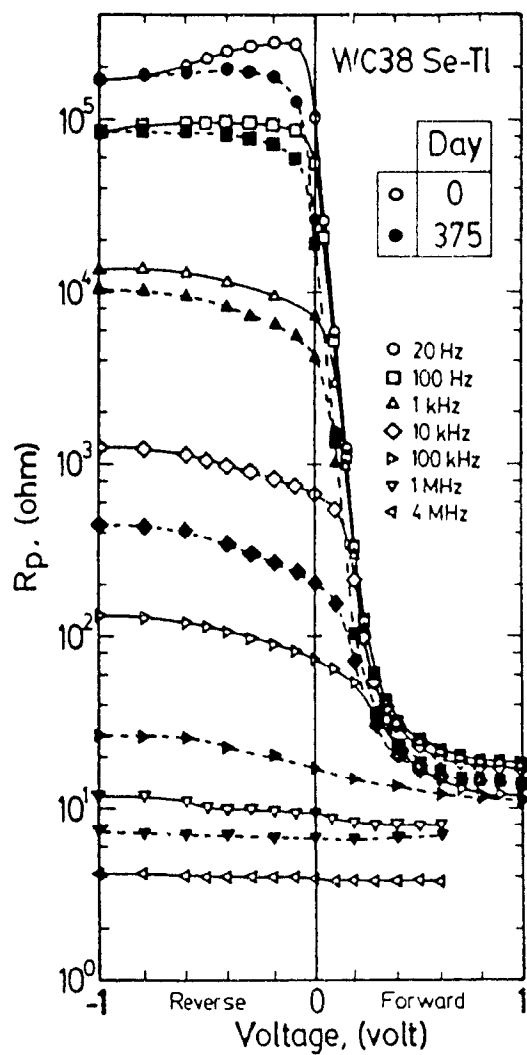


Fig.5.24. Resistance versus voltage plot for Se-Tl sample WC38 on day-0 and day-375 at different frequencies.

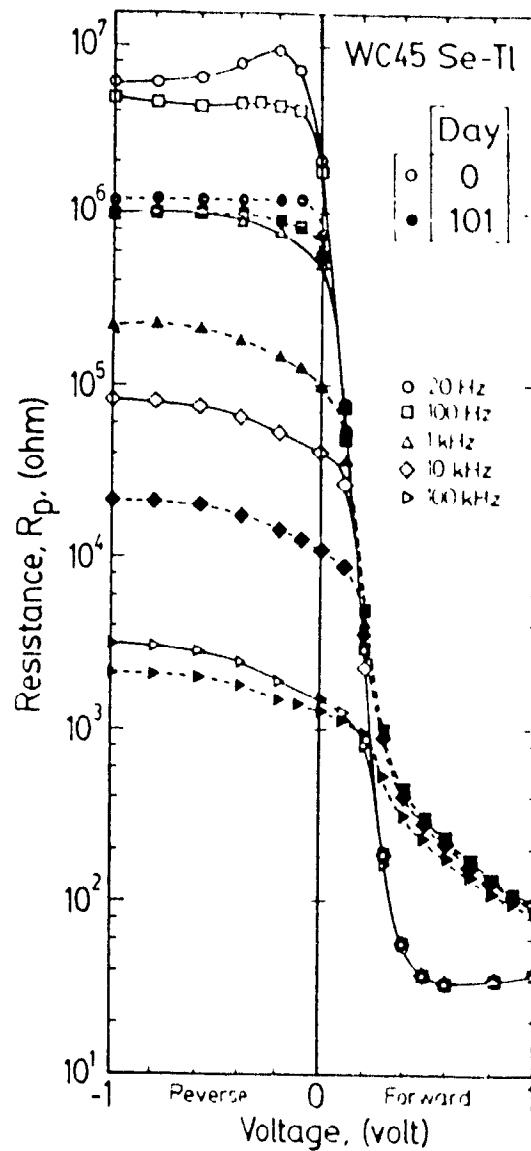


Fig.5.25. Resistance versus voltage plot for Se-Tl sample WC45 on day-0 and day-101 at different frequencies.

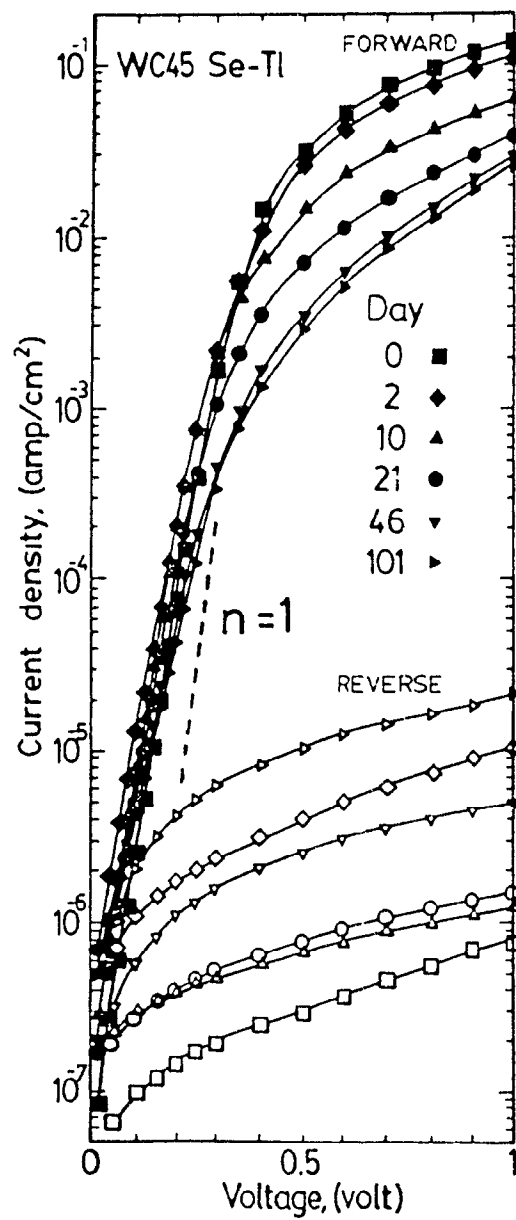


Fig.5.26. Plot of current-density against voltage for Se-Tl sample WC45 on days 0, 2, 10, 21, 46 and 101.

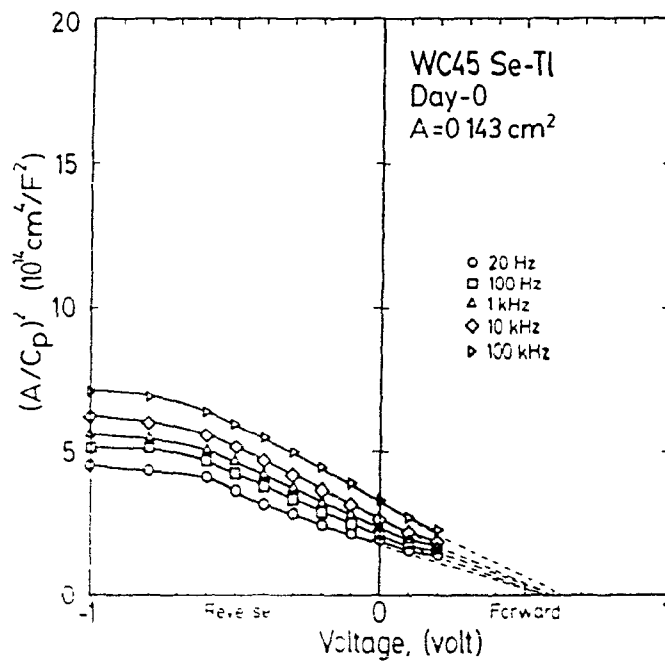


Fig 5.27. Mott-Schottky plot for Se-Tl sample WC45 on day-0 at different frequencies

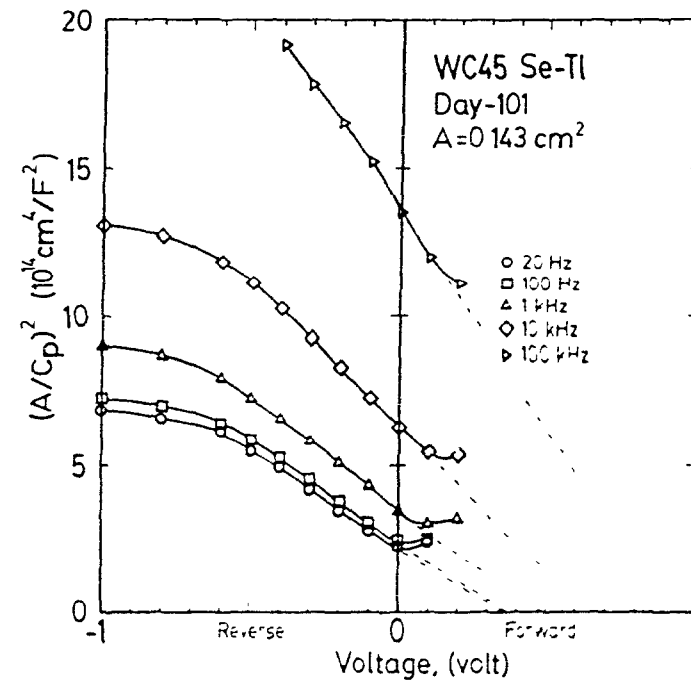


Fig 5.28. Mott-Schottky plot for Se-Tl sample WC45 on day-101 at different frequencies.

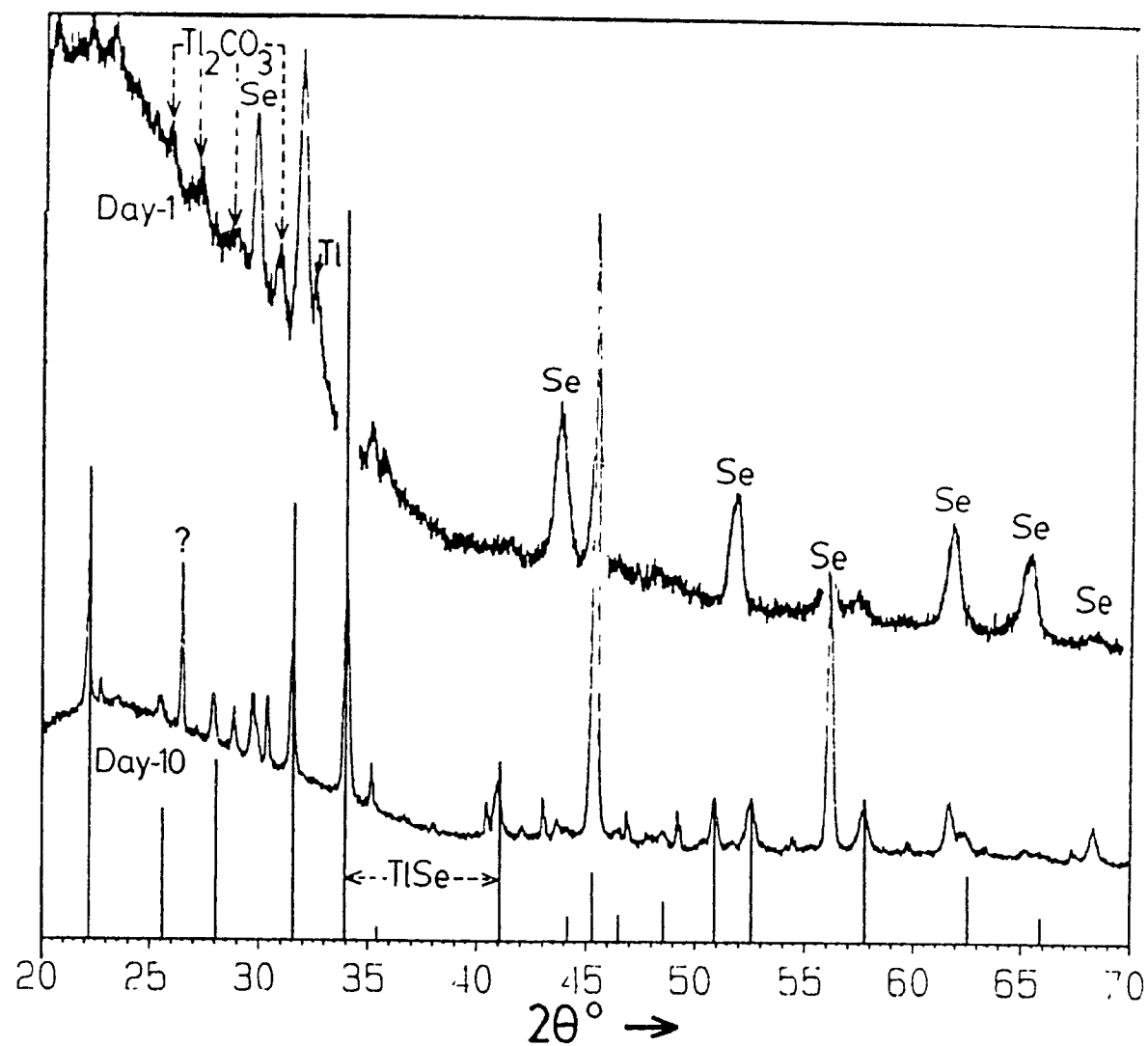


Fig.5.29. X-ray diffraction patterns obtained with $\text{Cu K}\alpha_1$ radiation for Se-Tl sample WC61 taken on day-1 and day-10.

Tl on glass

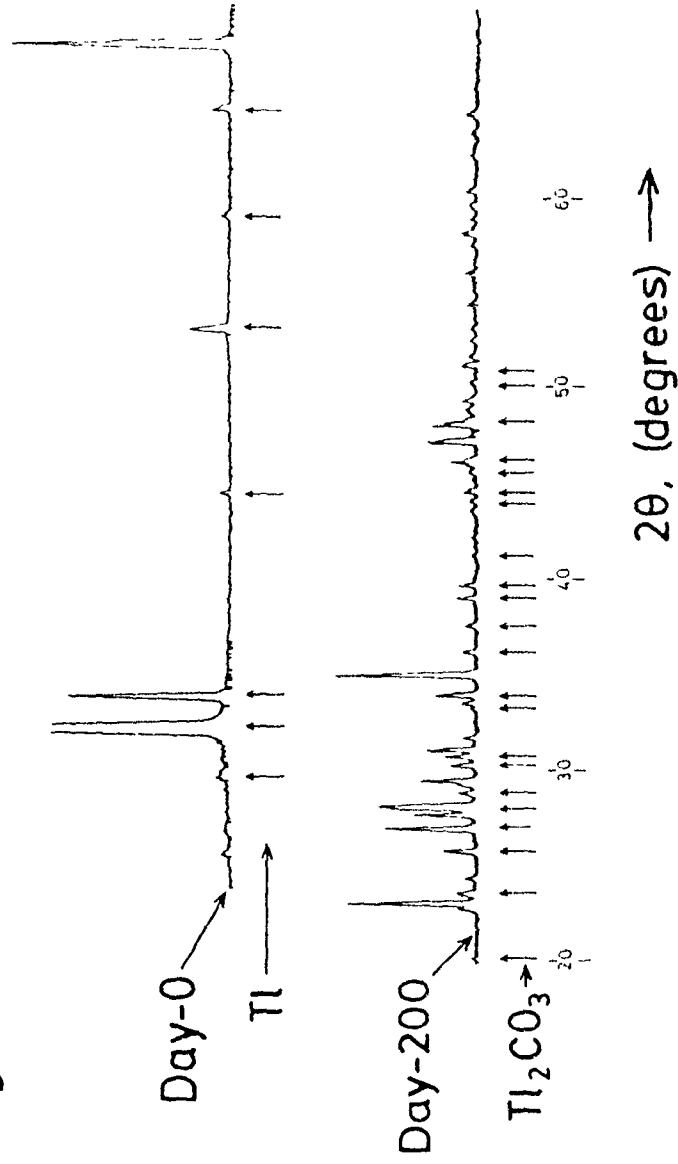


Fig.5.30. X-ray diffraction patterns obtained with Cu K α_1 radiation for a Tl film on glass when freshly deposited (day-0) and after 200 days (day-200). The vertical arrows correspond to expected peaks for the material indicated, according to ASTM data.

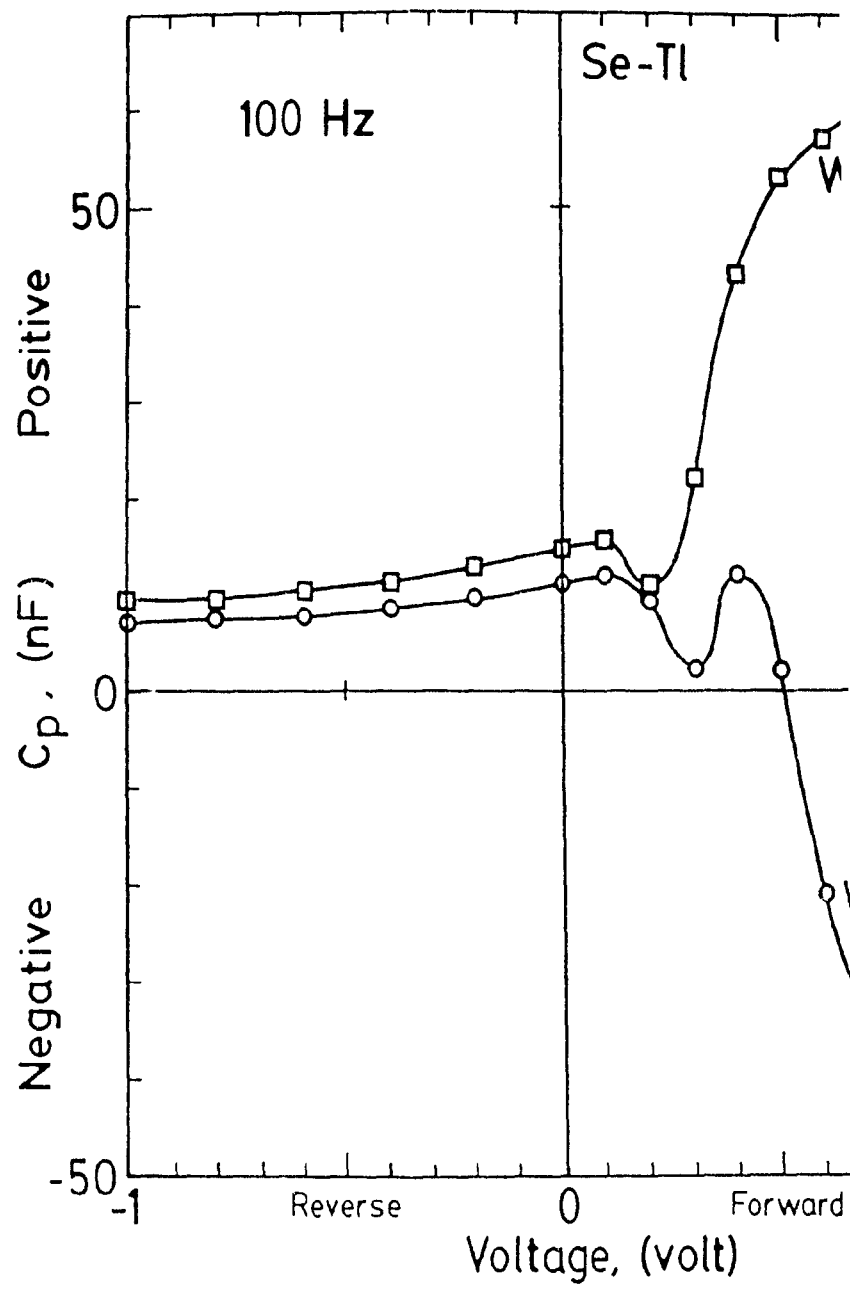
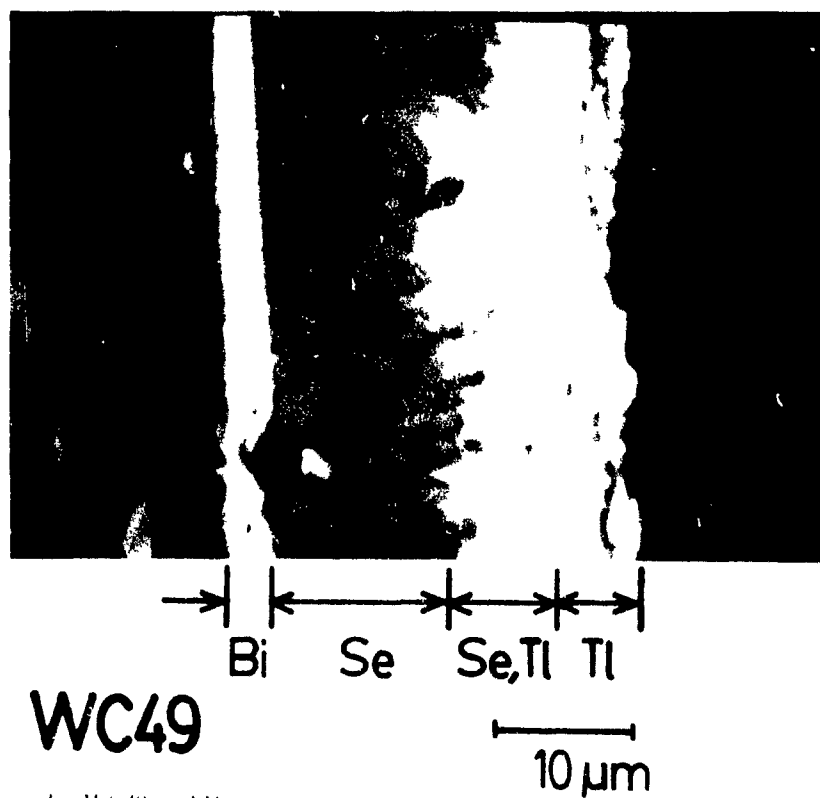
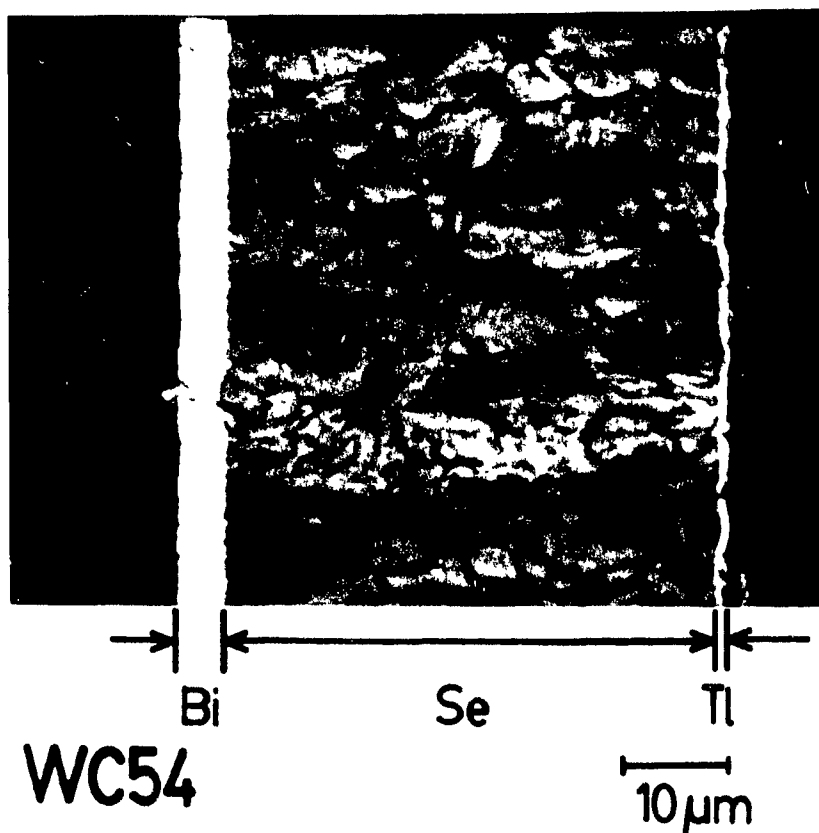
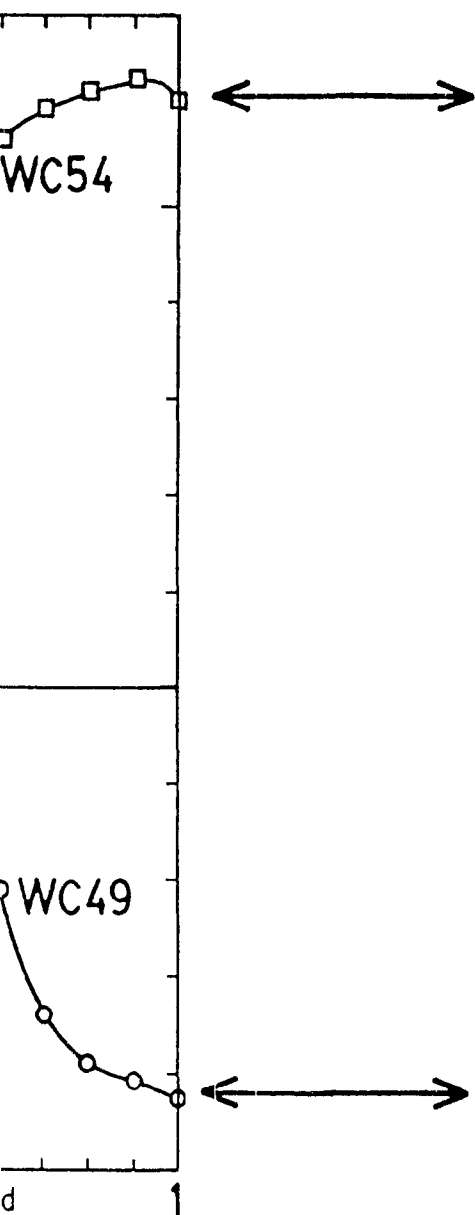


Fig.5.31. Plot of C_p vs. V on day-0 along



Plot of capacitance-versus-voltage at 100 Hz for Se-Tl samples WC 49 and WC 54 along with SEM back-scattered electron images of their cross-sections

6. RESULTS ON Bi AND Pt CONTACTS TO Se

6.1 Introduction

In the previous chapter it was mentioned that Se-Te diodes were studied because of their excellent rectifying characteristics. In this chapter, however, the thesis focuses on Bi and Pt contacts to Se, which, because of their higher work functions, are expected to give Schottky junctions with lower barrier energies. Accordingly, these should be of low resistance and only weakly rectifying. As seen in Table I, some 17 samples were made with Bi as the counterelectrode metal and 7 samples were made with Pt as the counterelectrode metal. Though Bi was the main back-contact metal used, several samples were made with Pt as the back-contact. Despite relatively few samples made with Pt, this work is, nevertheless, the first to report from this laboratory electrical characteristics of Pt contacts to Se, back or front.

With almost all of the metal-Se-metal samples studied in this laboratory, the forward j - V characteristics were obtained with the back-contact positively biased with respect to the counterelectrode. For samples made with Pt, however, it will be seen that this is often no longer the case. Therefore, to avoid ambiguity, the description in this chapter will refrain from using the words "forward" and "reverse" and a characteristic will be referred to as being in the "back-positive" direction when the back-contact is positively biased and, likewise, in the "back-negative" direction when the back-contact is negatively biased.

The first section of this chapter presents the j - V , R_p - V and Mott-Schottky characteristics

of Bi counterelectrode samples and Pt counterelectrode samples made with either Bi or Pt back-contacts. The section also describes how the rectifying characteristics for Bi contacts compare with those of Pt contacts. The next section presents C_p -V and C_p -f characteristics for the samples, where an interesting negative C_p effect is seen similar to that for the Se-Tl samples of chapter 5. Section 6.4 presents the results of aging studies on a Bi-Se-Bi sample. Though these results are not as extensive as those for the Tl samples, they are, nonetheless, quite informative.

6.2 Characteristics of Se-Bi and Se-Pt Structures with Bi and Pt Back-contacts

This section presents j-V, R_p -V and Mott-Schottky plots for several samples with the structures Bi-Se-Bi, Bi-Se-Pt, Pt-Se-Bi and Pt-Se-Pt. The first subsection compares the results for samples with Bi as the back-contact, while the second compares the results for Pt back-contact samples.

6.2.1 Samples with Bi as the Back-contact

The j-V characteristics for two Bi-Se-Bi samples, WC27 and WC32, are shown in Fig.6.1. These two samples had the lowest and highest rectification ratios respectively for samples with this type of structure. While WC32 shows a rectification ratio of almost three orders of magnitude, WC27 shows rectification of only about one order. This large difference is

mostly the result of a rather low forward j -values for WC27. It is also seen in the figure that, the back-positive (forward) curve for WC32 shows a straight line portion between about 0.05 and 0.15 volt, which corresponds to an ideality factor of about 1.3. The curve for WC27, on the other hand, shows no such straight line region.

The j -V characteristic for sample WC29, a Bi-Se-Pt structure, is shown in Fig.6.2, along with that for WC32 for comparison. At first glance it might seem that the two are quite similar. However, the direction of rectification for the Pt sample is actually opposite to that of the Bi sample, as indicated by the labeled voltage polarity of each curve. This is more clearly seen in Fig.6.3, where the current versus voltage (I -V) characteristics of the two samples are re-plotted on linear scales. While the high current direction for the Bi sample is when the back-contact is positive, the high current direction for the Pt sample is when the back-contact is negative. It is also interesting to note that the back-negative j -V curve for the Pt sample in Fig.6.2 actually rises to a slightly higher value than the back-positive (forward) j -V curve for the Bi sample at 1 volt, in spite of the fact that the Bi sample showed the highest current density of all the Bi-Se-Bi samples studied. Thus, it appears that a Pt counterelectrode contact gives a higher current density than any of the Bi/Se contacts, back or front. Inspection shows that with the two samples positively biased at the back-contact, the j -value for the Pt counterelectrode sample (WC29) is less than 5% that of the Bi sample (WC32). In fact, this smaller j -value is quite close to the 1 volt back-positive (forward) j -value of sample WC27 (Fig.6.1), which was the Bi-Se-Bi rectifier with the smallest back-positive current in this work. Fig.6.4 shows the j -V characteristics for another Bi-Se-Pt sample, WC64. It is seen in this case that, there is essentially no rectification at all

and furthermore, the $\log(j)$ - $\log(V)$ curves, shown in the inset, suggest a linear j - V relationship. Nevertheless, the j -value at 1 volt is still higher, though by only a slight margin, when the back-contact is negative than when it is positive. This is consistent with what is seen for sample WC29, another Bi-Se-Pt sample.

In Figs. 6.5 and 6.6 the R_p - V characteristics are displayed for samples WC32 and WC29 respectively. The Bi sample, WC32, shows a large dispersion of the curves for back-negative voltages, while the curves are relatively close together in the back-positive direction. Characteristics like these were common to all the Bi-Se-Bi samples of this work and are similar to those seen for the Se-Tl samples presented in the previous chapter. In contrast, the Pt sample, shows curves that are relatively dispersed in the back-positive voltage region and which are close together in the back-negative direction. Thus, if the curves for the Pt sample were reflected through the 0 volt axis, they would be quite similar to those of the Bi sample. This is consistent with the j - V plots for these two samples, which showed opposite directions of rectification. It is also interesting to note that there is a convergence of the low frequency curves (less than 100 kHz) in both R_p - V plots for both the positive and negative voltage regions. Such similarity between the curves at both voltage polarities was not observed with the Se-Tl samples.

Mott-Schottky plots for WC55, a Bi-Se-Bi sample and WC29, a Bi-Se-Pt sample, are shown in Figs. 6.7 and 6.8 respectively. The curves of the Bi sample, in Fig.6.7, for frequencies below 100 kHz are seen to show a straight line region for negative back-contact potentials, suggesting that a reverse biased junction is present. In contrast, the corresponding curves for the Bi-Se-Pt sample, WC29, in Fig.6.8, show a straight line region for positive

back-contact voltages. However, with this unusual polarity, it is of interest to note that, the values of the slope and extrapolated intercepts for this sample are about the same (though, with opposite sign) as those for sample WC55. The Mott-Schottky curves for WC27, the Bi-Se-Bi rectifier with the lowest back-positive current density, are shown in Fig.6.9. Interestingly, this plot displays some symmetry about the 0 volt axis, in that, it shows a straight line portion in its curves for both positive and negative polarities, at least for 1 and 10 kHz. It is seen here that, the slopes and voltage intercepts for the curves of one voltage direction are of about the same magnitude as those of the opposite voltage direction.

6.2.2 Samples with Pt as the Back-contact

The j - V characteristics for sample WC59, a Pt-Se-Bi structure, and sample WC66, a Pt-Se-Pt structure, are shown in Fig.6.10. While both samples show a rectification ratio of about a factor of 10, it is apparent that the characteristics are, in fact, quite different. The high current curve of WC59, the Bi sample, is for positive back-contact voltages, whereas, WC66, the Pt sample, has its high current curve for negative back-contact voltages. Thus, the rectification direction for the Pt sample is opposite to that of the Bi sample. Comparing the two curves for one polarity at a time, it is seen that both back-positive curves are relatively near each other, while on the other hand, the back-negative curve for the Pt sample is seen to be more than 2 orders of magnitude higher than that for the Bi sample at 1 volt.

In Figs. 6.11 and 6.12 the R_p - V characteristics are shown respectively for WC56, a Pt-Se-Bi sample, and WC66, a Pt-Se-Pt sample. It is seen that like the R_p - V characteristics for

samples WC32 and WC29, (displayed in Figs. 6.5 and 6.6 respectively) the characteristics for the Bi sample appear again to be the inverse of those of the Pt sample. Fig.6.11 shows that the curves for the Bi sample are more dispersed in the back-negative (reverse) direction than in the back-positive direction. In contrast, the curves for the Pt sample, shown in Fig.6.12, show greater dispersion in the back-positive direction than in the back-negative direction. This is again consistent with the reverse rectification direction observed in the Pt counterelectrode samples. It is also of interest to note the existence of the minimum at 0.1 volt in the back-positive direction for the curves of WC56. Such a minimum was seen in the characteristics of each of the Pt-Se-Bi samples and was also seen for WC27, the sample with the lowest back-positive curve of all the Bi-Se-Bi samples. Furthermore, it is seen in Figs. 6.11 and 6.12 that, the low frequency curves (less than 100 kHz) are again relatively close together at all voltages. Such a trend was also noted for the Bi back-contact samples in the previous subsection.

The Mott-Schottky plot for the Pt-Se-Bi sample, WC30, is shown in Fig.6.13. Straight line portions in its curves for both voltage polarities are observed, at least for 10 and 100 kHz. What is most striking, is that the magnitude of the slope of these curves is about 10 times higher in the back-positive direction than in the back-negative direction. Such a difference in slope, from one polarity to the other, was also observed in the other Pt-Se-Bi samples, WC56 and 59 (not shown), as well as in two Bi-Se-Bi samples, WC60 and 63 (not shown). In spite of the different slopes, the magnitude of the voltage intercepts for the WC30 curves is about the same for both polarities, at about 0.2 volt. The Mott-Schottky characteristics for sample WC66, a Pt-Se-Pt structure, are shown in Fig.6.14. Unlike the plot for the Pt-Se-Bi

sample, this one shows a straight line portion in its curves only for the back-positive direction. While the slope of the 10 and 100 kHz curves is found to be somewhat smaller than that of WC56 in the same voltage region, it is, nevertheless, higher than that usually found for the Bi back-contact samples. The extrapolated intercept of these curves is at about 0.1 volt, which is similar to that seen previously for both Bi and Pt samples.

6.3 C_p versus Voltage and Frequency Characteristics

This section presents the C_p -V and C_p -f characteristics for several samples with the structures Bi-Se-Bi, Bi-Se-Pt, Pt-Se-Bi and Pt-Se-Pt. The first subsection describes the characteristics of the Bi back-contact samples, while the second subsection presents results for Pt back-contact samples.

6.3.1 Characteristics for Bi Back-contact Samples

Prior to comparing the C_p -V characteristics of Bi-Se-Bi samples with those of a Bi-Se-Pt sample, the curves of several Bi-Se-Bi structures are described. The C_p -V plots for Bi-Se-Bi samples WC24, WC27, WC33 and WC55 are shown in Figs. 6.15 to 6.18. It is observed that, for the most part, each sample displays the usual decrease in C_p values with increase of back-negative (reverse) voltage. Furthermore, it is seen that all of these plots show that C_p is less dependent on voltage for higher frequencies than for lower frequencies. For example, the 1 and 10 MHz curves for WC55 are almost flat right across the figure, whereas the

curves for lower frequencies show much more variation. However, it is in the back-positive (forward) voltage range at lower frequencies, where there is considerable variation between the plots. In this voltage range the plot for sample WC24 in Fig.6.15 shows a very strong negative capacitance effect for the lower frequencies of 20 and 100 Hz. Furthermore, the curves at these frequencies show a broad negative minimum at about 0.5 volt. A minimum for 10 and 100 kHz is also seen but at 0.2 volt. The plot for sample WC27 in Fig.6.16 also shows curves in the forward direction with a minimum between 0 and 0.1 volt for frequencies up to 100 kHz but with no negative C_p -values. It is also seen that, the 20 Hz curve for this sample deviates quite substantially from the others for back positive voltages above about 0.3 volt. The 20 and 100 Hz curves for sample WC33, shown in Fig.6.17, also display negative C_p values but only above about 0.8 volt in the back-positive voltage direction. The 100 kHz curve in this figure shows a broad minimum at about 0.6 volt in the back-positive direction but an unusual bow-like shape in the back-negative direction (reverse). The curves for sample WC55, shown in Fig.6.18, are relatively free of anomalies. This plot shows no negative C_p values at any frequency, and only a very weak minimum in the 100 Hz curve at 0.1 volt in the back-positive direction and possibly also in the 20 Hz curve at 0 volt. The 20 Hz C_p values for back-positive voltages above 0.6 volt, however, showed great instability when measured and, hence, were left off this plot.

The C_p -V characteristics of Bi-Se-Pt sample, WC29, in Fig.6.19, are now compared with those above for the Bi-Se-Bi samples. It is seen that the plot for WC29 is quite different from those of the Bi-Se-Bi samples. In the back-negative direction the curves for the Pt counterelectrode sample are very dispersed, whereas in the back-positive direction they tend

to converge together, with the exception of the 20 Hz curve. In contrast the curves for the Bi-Se-Bi samples, shown in Figs. 6.15 to 6.18, are relatively convergent in the back-negative direction and are quite dispersed in the back-positive direction. Thus, even the C_p -V characteristics of Bi-Se-Pt sample, WC29, appear inverted in comparison with those of the Bi-Se-Bi samples. It is of interest to note that, the C_p appears to be a double minimum in the 20 Hz curve for WC29, with one minimum at 0 volt and the other at 0.2 volt in the back-positive direction. Such a multiple minimum was not seen in any of the Bi-Se-Bi samples and, in fact, Se-Te structures were the only other samples in this work where a multiple minimum was observed on day-0.

Using the C_p -V data at the different frequencies, C_p -f plots were made for the samples. Though there is a somewhat large variation in these plots, some interesting consistencies are also seen.

The C_p -f characteristics for the Bi samples, WC34 and WC55, both Bi-Se-Bi structures, are shown in Figs. 6.20 and 6.21. It is seen that these two Bi counterelectrode samples have characteristics that resemble one another in many ways. All of the curves converge together at high frequencies (around 10^6 Hz) where they show a relatively steep decrease with increase of frequency. In fact, the C_p values for WC55 in this range decrease approximately as $1/f$. The 0 and -1.0 volt curves, in each case, show relatively little variation from 20 Hz to around 10^4 Hz. Interestingly, the 1 volt back-positive (forward) curve for each sample actually shows a broad minimum at 10^3 Hz. Furthermore, the 0.2 and 0.3 volt curves, for WC55 and WC34 respectively, are seen to decrease steeply and cross under the -1.0 and 0 volt curves as the frequency rises from 20 Hz to about 10^3 Hz. Such a cross under was also

seen for Se-Tl diodes in chapter 5 but at a somewhat higher frequency, around 10^5 Hz.

The C_p -f plot for sample WC29, a Bi-Se-Pt sample, is shown in Fig.6.22. At first glance the curves seem quite similar to those of the Bi-Se-Bi samples. The 0 volt curve is quite similar to those of the Bi-Se-Bi samples. However, in Fig.6.22 it is the 1.0 volt back-positive curve that is relatively flat between 20 Hz and 10^6 Hz, not the -1.0 volt curve, as for the Bi-Se-Bi samples. Furthermore, the -1.0 volt back-negative curve for the Pt-counterelectrode sample resembles the 0.3 volt back-positive curve for Bi-Se-Bi sample, WC34 (Fig.6.20), in that both curves show a relatively steep decline from 20 Hz to above 10^3 Hz.

At this point it is informative to display some characteristics of the very interesting sample WC65, a Bi-Se-Pt structure. Fig.6.23 shows the j-V characteristics and it is seen that they resemble those of WC64 in Fig.6.4. The rectification ratio is relatively small and its direction is opposite to that found in samples made with Tl and Bi as the front-contact. Fig.6.24 shows the R_f -V and C_p -V characteristics for the sample, where it is seen that the R_p value is essentially invariant with bias voltage and frequency, at least between -1 and 1 volt and between 100 Hz and 100 kHz. Similarly, the value of C_p is relatively independent of bias voltage and frequency, having a value near 100 nF, at least for bias voltages between -1 and 1 volt and frequencies between 100 Hz and 10 kHz. These results are given special attention in the discussion section later in this chapter.

6.3.2 Characteristics of Pt Back-contact Samples

The C_p -V curves for two samples, WC56 (Pt-Se-Bi) and WC66 (Pt-Se-Pt), which had Pt

as their back-contact are shown in Figs. 6.25 and 6.26 respectively. It is observed that, the plot for WC56, the Bi counterelectrode sample, displays very little in the way of anomalies outside of a weak minimum at 0.1 volt in the back positive direction for the 100 kHz curve and only a tendency to a minimum between 0 and 0.1 volt for the 20 Hz curve. In fact, this plot resembles that of WC55 shown in Fig 6.20. On the other hand, the plot for WC66, the Pt counterelectrode sample, is very different from that of WC56. Firstly, the plot for WC66 in Fig.6.26 shows larger dispersion of the curves in both bias directions than for sample WC56 as well as the other samples of this work. Even more striking though, is the pronounced minimum in the 20 Hz curve at 0.1 volt in the back-negative direction, which actually extends to negative C_p values. A minimum is also seen in the curves for 100 Hz, 10 kHz, 100kHz and 1 MHz between -0.1 and -0.3 volt in the back-negative direction but not for 1 kHz. Other samples of this work showed such minima only in the back-positive bias direction. This again is consistent with an inverted rectification direction for samples where Pt is the counterelectrode metal.

In a similar manner to that for the Bi back-contact samples, C_p -f plots were also made for Pt back-contact samples. These also show some interesting features and they are now presented.

The C_p -f curves for three Pt back-contact samples, WC30 (Pt-Se-Bi), WC59 (Pt-Se-Bi) and WC66 (Pt-Se-Pt) are displayed in Figs. 6.27 to 6.29. While the curves for WC30 are relatively free of anomalies, those for WC59 and WC66 are not so well behaved, in that, these have negative C_p values, as well as, a minimum for sample WC66. The back-positive 1.0 volt curve for WC59 shows strong negative C_p values for frequencies below 100 Hz. It

also shows an increase as the frequency increases for low frequencies. A rise with frequency at low frequencies is also seen in the 0.3 volt curve, as well as, in the -1.0 volt back-negative (reverse) curve. Sample WC66 also shows a curve that passes into the negative C_p domain at low frequency but in this case for 0 bias. Furthermore, while both the 0.8 and -0.8 curves show a steep decrease with frequency from 20 Hz to about 10^3 Hz, a strong minimum is present in the -0.8 volt curve at 10^3 Hz. A similar minimum was seen also for several Bi-Se-Bi samples (Figs. 6.22 and 6.23).

When presenting the R_p -V characteristics earlier, in section 6.2, it was seen that the curves at low frequencies were very near one another at all bias values, while the high frequency curves were somewhat spread out. Plots of R_p against f are now presented which show this trend more clearly. The R_p - f plot for sample WC32 (Bi-Se-Bi) is shown in Fig. 6.30 for 1.0, 0 and -1.0 volt bias values. It is seen that the 1.0 volt back-positive (forward) curve is almost flat from 20 Hz all the way to 10^6 Hz. On the other hand, the curves for 0 and -1.0 volt show a relatively flat region only between 20 Hz and about 10^4 Hz and then a relatively steep decline with frequency for higher frequencies. It is also seen that all three curves converge together at higher frequencies, above about 10^6 Hz. Similar features are seen in the R_p - f plot for sample WC66 (Pt-Se-Pt) in Fig. 6.31. However, in this case, it is the -0.8 volt back-negative curve that is seen to be relatively flat over the entire frequency range and it is the 0.8 volt back-positive curve that shows the relatively large variation. It is interesting that, despite showing rather anomalous C_p - f curves (Fig. 6.29), such anomalies are not apparent in the R_p - f plot for this sample.

6.4 Evidence for Aging in Bi-Se-Bi Samples

It was seen in chapter 5 that negative capacitance was observed in most of the Se-Te samples of this work and this negative effect seemed to coincide with the formation of the semiconductor TeSe. Several Bi-Se-Bi samples of this work also showed negative C_p -V characteristics similar to those of the Te samples. In this section results are presented on some aging studies of Bi-Se-Bi sample WC55, which initially did not show negative capacitance values. Though these studies were not nearly as extensive as those of the Te samples, they were, nevertheless, quite informative. The C_p -V, R_p -V, J-V and Mott-Schottky plots for this sample on day-0 and day-151 are now presented.

The 20 and 100 Hz C_p -V characteristics for the sample on day-0 and day-151 are shown in Fig.6.32. While the curves for the back-negative (reverse) voltage are almost identical, the curves in the back-positive region are quite different after the 151 days of storage. Firstly, the 20 Hz day-0 curve shows no negative values, while that for day-151 shows a strong negative C_p effect in the back-positive direction beyond 0.6 volt. Thus, it would seem that the presence of negative C_p values has grown with storage time. Secondly, it is also seen that, there is only a tendency to a minimum at this frequency in the day-0 curve near 0 volt, while a strong minimum is present in the day-151 curve shifted to 0.1 volt. The 100 Hz curves show a similar trend with a shift of also 0.1 volt. Thus, it appears that the minimum has also become more pronounced with storage time and has shifted to a slightly greater back-positive voltage. Similar aging effects were also seen for Se-Te samples described in chapter 5.

Figs. 6.33 and 6.34 show the R_p -V plots for this sample on day-0 and day-151 respectively. It is seen that, the two plots are quite similar in shape; they differ only, in that, the low frequency R_p values for back-negative voltages are somewhat smaller for day-151 than day-0. Thus, these characteristics have not changed dramatically with storage time as did the C_p -V characteristics.

The j-V characteristics for the two storage times, day-0 and day-151, are shown in Fig.6.35. It is seen that, while the back-positive (forward) j-values decreased only slightly from their day-0 values, the back-negative values increased by a factor of four. Thus, the rectification ratio decreased from about 2 orders of magnitude on day-0 to just above 1 order of magnitude on day-151. Nevertheless, the j-V characteristics do not show the emergence of anomalies with storage time such as displayed in the C_p -V characteristics.

As mentioned previously, the back-negative C_p -V characteristics changed very little with storage time. Reflecting this fact, it is seen that the Mott-Schottky plots too, in Figs. 6.36 and 6.37, show relatively little variation over this storage time period. Though, the curves are slightly more dispersed for day-151 (Fig.6.37) than day-0 (Fig.6.36), their slopes and intercepts are still about the same.

6.5 Discussion

The most interesting result in this chapter is that the Pt counterelectrodes provided low resistance contacts to Se. Hence, diodes made with Pt as their counterelectrode rectified in a direction that was opposite to that observed for all other Se-metal samples made in this

laboratory with the counterelectrode metals Te, Bi, Mg, Au, Al, Cd, and Cu. Such a low resistance at the Pt front-contact may have come about in the following way. Since Pt has such a high melting point (1769°C) and because the filament to substrate distance was rather small during the Pt counterelectrode evaporation (2 cm), it is expected that the metal was quite hot after it was deposited on to the Se film. At such a high temperature, it is speculated that the small energy gap semiconductor PtSe₂ ($E_g = 0.1$ eV [16]) may have formed at the Pt/Se interface. It is further speculated that this semiconductor formed a low resistance and essentially ohmic contact to the Se, while the contact between the Pt and the PtSe₂ was also ohmic. In this case, the current-voltage characteristics would be dominated by the higher resistance back-contact. Thus, if the back-contact metal was Bi, the j - V characteristics would represent those of a Bi-Se contact, while if the back-contact was Pt, they would represent those of a Pt-Se contact. While it was seen in this work that most of the Bi back-contacts were also of low resistance, the Pt back-contacts did not show low resistance properties and, in fact, displayed characteristics which resembled that of a rectifying junction. The Pt contacts were not of low resistance perhaps because their formation during the Se deposition step involved relatively low temperatures (substrate temperature 130°C; Se melting point 217°C), which were not high enough to form PtSe₂. While it may have been thought that the rectifying nature of the Pt back-contact depended on the method by which the Pt was deposited (sputtered vs evaporated), this was actually not the case, since sample WC66 was made with a Pt back-contact that was deposited by evaporation and it was seen that it too showed the inverted rectification properties. Of course these speculations must be verified by further experimentation.

While in almost all cases, the Bi back-contact in the samples of this work was of relatively low resistance, some were of relatively high resistance and in fact evidence suggests that these were also partially rectifying. In particular, sample WC29, showing inverted rectification and sample WC27, showing normal rectification both exhibited Mott-Schottky plots which suggest that a junction was present at the Bi/Se back-contact. From the fabrication data of these samples in Table I, it is seen that the Bi back-contact films for these two samples were unusually thin. Thus, it would seem that a thin Bi back-contact produced a relatively high resistance, rectifying back-contact. It is speculated that the thin Bi back-contact layer only partially covered the surface of the Al substrate. Thus, the Al substrate was exposed in certain areas to the Se, which gave rise to high resistance, rectifying Al-Se contact areas. Another possible explanation is that the thin Bi layer was completely consumed in the formation of Bi_2Se_3 at the back-contact during the Se deposition. Thus, the back-contact was actually a heterojunction of the form Al- Bi_2Se_3 -Se, which was rectifying since the Al did not make an ohmic contact to the selenide. A thicker Bi layer would not have been completely consumed, so that the back-contact junction would be of the form Bi- Bi_2Se_3 -Se and in this case the Bi provided an ohmic contact to the selenide. The selenide here has such a low gap energy (0.35 eV [17]) that it would make only a weakly rectifying contact to the Se.

It is believed that the low resistance Pt front-contact, as well as, the low resistance Bi back-contact to the Se were actually not uniform. That is, ohmic contacts to the Se layer were only present in small areas and acted as bridges between the metal and the Se. The remaining areas are believed to have been Schottky contacts between the Se and the Pt or

the Se and the Bi. This would explain why in sample WC65 the values of C_p and R_p were essentially independent of voltage. The low resistance areas or bridges would tend to short out the Schottky junction areas so that varying the bias across the entire sample would not result in much bias change across the actual junctions. Therefore, the capacitance and resistance of the Schottky junction areas would vary only slightly as the bias voltage across the sample was changed. Furthermore, the capacitance value of 100 nF observed in this sample corresponded to the zero bias value measured for sample WC55, a Bi-Se-Bi sample, as well as other samples (not shown), which suggests further that any junction present in sample WC65 was, essentially, at zero bias.

In several samples of this work the Mott-Schottky plots showed straight line regions for both bias polarities. Such behaviour corresponded to what is expected for two back-to-back diodes. When the counterelectrode was forward biased, the back-contact was in reverse, so that most of the voltage applied to the structure was actually across the back-contact. Thus, it was primarily the back-contact capacitance that was measured under these circumstances. Conversely, when the counterelectrode was reverse biased, the back-contact was forward biased and the capacitance measured was that at the counterelectrode. It was seen in this work that the Bi-Se-Bi sample WC27, showed Mott-Schottky curves with a slope of about the same magnitude for both bias directions, suggesting that the nominal hole concentration in the Se was about the same at both contacts. On the other hand, the Pt-Se-Bi sample WC30 showed a slope in the back-positive direction about 10 times larger than that for the curves in the back-negative direction. This suggests that the nominal hole concentration at the Pt back-contact was about an order of magnitude lower than that at the Bi

counterelectrode. Further evidence suggesting that these samples were actually back-to-back diodes was seen in the R_p - V characteristics, where a clear minimum was observed. Such a minimum comes about when the two diodes have equal voltages across them as explained by van Opdorp and Kanerva [18], which is at zero bias when the diodes are identical.

In chapter 5, it was seen that a low frequency inductive effect was quite strong in the Se-Tl samples. Such an inductive effect was also seen for samples presented in this chapter and this was despite there being no Tl present. In fact, the effect was also seen for a Pt-Se-Pt sample (WC66), which had neither Bi nor Tl present. Thus, the appearance of this inductive effect does not depend especially on whether Tl or Bi are present. It was also seen with the Tl samples that the inductive effect grows with time, at least in the initial stages after fabrication. A Bi-Se-Bi sample (WC55) also displayed such a growing inductive effect and it is speculated that, like the Tl samples, it may also be due to selenide formation at the counterelectrode-Se interface, specifically Bi_2Se_3 which was not detected by x-ray diffraction in this work but was detected in a previous study [19].

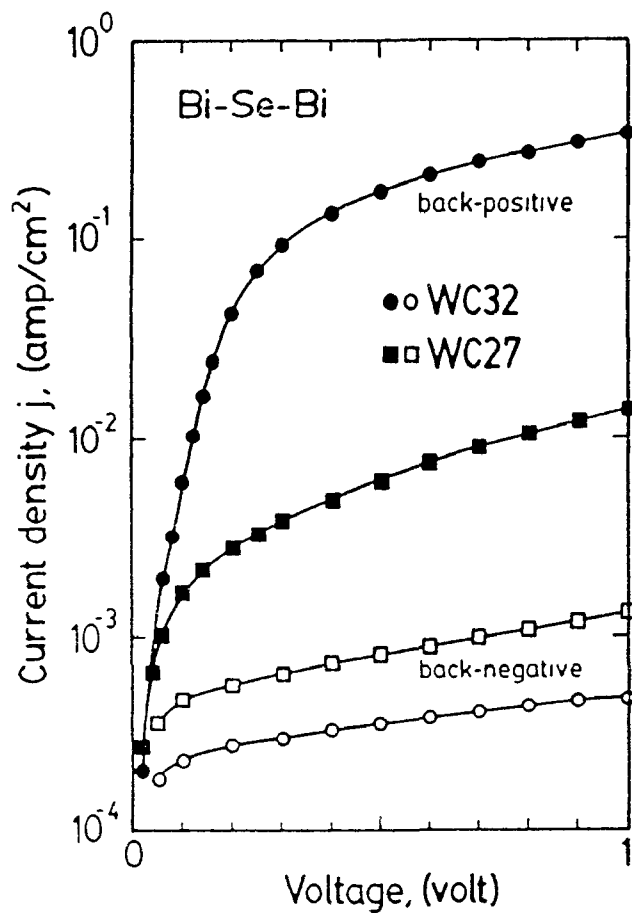


Fig.6.1. Plot of current-density against voltage for Bi-Se-Bi samples WC27 and WC32.

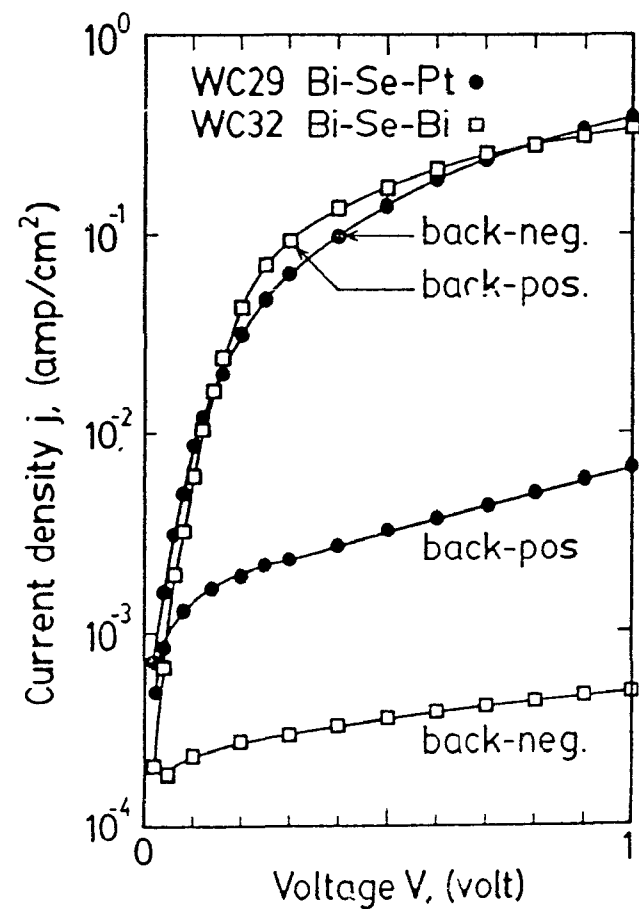


Fig.6.2. Plot of current-density against voltage for Bi-Se-Pt sample WC29 and Bi-Se-Bi sample WC32.

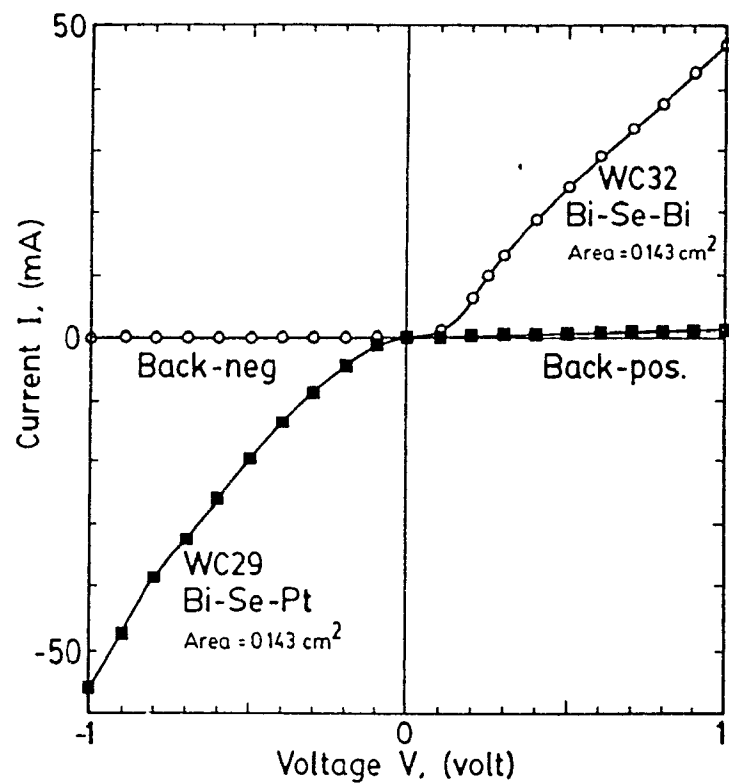


Fig.6.3. Plot of current against voltage on linear scales for Bi-Se-Pt sample WC29 and Bi-Se-Bi sample WC32.

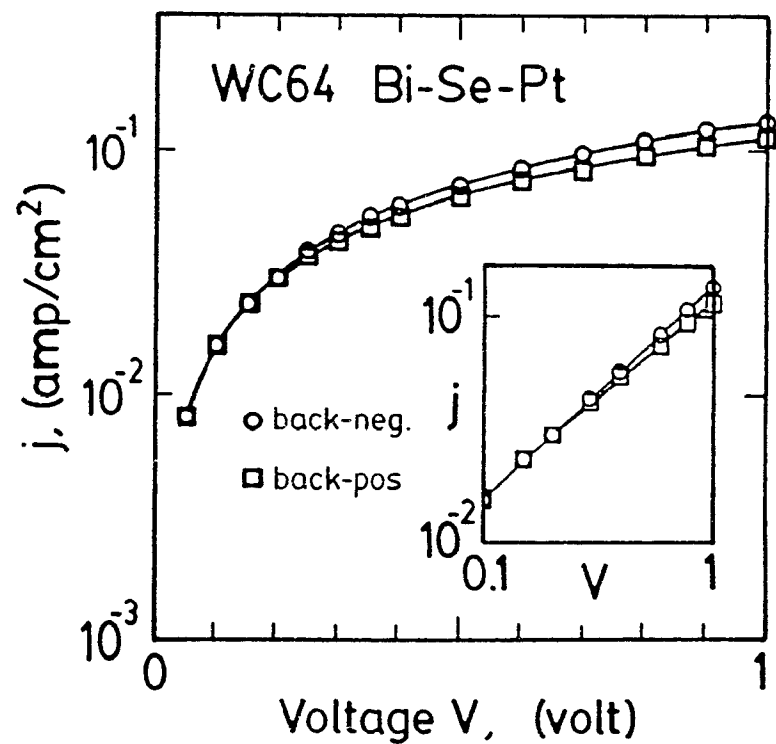


Fig.6.4. Plot of current-density against voltage for Bi-Se-Pt sample WC64.

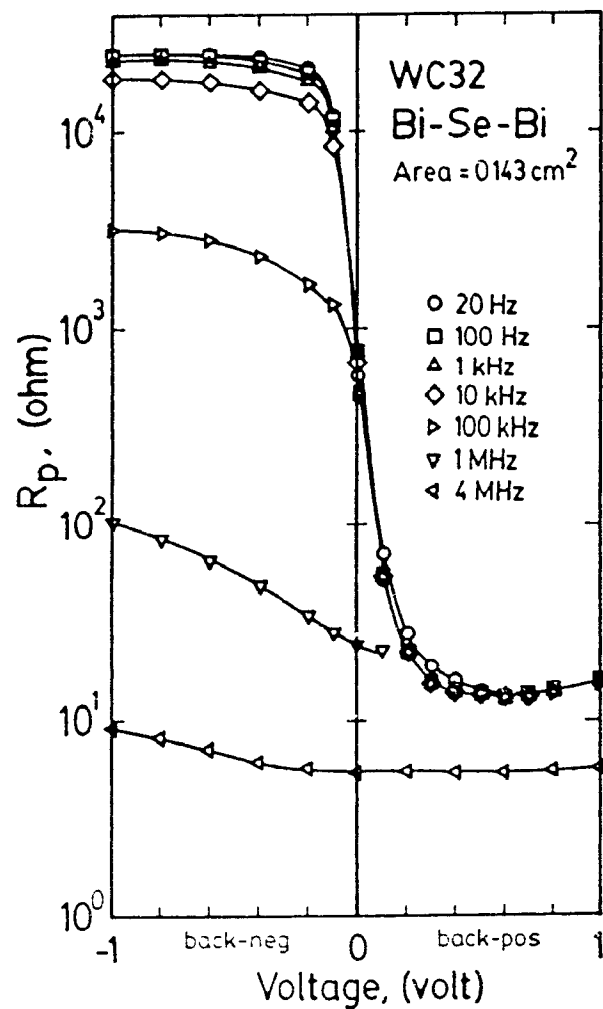


Fig.6.5. Resistance versus voltage plot for Bi-Se-Bi sample WC32 measured at different frequencies.

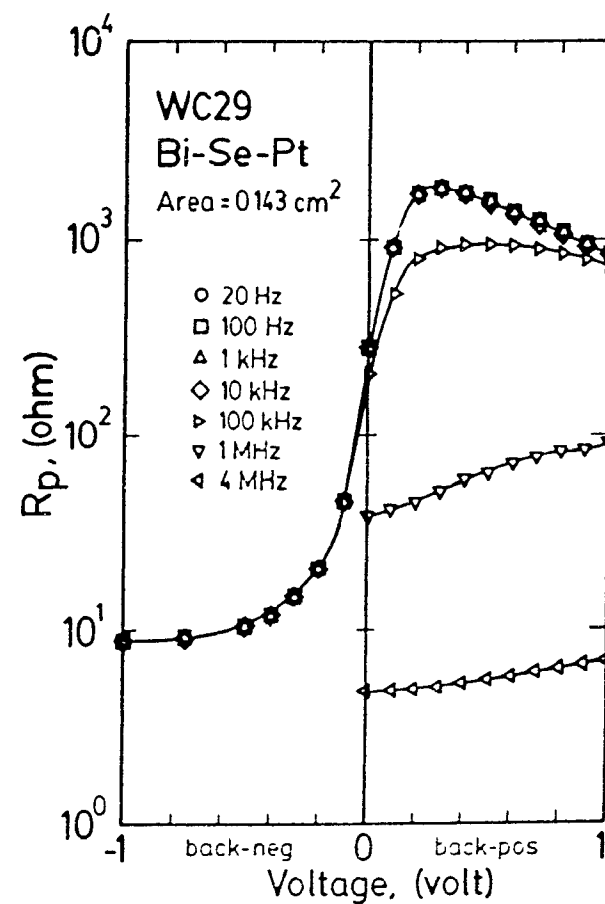


Fig.6.6. Resistance versus voltage plot for Bi-Se-Pt sample WC29 measured at different frequencies.

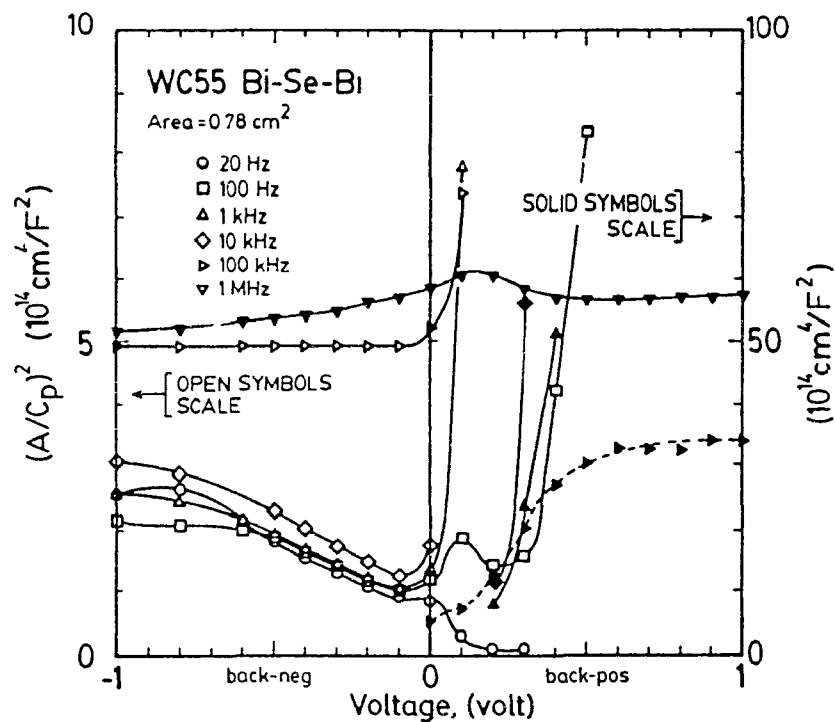


Fig.6.7. Mott-Schottky plot for Bi-Se-Bi sample WC55 at different frequencies.

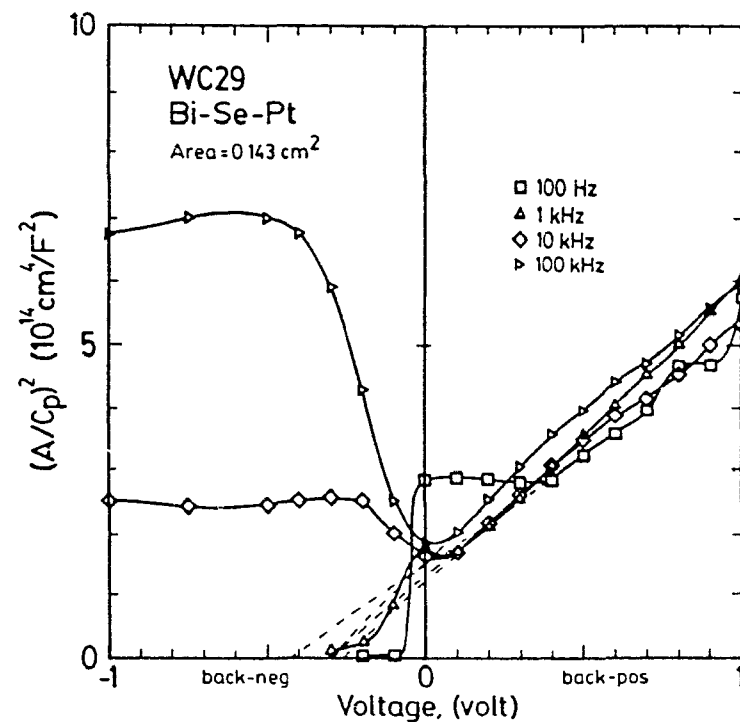


Fig.6.8. Mott-Schottky plot for Bi-Se-Pt sample WC29 at different frequencies.

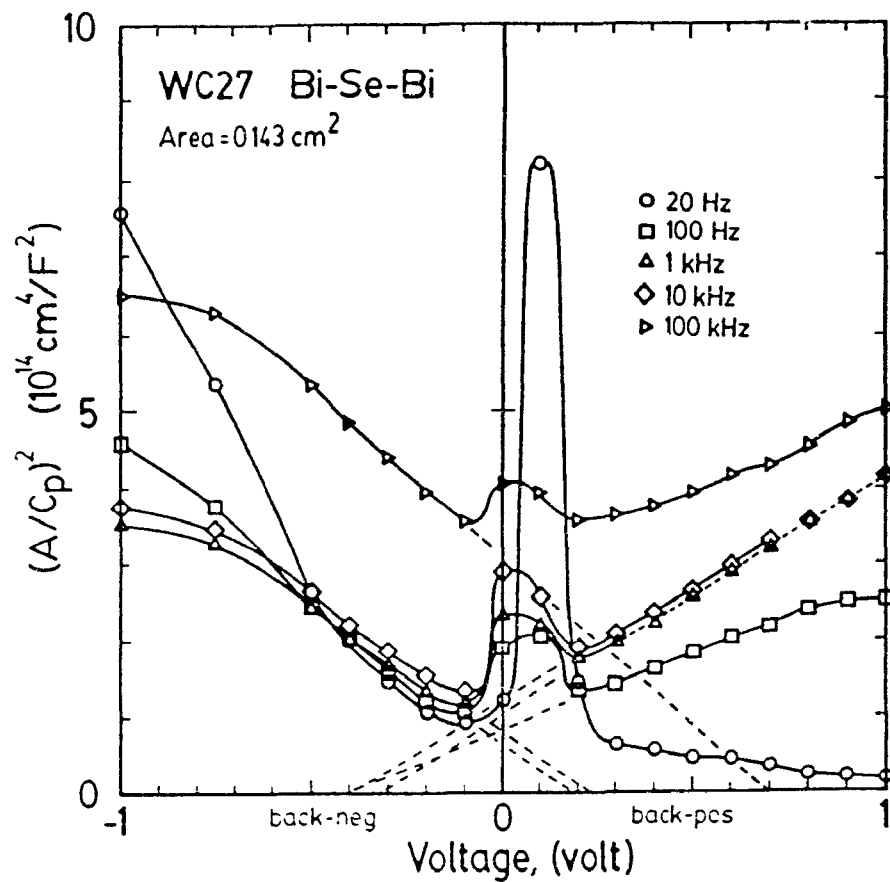


Fig.6.9. Mott-Schottky plot for Bi-Se-Bi sample WC27 at different frequencies.

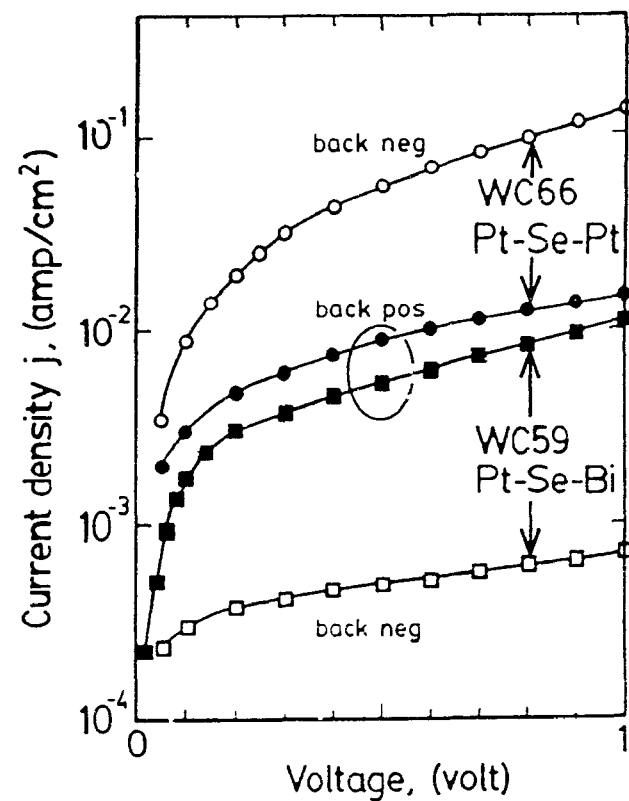


Fig.6.10. Plot of current-density against voltage for Pt-Se-Bi sample WC59 and Pt-Se-Pt sample WC66.

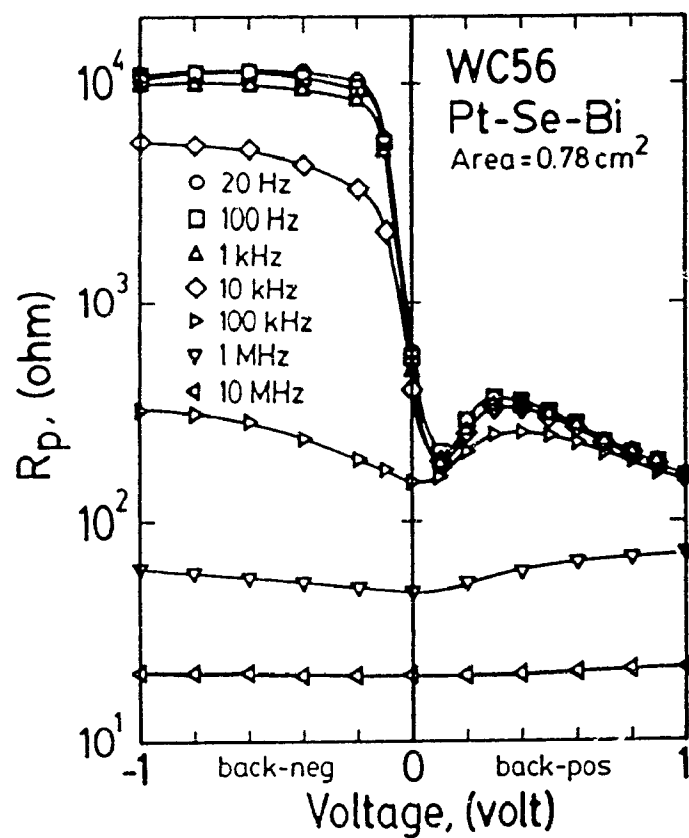


Fig.6.11. Resistance versus voltage plot for Pt-Se-Bi sample WC56 measured at different frequencies.

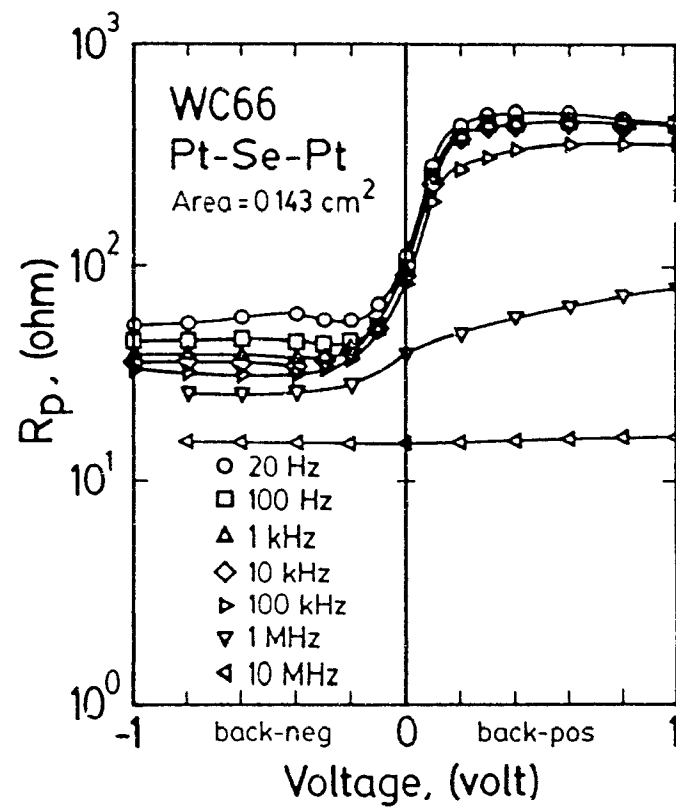


Fig.6.12. Resistance versus voltage plot for Pt-Se-Pt sample WC66 measured at different frequencies.

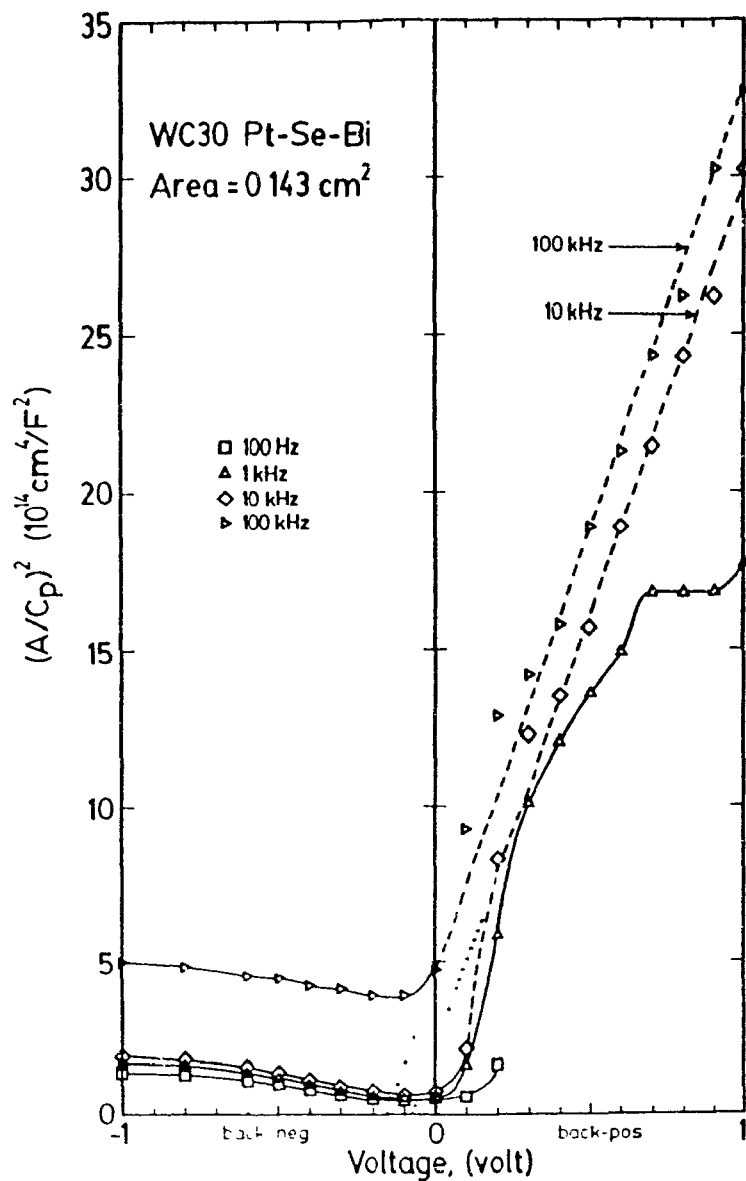


Fig.6.13. Mott-Schottky plot for Pt-Se-Bi sample WC30 at different frequencies

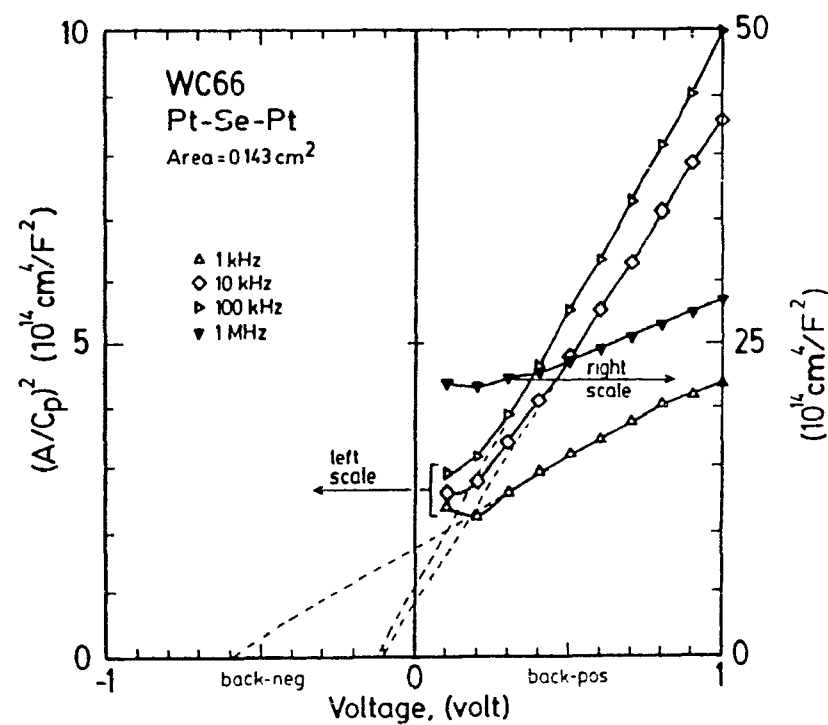


Fig.6.14. Mott-Schottky plot for Pt-Se-Pt sample WC66 at different frequencies.

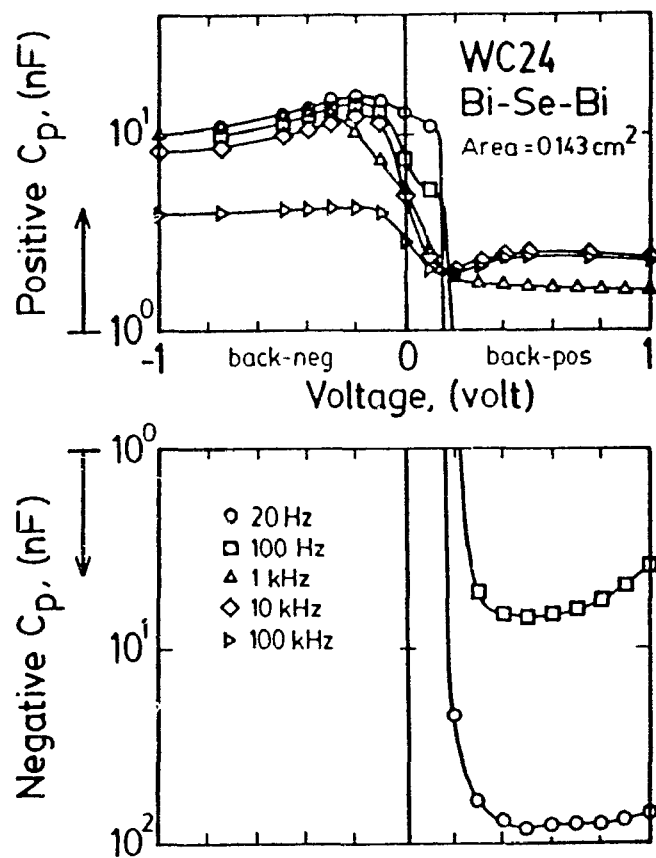


Fig.6.15. Capacitance versus voltage plot for Bi-Se-Bi sample WC24 measured at different frequencies.

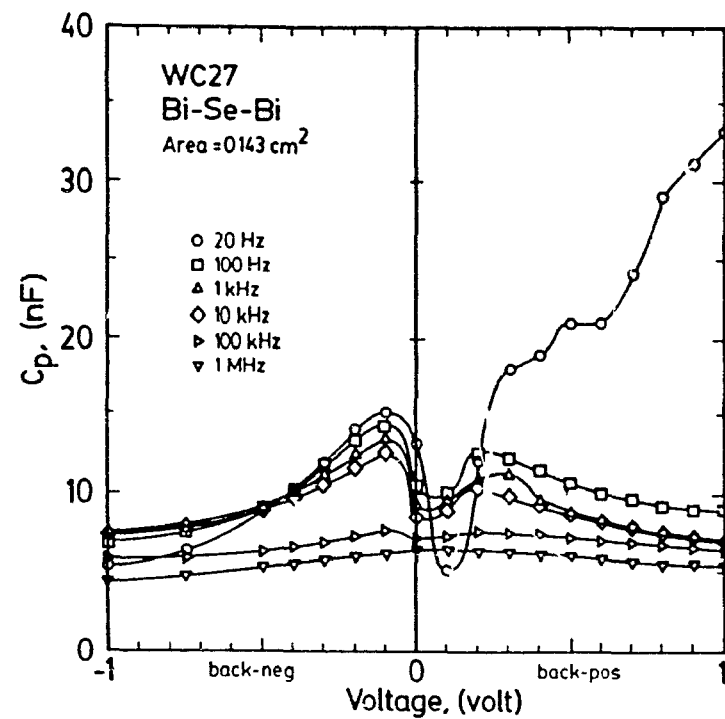


Fig.6.16. Capacitance versus voltage plot for Bi-Se-Bi sample WC27 measured at different frequencies.

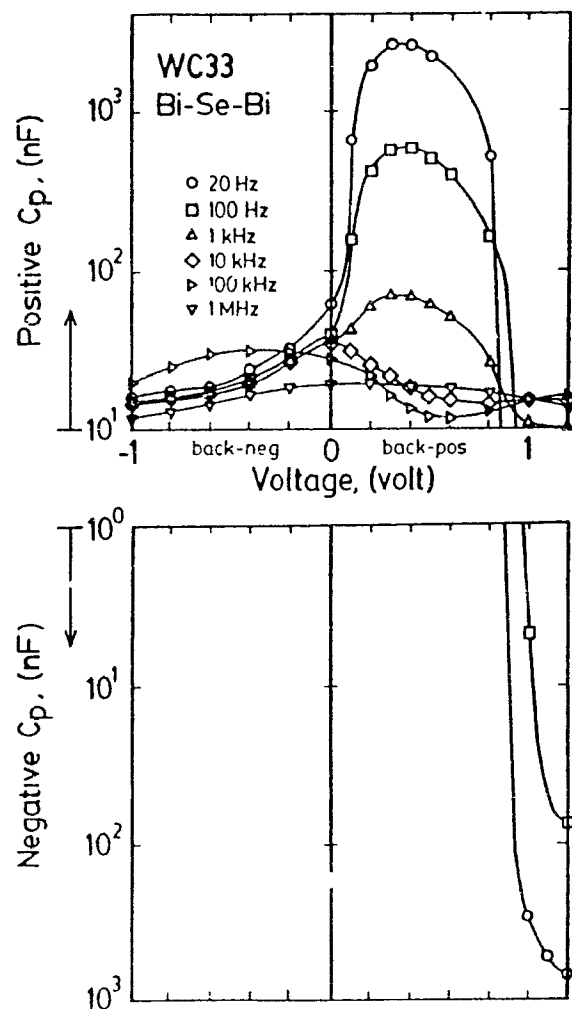


Fig.6.17. Capacitance versus voltage plot for Bi-Se-Bi sample WC33 measured at different frequencies.

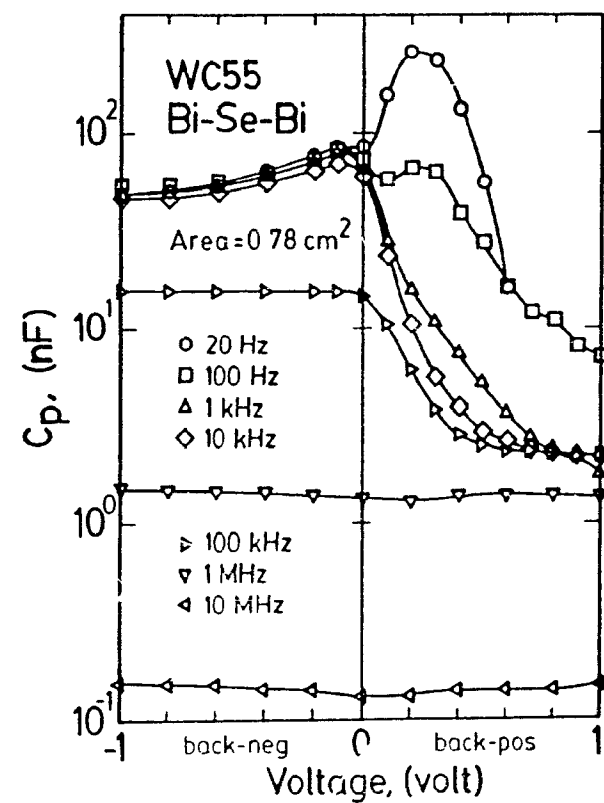


Fig.6.18. Capacitance versus voltage plot for Bi-Se-Bi sample WC55 measured at different frequencies.

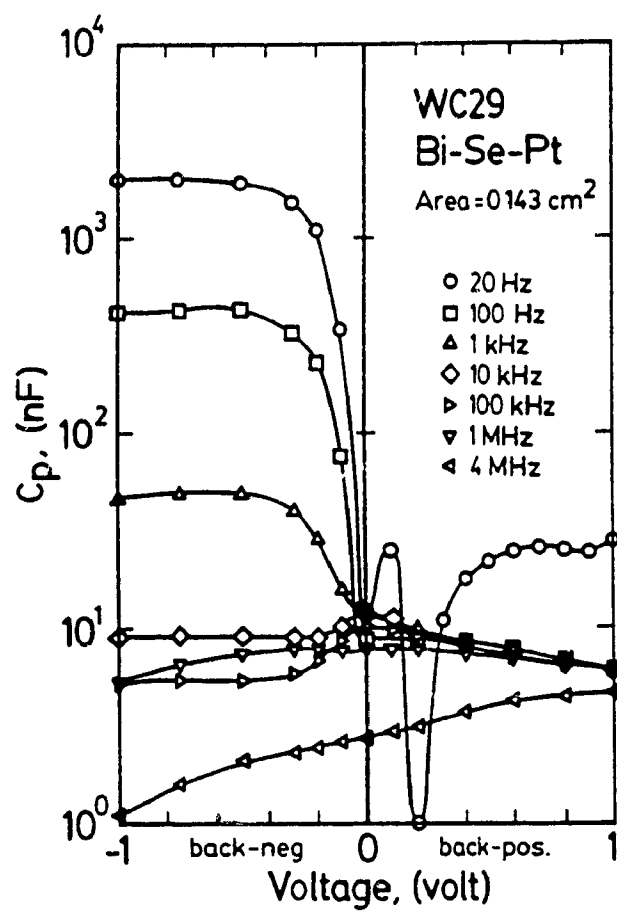


Fig.6.19. Capacitance versus voltage plot for Bi-Se-Pt sample WC29 measured at different frequencies.

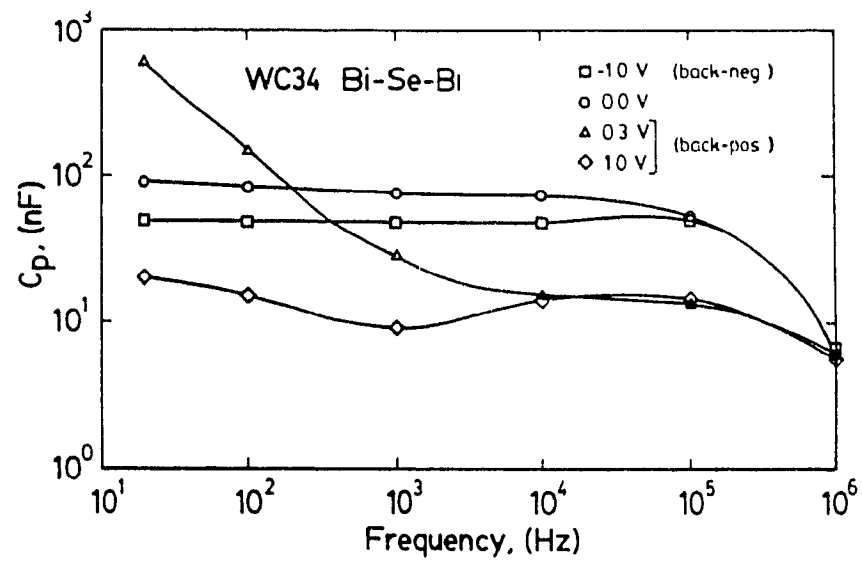


Fig.6.20. Capacitance versus frequency plot for Bi-Se-Bi sample WC34 at different bias voltages.

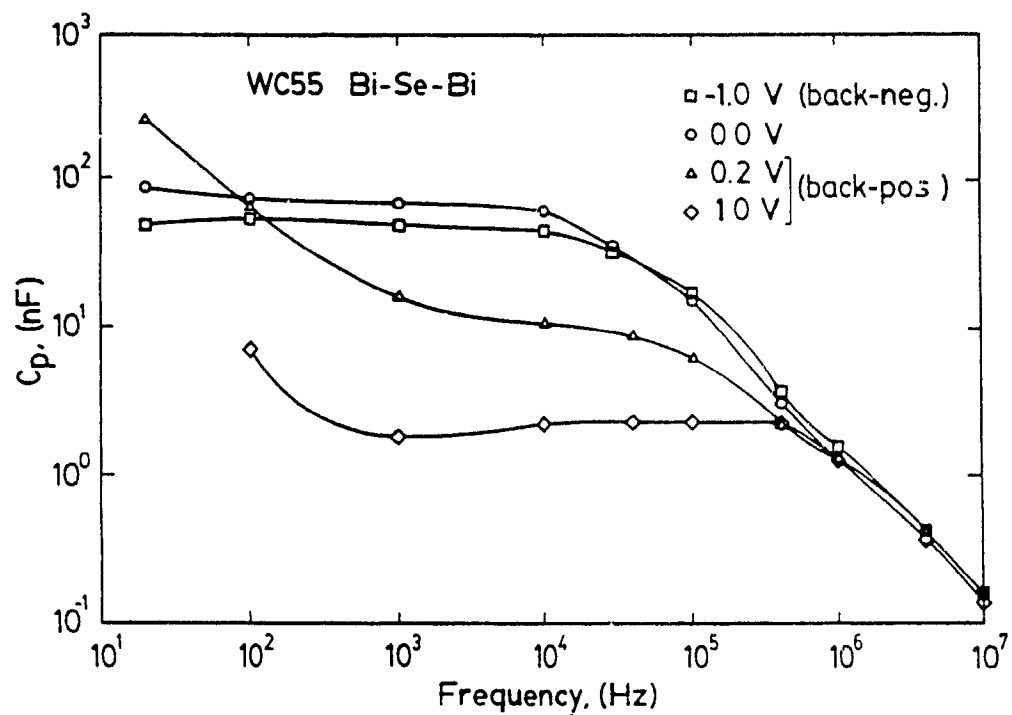


Fig.6.21. Capacitance versus frequency plot for Bi-Se-Bi sample WC55 at different bias voltages.

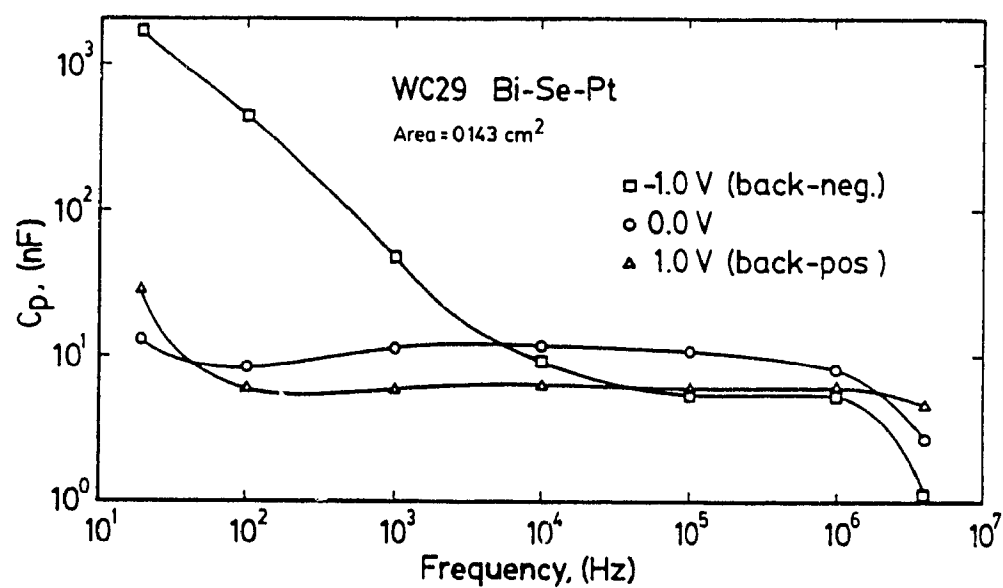


Fig.6.22. Capacitance versus frequency plot for Bi-Se-Pt sample WC29 at different bias voltages.

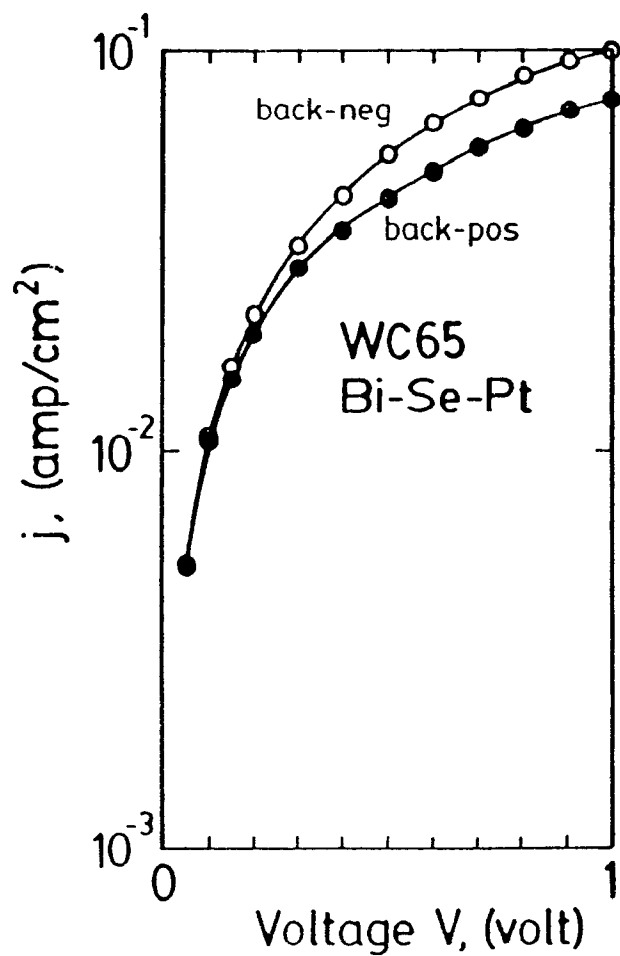


Fig.6.23. Plot of current-density against voltage for Bi-Se-Pt sample WC65.

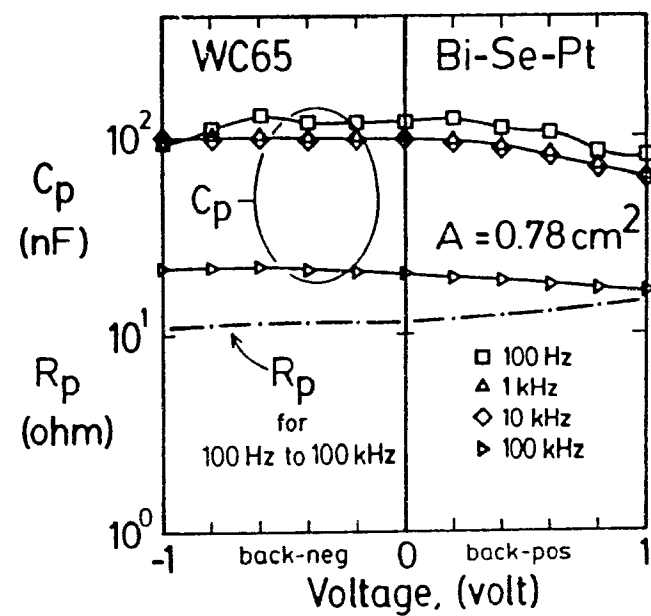


Fig.6.24. Plot of capacitance and resistance against voltage for Bi-Se-Pt sample WC65 measured at different frequencies.

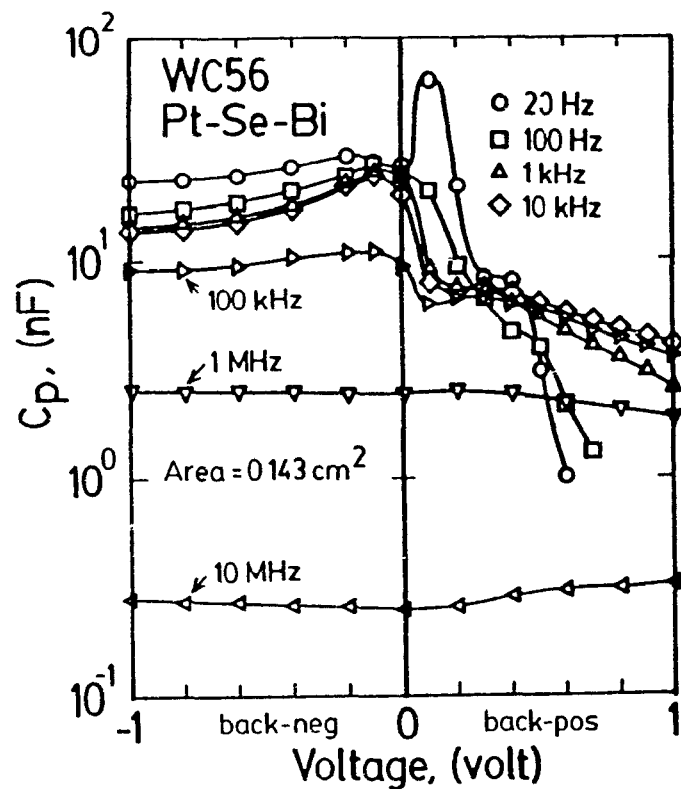


Fig.6.25. Capacitance versus voltage plot for Pt-Se-Bi sample WC56 measured at different frequencies.

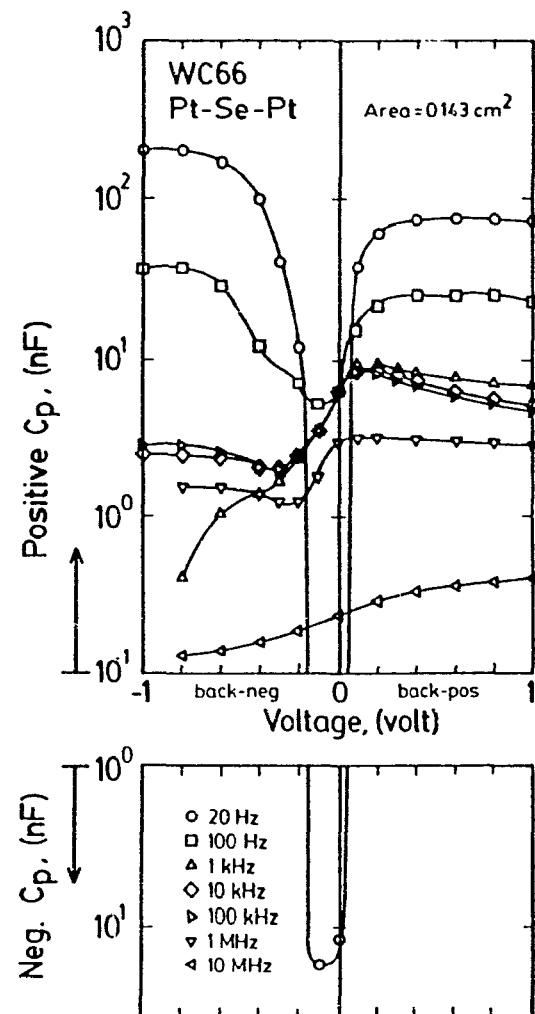


Fig.6.26. Capacitance versus voltage plot for Pt-Se-Pt sample WC66 measured at different frequencies.

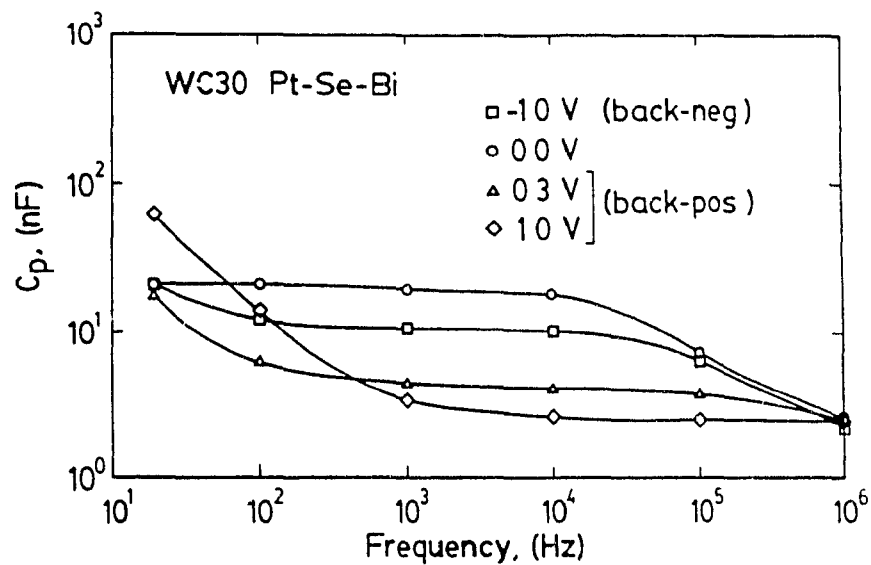


Fig.6.27. Capacitance versus frequency plot for Pt-Se-Bi sample WC30 at different bias voltages.

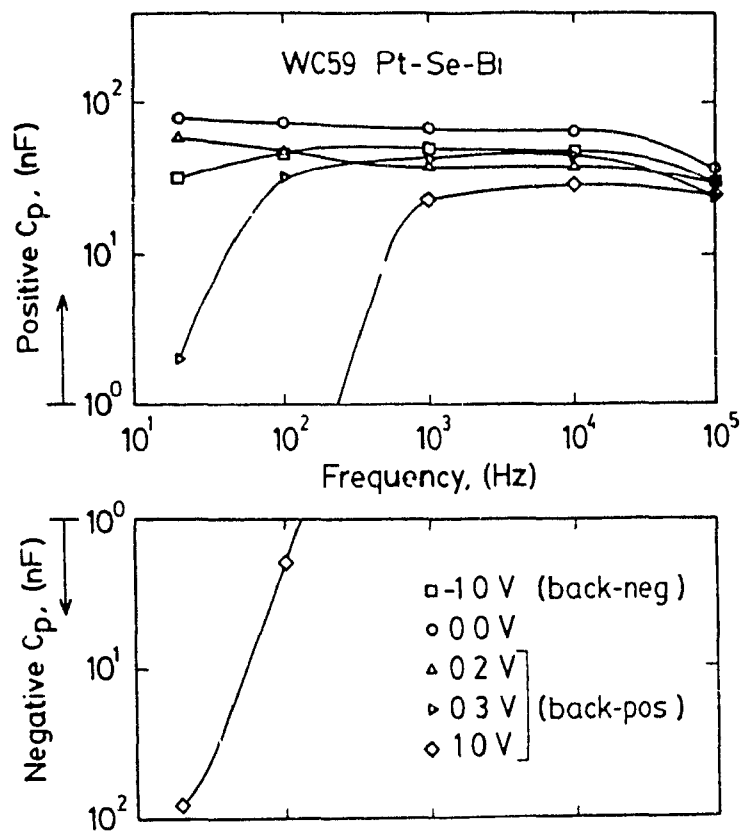


Fig.6.28. Capacitance versus frequency plot for Pt-Se-Bi sample WC59 at different bias voltages

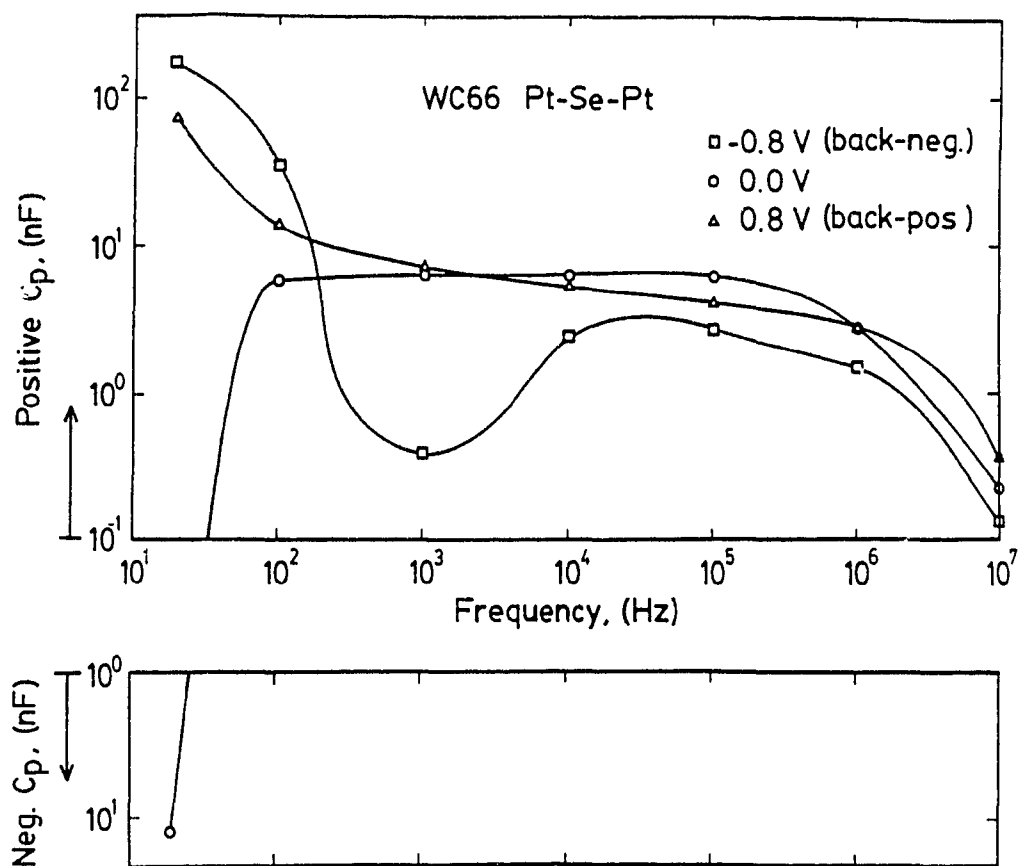


Fig.6.29. Capacitance versus frequency plot for Pt-Se-Pt sample WC66 at different bias voltages.

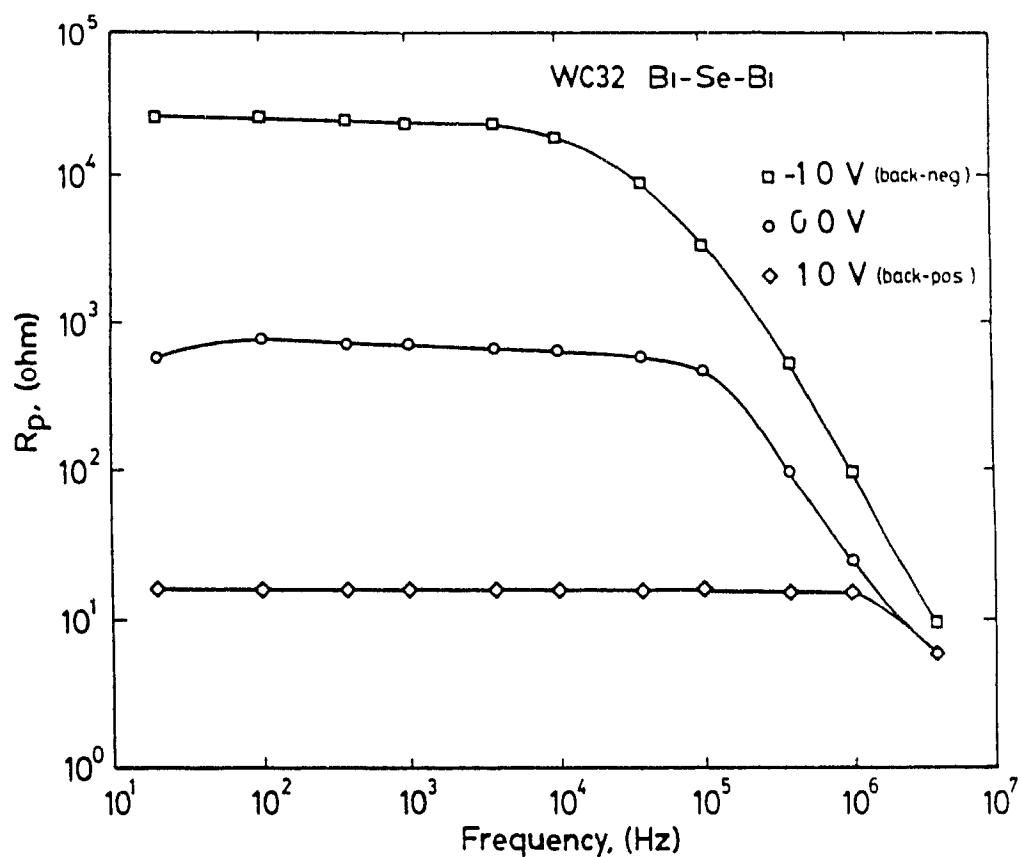


Fig.6.30. Resistance versus frequency plot for Bi-Se-Bi sample WC32 at different bias voltages.

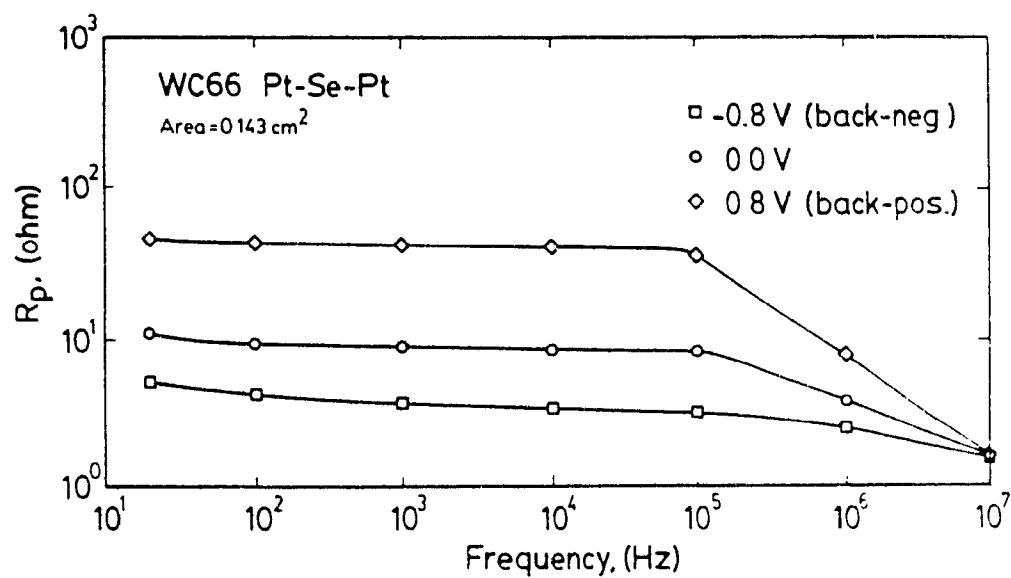


Fig.6.31. Resistance versus frequency plot for Pt-Se-Pt sample WC66 at different bias voltages.

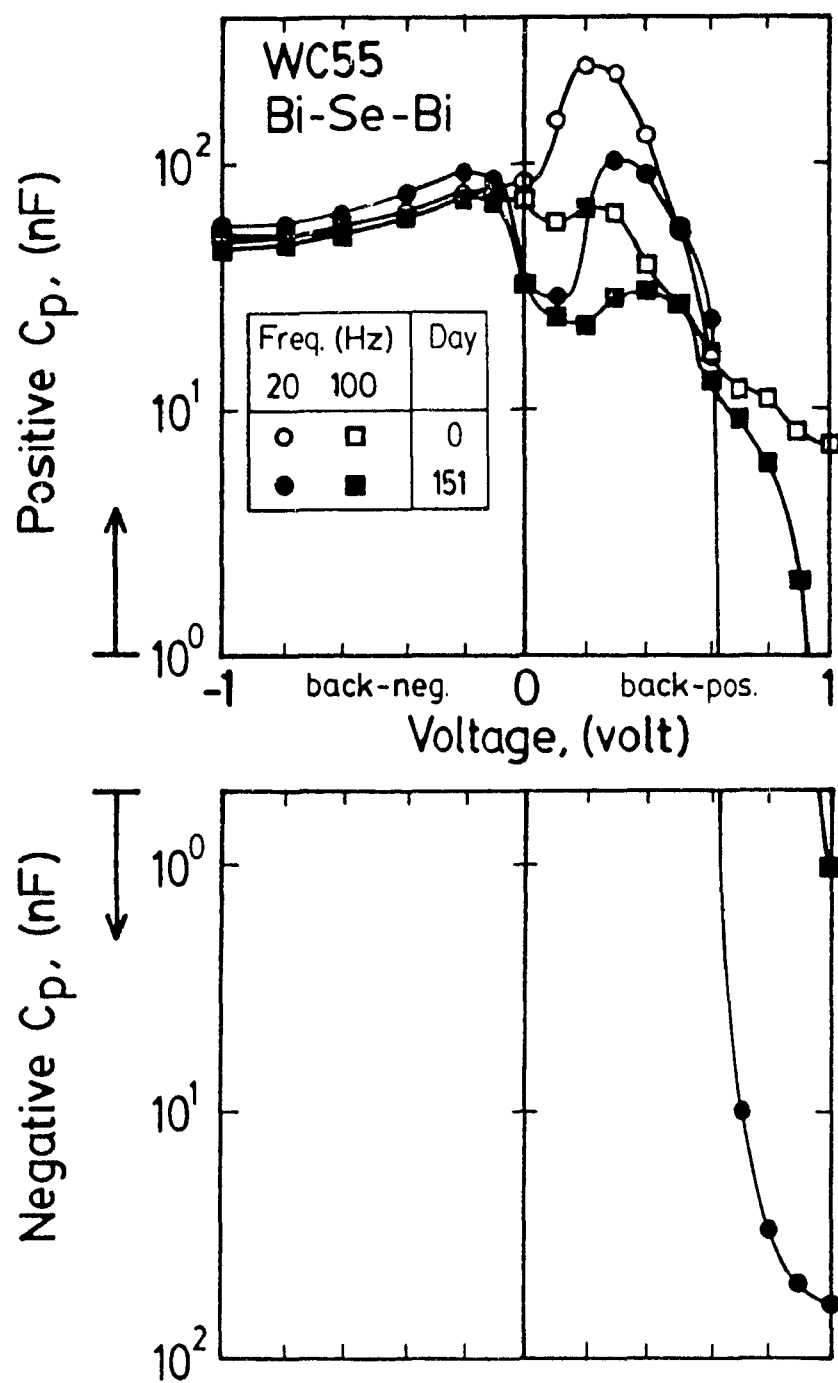


Fig.6.32. Capacitance versus voltage plot for Bi-Se-Bi sample WC55 on day-0 and day-151 measured at 20 and 100 Hz.

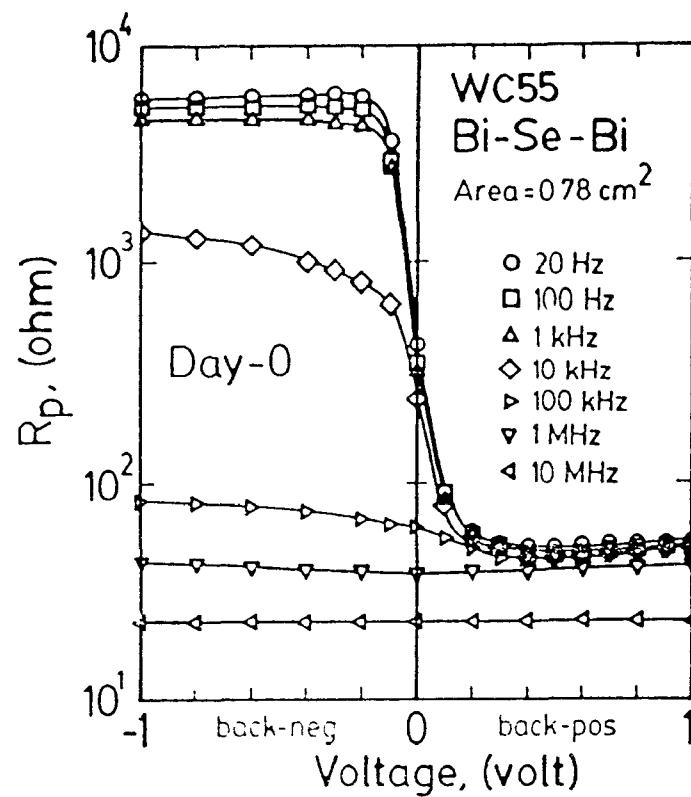


Fig.6.33. Resistance versus voltage plot for Bi-Se-Bi sample WC55 on day-0 at different frequencies.

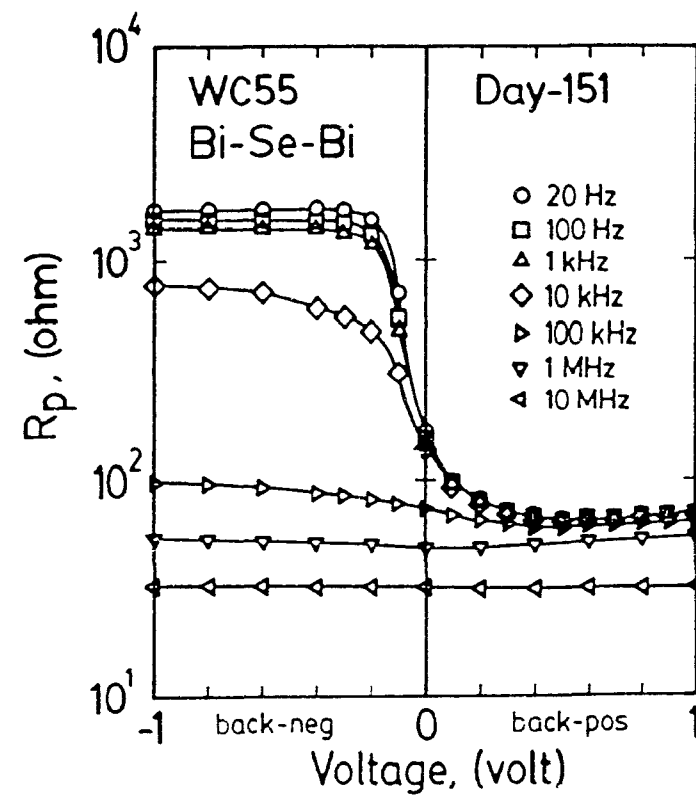


Fig.6.34. Resistance versus voltage plot for Bi-Se-Bi sample WC55 on day-151 at different frequencies.

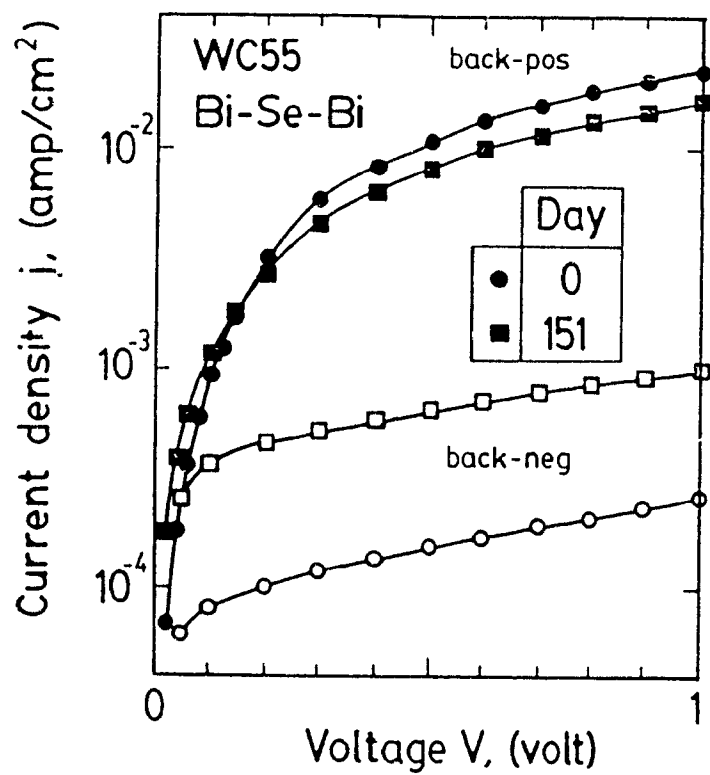


Fig.6.35. Plot of current-density against voltage for Bi-Se-Bi sample WC55 on day-0 and day-151.

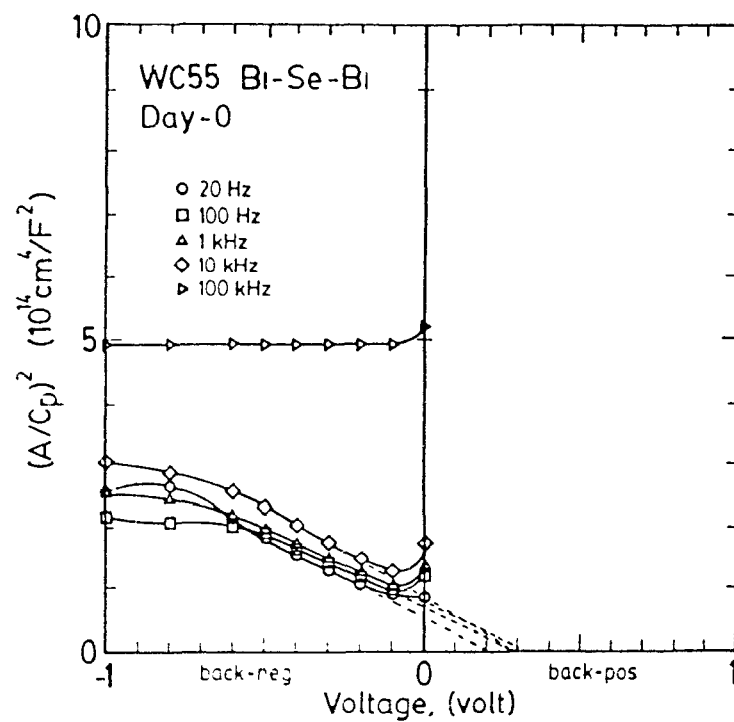


Fig.6.36. Mott-Schottky plot for Bi-Se-Bi sample WC55 on day-0 at different frequencies.

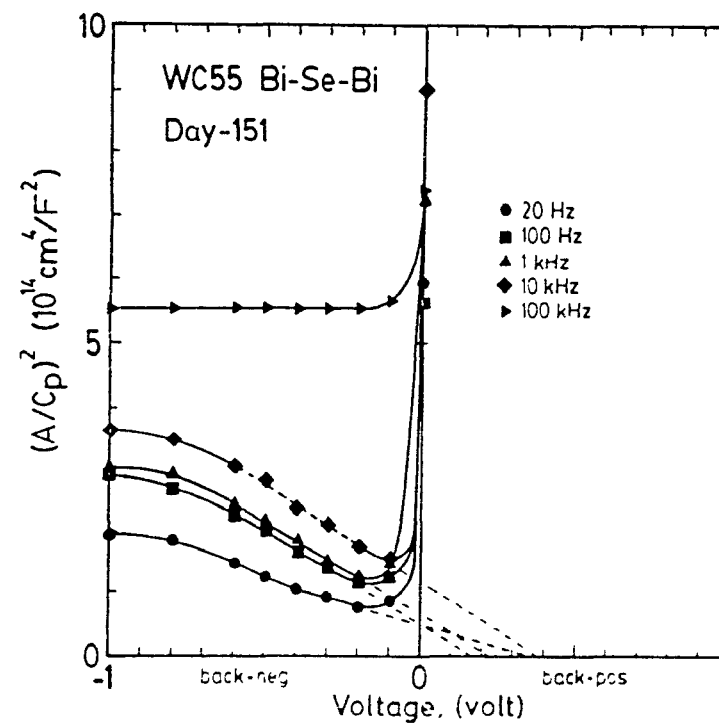


Fig.6.37. Mott-Schottky plot for Bi-Se-Bi sample WC55 on day-151 at different frequencies.

7. BARRIER HEIGHTS OF Se-METAL CONTACTS

7.1 Introduction

As is evident from the results given in chapters 5 and 6, the characteristics of the Se-Tl, Se-Bi and Se-Pt diodes are quite different. These differences arise in large part as a result of the difference in their barrier heights. It is therefore very important to determine this quantity and this is attempted in this chapter. The barrier heights of the Se-metal contacts in this work were determined from j -V, C_p -V and photoelectric measurements, as previously described in chapter 2. In the present chapter, the results of these measurements are presented. A summary of these results are tabulated in Table II, where the barrier height values, determined from these measurements, for Tl, Bi and Pt contacts to Se are listed.

7.2 Barrier Heights from j -V Measurements

The barrier height of a Schottky junction can be determined from forward j -V measurements, particularly from the intercept value J_0 , as explained in chapter 2. In this section, the barrier heights for a representative Se-Tl sample, WC44 and a representative Se-Bi sample, WC32, are determined from these measurements. A reliable barrier height value for a Pt contact to Se could not be obtained from the j -V data and so, Pt results are not presented here.

In Fig.7 1, the forward j -V characteristics for two samples, WC44, a Se-Tl sample and

WC32, a Se-Bi sample are shown. Both curves display a straight line region around 0.1 volt corresponding to an exponential j - V dependence. These straight line regions are seen to have extrapolated intercepts on the j -axis of about 3×10^{-8} and 4.5×10^{-4} amp/cm² for the Se-Tl and Se-Bi samples respectively. Assuming these values correspond to j_0 , the barrier heights are found to be 0.85 and 0.62 eV respectively. These values, as well as those determined for other samples from their respective j - V plots (not shown), are listed in Table II(a) column 2 for Tl samples and Table II(b) column 2 for Bi samples.

7.3 Barrier Heights from Capacitance Measurements

As was already mentioned in chapter 2, the barrier height of a Schottky junction can be determined from C_p - V measurements that are plotted in the form of a Mott-Schottky plot. In this section Mott-Schottky plots for Se-Tl, Se-Bi and Se-Pt junctions are presented, along with their corresponding barrier heights, as listed in Table II. Though the C_p - V measurements were carried out at many different frequencies for a given sample, only the 100 Hz or 1 kHz data are presented here, as these frequencies provided the most consistent results. Note that there was little difference between the 100 Hz and 1 kHz results for a given sample and so, often, the data for only one of these frequencies is presented here. The characteristics shown for the Tl samples are all for 100 Hz only, while those for the Bi counterelectrode samples are for 1 kHz.

Mott-Schottky plots for the Se-Tl samples are shown in Figs. 7.2 and 7.3 for 100 Hz. It is seen that most of the curves have an intercept, V_p , of between 0.5 and 0.65 volt. It is also

found that their slopes range between about 1×10^{14} and $5 \times 10^{14} \text{ cm}^{-4} \text{ F}^{-2} \text{ V}^{-1}$, corresponding to carrier concentrations of between about $1.5 \times 10^{17} \text{ cm}^{-3}$ and $3.5 \times 10^{16} \text{ cm}^{-3}$ respectively. Despite their apparently large spread in values, these concentrations, in turn, correspond to Fermi levels in the bulk Se situated in a relatively narrow zone between about 0.13 eV and 0.16 eV above the valence band edge. This assumes that the valence band density of states can be taken as $2.5 \times 10^{19} \text{ cm}^{-3}$ for Se. From the intercept values and the Fermi level positions above the valence band, the barrier height for most of the samples was found to lie between about 0.65 and 0.80 eV, as listed in Table II(a) column 3. Only 2 out of the 13 Se-Tl samples with values listed here have barrier heights outside this range, namely WC46, the sample made with undoped Se and WC38. These samples display Mott-Schottky curves with the two lowest slopes and the two smallest intercept values. Furthermore, the curve for WC46 is not particularly straight, so the extrapolated intercept shown is somewhat arbitrary.

The 1 kHz Mott-Schottky curves for the Se-Bi (Bi counterelectrode) samples are shown in Figs. 7.4 and 7.5. It is seen that for the most part the curves have an intercept between 0.1 and 0.2 volt. Like the curves for the Tl samples, these also show a spread in slope and correspond to carrier concentrations between about $1.5 \times 10^{17} \text{ cm}^{-3}$ and $2.5 \times 10^{16} \text{ cm}^{-3}$. Once again, despite this spread in concentration values, the Fermi level position in the bulk Se corresponding to these concentrations is found to lie in a relatively narrow range, between about 0.13 eV and 0.17 eV above the valence band edge. The barrier heights determined from these values are listed in Tables II(b) and II(c) column 3, where it is seen that most of them fall between about 0.25 eV and 0.35 eV. The one exception, that for sample WC55, is somewhat higher at about 0.42 eV, as the curve for this sample shows an unusually high

intercept at 0.27 volt. It is also of interest to note that the Se-Bi samples with Pt back-contacts, WC30, WC56 and WC59, all show barrier height values (Table II(c) column 3) which are not all that different from those of the Bi back-contact samples. However, it is also seen from Figs. 7.4 and 7.5 that, these Pt back-contact samples show curves with the smallest slopes (though, they are not unusually small) of all the Se-Bi samples.

Fig.7.6 shows the Mott-Schottky plot for sample WC29, a Bi-Se-Pt structure. In chapter 6 it was seen that a Pt counterelectrode behaves like a low resistance ohmic contact. Therefore, the straight line portion of the curves in the back-positive direction in this figure correspond to the capacitance of the Bi-Se back contact rather than that of the Pt counterelectrode. These curves are quite interesting, in that, they show a slope of about $4 \times 10^{14} \text{ cm}^2 \text{ F}^{-2} \text{ V}^{-1}$, which is about the same as that observed for the Bi counterelectrode samples in Figs. 7.4 and 7.5. However, their intercepts, at about 0.40 volt for 100 Hz and 0.25 volt for 1 kHz, are somewhat higher than those seen for the Se-Bi samples. Hence, the barrier height values found for this sample are also somewhat higher, at about 0.55 eV and 0.40 eV for the 100 Hz and 1 kHz curves respectively. However, these values are not listed in Table II.

The Mott-Schottky plot for sample WC66, a Pt-Se-Pt structure, is shown in Fig.7.7 where 4 curves for the frequencies 1 kHz, 10 kHz, 100 kHz and 1 MHz are seen. As mentioned earlier, a Pt counterelectrode on Se acts like a low resistance ohmic contact and so the curves in this figure correspond to the capacitance at the Pt-Se back-contact. While the curves for 1 kHz and 1 MHz have rather large intercepts, those for 10 and 100 kHz are seen to be more consistent at about 0.1 V. It is also found that the slopes of the 10 and 100 kHz

curves correspond to a carrier concentration value of about $2 \times 10^{16} \text{cm}^{-3}$. This concentration, in turn, corresponds to a Fermi level in the bulk Se of about 0.18 eV above the valence band. Thus, the barrier height of this Pt-Se back-contact was found from the 10 and 100 kHz curves to be about 0.28 eV, as indicated in Table II(d) column 3.

7.4 Barrier Heights from Photoelectric Threshold Measurements

The barrier height of a Schottky junction can also be determined from photoresponse characteristics that are in the form of a Fowler plot, as explained in chapter 2. This section presents such results for several Se-Bi samples and represents the first time this method has been used in this laboratory to determine barrier heights.

The Fowler curves for two samples, WC60 and WC63, both on day-0, are shown in Fig.7.8. The intercepts of the straight line region of each curve at lower energies are seen to be relatively close to each other, corresponding to Schottky barrier heights of 0.67 and 0.70 eV respectively. These barrier heights, along with those found for other Se-Bi samples using this method, are listed in Table II(b) column 4, where it is seen that most of the values lie between 0.67 and 0.75 eV. Sample WC55, however, shows curves in Fig.7.9 for the two slit widths of 0.3 and 0.6 mm, each having a straight line portion between about 1.1 and 1.5 eV with an intercept value at 0.93 eV. This intercept is considerably larger than those seen in Fig.7.8. However, it was obtained from measurements made with photon energies between 1.1 and 1.5 eV. The intercept values between 0.67 and 0.75 eV listed in Table II, on the other hand, were all obtained from measurements made with lower photon energies

between about 0.8 and 1.2 eV. The Fowler curves for WC57 in Fig.7.10 also show an intercept value at 0.93 eV from the higher energy points but it should be noted that the curve for the 0.6 mm slit width shows a tendency to a second straight line region, at lower energies, between about 0.8 and 0.9 eV, which has an intercept value at 0.70 eV. Thus, there appear to be two different photothreshold energies present in this sample, one at about 0.7 eV, which corresponds to those seen for the majority of the samples in this study, while the other one, at about 0.93 eV, corresponds to that seen for sample WC55 at higher energies. Note that a 0.70 eV threshold value was obtained with both a NaCl prism (Fig.7.8 for sample WC63) as well as a SiO₂ prism (Fig.7.10 for sample WC57). This consistency from one prism to the other is more clearly seen in Fig.7.11, where the Fowler curves for WC57 on day-100 are shown. Both curves have a straight line portion between about 1.1 and 1.3 eV with an intercept at 1.00 eV. Note also, however, that the NaCl curve has a second straight line region between about 0.85 and 1.0 eV with an intercept at 0.72 eV. When the SiO₂ prism was used, the photocurrent values were too small to measure in this energy range and so the corresponding points for this curve are absent from the plot. It is of further interest to note from Figs. 7.10 and 7.11 that the lower energy intercept has remained at about 0.7 eV from day-0 to day-100, whereas the higher energy intercept has shifted up from 0.93 eV on day-0 to 1.00 eV on day-100.

7.5 Discussion

A plot of the average of the barrier heights, ϕ'_{bp} , determined for each metal, Tl, Bi and

Pt, versus the metal work function, ϕ_M , is shown in Fig.7.12. The points in this plot correspond to values obtained from j-V and C-V measurements. In addition to the points for the metals used in this work, points determined by the candidate for a Mg counterelectrode sample are also shown from previous work. Table III lists some of the results of this previous work. It is seen from the plot that, in general, the barrier height decreased as the work function increased for a given measurement technique, either j-V or C_p -V. This decrease in barrier height with work function was at least qualitatively consistent with that found from capacitance measurements by Chan (dashed curve in the figure) and suggests that the Fermi level in the semiconductor was not pinned at the interface by the presence of surface states [9] [10].

It is also of interest to note that, as seen from Tables II and III, there was a variation of barrier height values for a given counterelectrode metal depending on the method of determination used. The barrier heights determined from j-V characteristics were frequently higher than those determined with C_p -V measurements. The barrier heights determined from j-V measurements with variation of temperature, also known as activation energy measurements, from previous work shown in Table III, gave barrier height values that were different from those determined by both the room temperature j-V and the C_p -V measurements. The Fowler plots gave barrier heights for the Se-Bi contact of about 0.7 eV, which was higher than that obtained from the other methods, though it was not much higher than the 0.63 eV value obtained from the j-V measurements. If this 0.7 eV barrier height value is, in fact, correct and if the voltage intercept value in the Mott-Schottky plots is also the actual built-in potential of the junction, then it suggests that the Fermi level energy in

the bulk Se semiconductor was actually about 0.5 eV above the top of the valence band, instead of only about 0.15 eV obtained from the $(A/C_p)^2$ -V slopes, at least for the Bi samples. This corresponds to a free carrier concentration of only about 10^{11}cm^{-3} , which was only about 10^{-5} that of the doping concentration N_A found from the slope of the Mott-Schottky plots. Thus, it is speculated that the free carrier concentration in the Se was far less than the apparent acceptor concentration and, it is further speculated that, a high concentration of acceptor-like trapping centres in the Se layer was responsible.

The barrier height values determined from the j-V and C_p -V data were seen to be closer to each other for the Tl samples (0.05 eV difference) than for the Bi counterelectrode samples (0.3 eV difference). This may have been because of back-contact effects. These effects would have been less apparent for Tl samples because of the large Se-Tl barrier height, which resulted in the front contact dominating the reverse characteristics. On the other hand, Bi samples had a somewhat lower front contact barrier height which was not so dominant over the effects of the back-contact. Thus, the barrier heights determined from the C_p -V data for the Bi front-contact samples may have been unusually low also because of the influence of the back-contact.

It was also seen in the Fowler plots that two straight line regions of the Fowler curve were present, giving two distinct intercepts. It is speculated that, while the smaller intercept was due to the barrier height of the Se-Bi interface, the larger one was due to the presence of a deep level in the Se at an energy near the middle of the gap. Holes from this level in the depletion region of the Se layer may have been excited into the valence band and swept into the bulk Se by the high field of the depletion region. Thus, an additional contribution to the

photocurrent would have been made and this resulted in a change in slope of the Fowler curve that corresponded to a second apparent photothreshold value. The additional photoresponse from this level was seen in this work to be comparable to that from the metal itself. This would suggest that a very high concentration of trapping states was present. It was also seen that the higher intercept shifted up somewhat with storage time. It is further speculated that the deep level was the result of the diffusion of Bi into the Se. The energy of the level thus changed as the Bi atoms tended toward an equilibrium level between the Se atoms of the crystal lattice.

Of course, the photoelectric measurement technique had some degree of error associated with it. The largest source of error came from the fact that the incident beam was not actually monochromatic. In fact, as mentioned earlier in chapter 4, the beam was made up of a range of wavelengths $\Delta\lambda$, amounting to about 10% of the middle wavelength. This corresponded to an approximate spread in the E_{ph} value of about $\pm 5\%$. Other sources of error included the wavelength calibration, accurate to $0.01 \mu m$ (less than 2% error) in the wavelength range used here and the photocurrent value I_{ph} , which was accurate to less than 5%. It is seen from Table II(b) column 4 that, 6 out of 7 Se-Bi samples showed barrier height values within $\pm 4\%$ of 0.71 eV, which is consistent with the limits of accuracy of this photoelectric technique. It is also seen that, despite a change of slit width from 0.3 to 0.6 mm, which corresponded to a doubling of the wavelength interval $\Delta\lambda$, the intercept of the Fowler curve for each slit width was the same. This was consistent with the fact that both slit widths corresponded to quite narrow wavelength intervals anyway (less than 10%). Furthermore, both the NaCl and the SiO₂ prisms gave the same intercept value for a given

sample on a given day. Thus, the barrier height values determined were quite consistent, despite changes in the monochromator prism. A contribution to the photocurrent may have also come from the Bi-Se back contact junction. This is because the long wavelength photons not absorbed at the front contact, with energies less than the gap energy of Se, would pass right through the Se layer to the Bi-Se back-contact junction. A photocurrent at this junction would also result causing an additional source of error. However, it is believed to be insignificant from photoelectric tests (not presented in this thesis) made on Bi-Se-Pt samples WC64 and WC65. Here, the Pt counterelectrode behaved like an ohmic contact and under illumination the photocurrent of the samples was immeasurably small, even under strong white light.

The three main methods of barrier height determination described in chapter 2 were used and while these theoretically should have yielded the same values, in practice there were many experimental difficulties which rendered the barrier height values uncertain. Until ways of overcoming these are found or until realistic corrections can be made, any values determined must be taken as only preliminary.

Table II(a)**Se-Tl samples**

sample number	ϕ_{bp} (eV) from	
	j-V	Mott-Schottky
WC35	0.82	--
36	0.74	--
37	0.82	0.77
38	0.80	0.51
39	0.82	0.77
40	0.82	0.77
41	0.82	0.77
43	0.82	0.76
44	0.83	0.66
45	0.81	0.72
46	0.74	0.60
48	0.77	--
49	0.82	0.71
52	0.83	--
53	0.84	--
54	0.82	0.70
61	0.82	0.67
62	0.82	0.70
AVE.	0.81	0.76

Table II(b)**Bi-Se-Bi samples**

sample number	ϕ_{bp} (eV) from		
	j-V	Mott-Schottky	Fowler
WC24	--	0.35	--
26	--	0.23	--
27	--	0.27	--
32	0.61	0.34	0.70
33	0.63	0.35	0.75
34	0.61	0.29	0.72
42	0.66	--	--
55	0.65	0.42	0.93
57	0.64	--	0.70, 0.93
60	0.62	0.33	0.67
63	0.62	0.30	0.70
AVE.	0.63	0.32	0.71

Table II(c)**Pt-Se-Bi samples**

sample number	ϕ_{bp} (eV) from	
	j-V	Mott-Schottky
WC30	--	0.27
56	--	0.26
58	0.62	--
59	--	0.28

Table II(d)**Pt-Se-Pt samples**

sample number	ϕ_{bp} (eV)	
	from	
	j-V ^(a)	Mott-Schottky ^(b)
WC31	0.5	0.47
WC66	0.5	0.28

(a) Estimated barrier height values.

(b) Barrier heights here were determined from back-positive C_p -V data.

Table III**Results from previous studies by the author.**

structure	sample number	ϕ_{bp} (eV)		
		from		
		j-V	Mott-Schottky	(j-V) vs T
Bi-Se-Tl	WC16	0.80	0.76	0.55
Bi-Se-Bi	WC14	0.62	0.36	0.45
Bi-Se-Mg	WC18	0.92	1.02	0.78

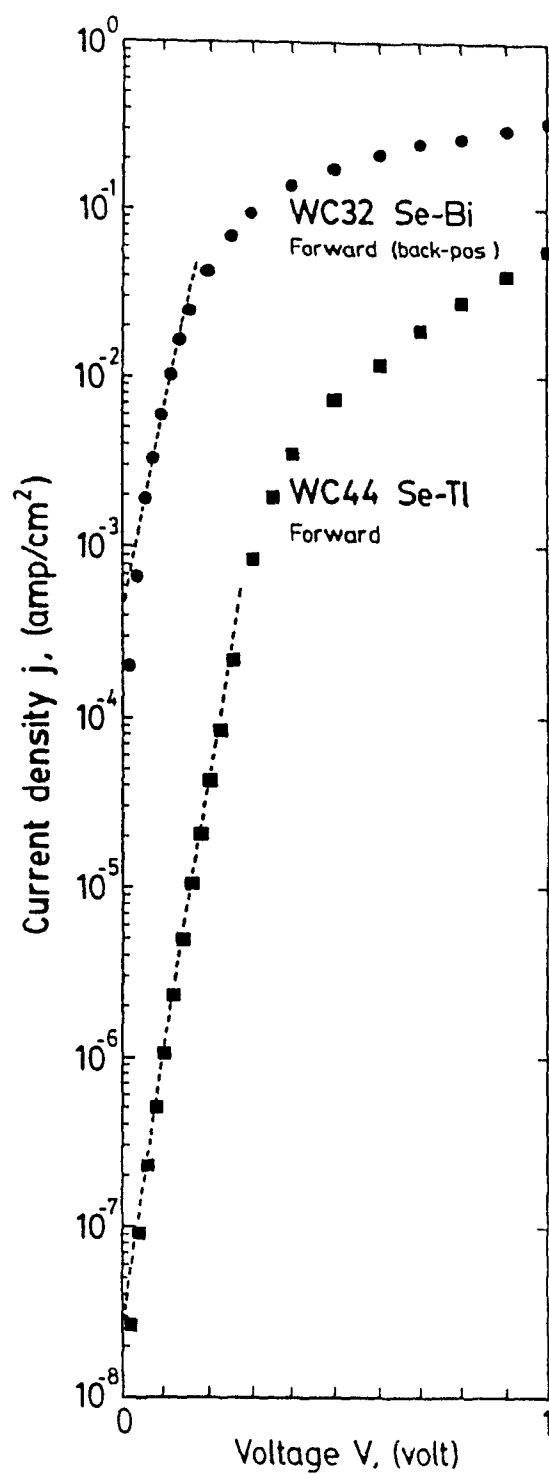


Fig.7.1. Plot of forward (back-positive) current-density against voltage for Se-Tl sample WC44 and Bi-Se-Bi sample WC32.

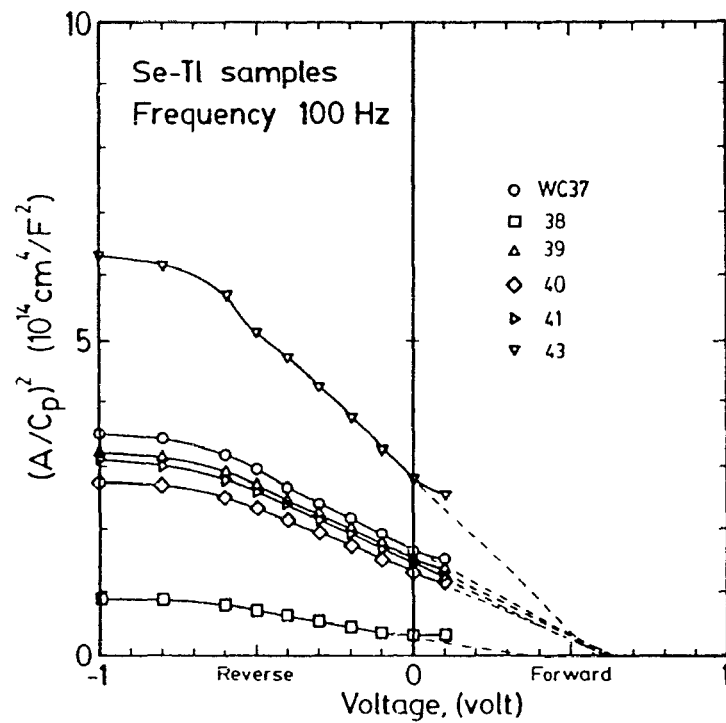


Fig.7.2. Mott-Schottky plot for Se-Tl (Tl counterelectrode) samples WC37, WC38, WC39, WC40, WC41 and WC43 at 100 Hz.

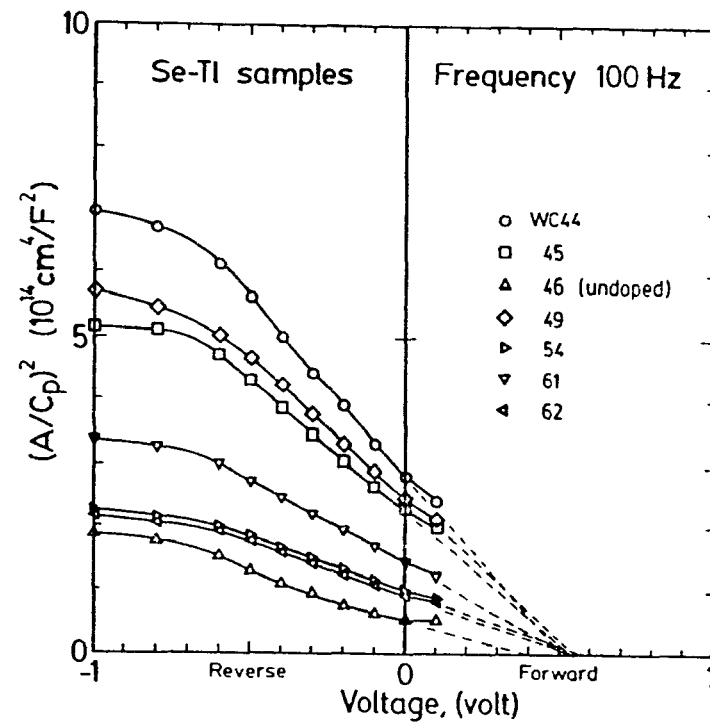


Fig.7.3. Mott-Schottky plot for Se-Tl (Tl counterelectrode) samples WC44, WC45, WC46, WC49, WC54, WC61 and WC62 at 100 Hz.

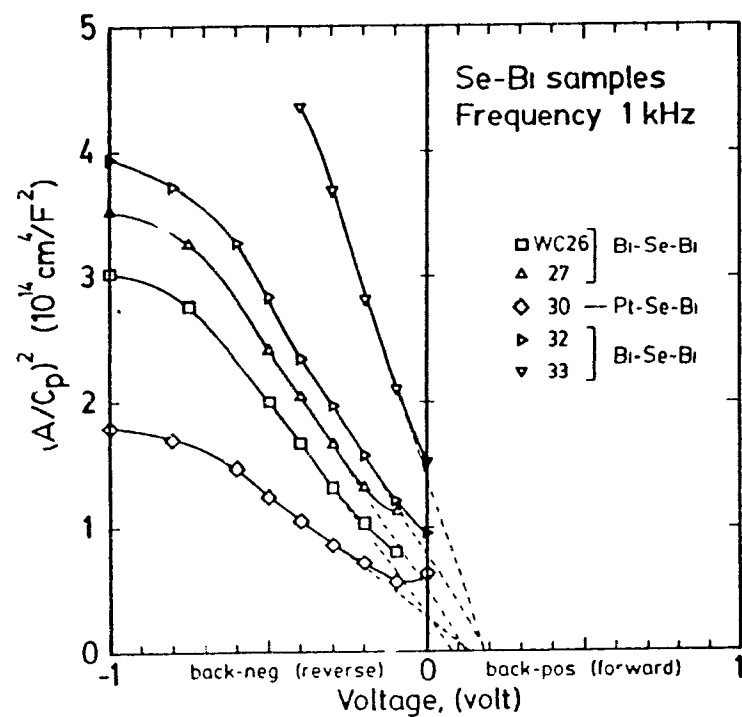


Fig.7.4. Mott-Schottky plot for Se-Bi (Bi counterelectrode) samples WC26, WC27, WC30, WC32 and WC33 at 1 kHz.

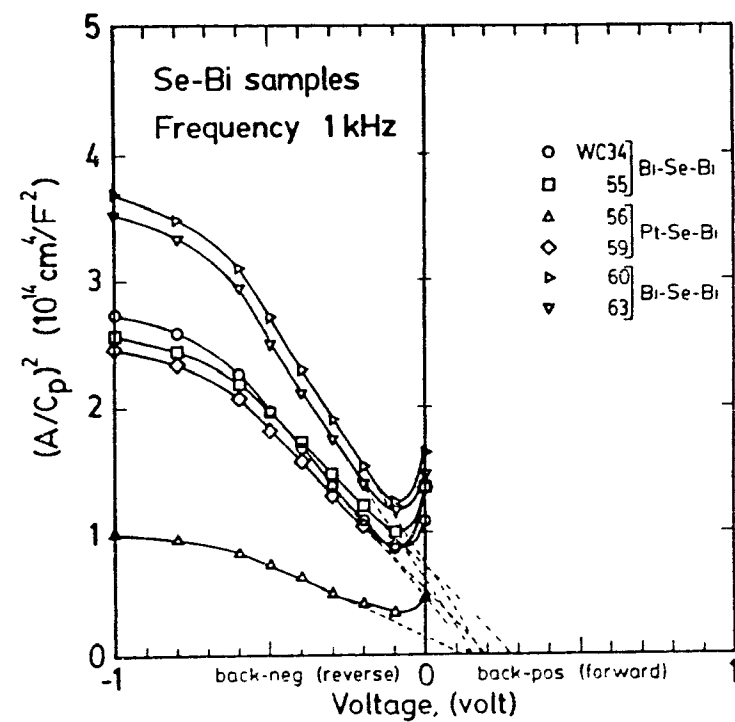


Fig.7.5. Mott-Schottky plot for Se-Bi (Bi counterelectrode) samples WC34, WC55, WC56, WC59, WC60 and WC63 at 1 kHz.

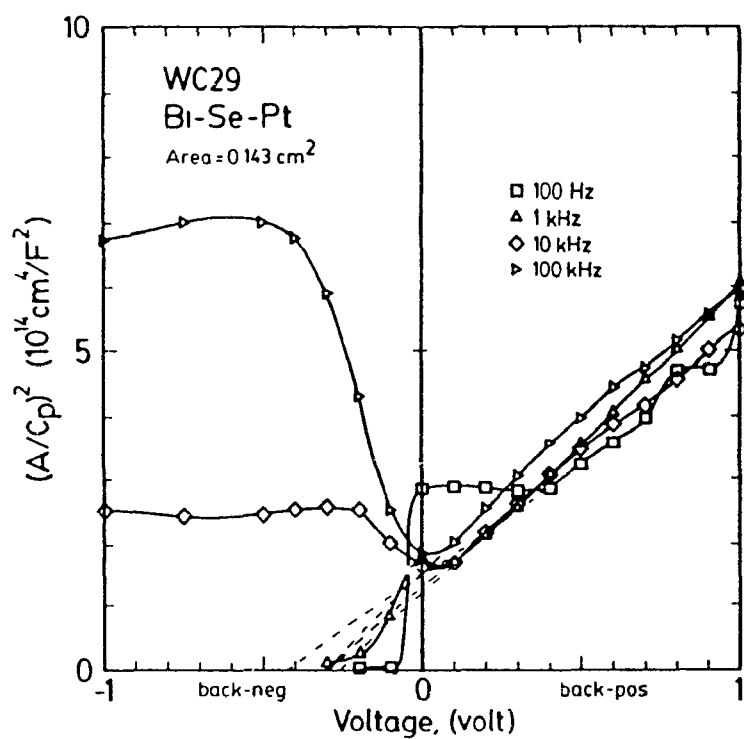


Fig.7.6. Mott-Schottky plot for Bi-Se-Pt sample WC29 at different frequencies.

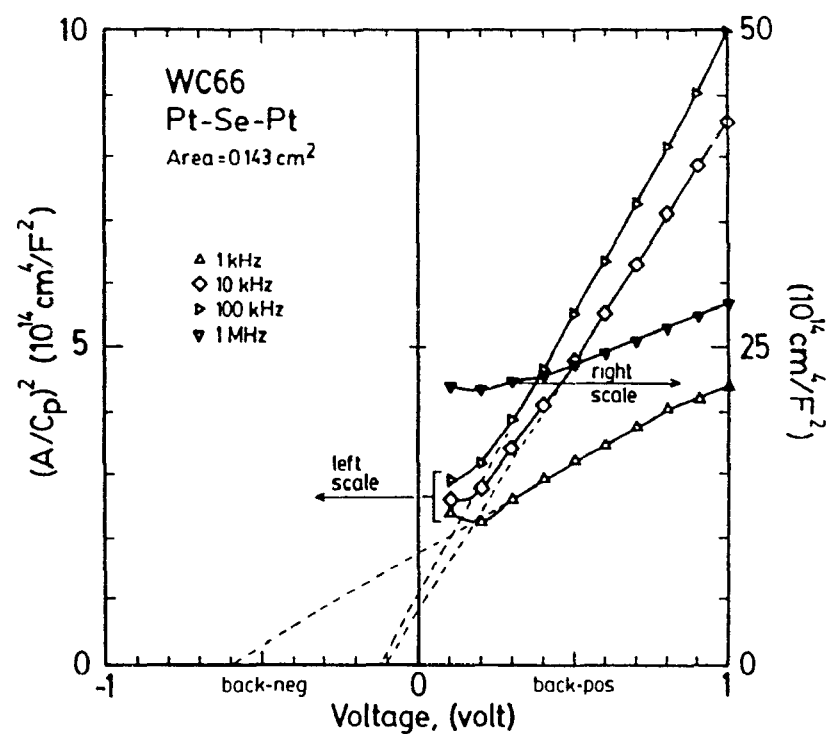


Fig.7.7. Mott-Schottky plot for Pt-Se-Pt sample WC66 at different frequencies.

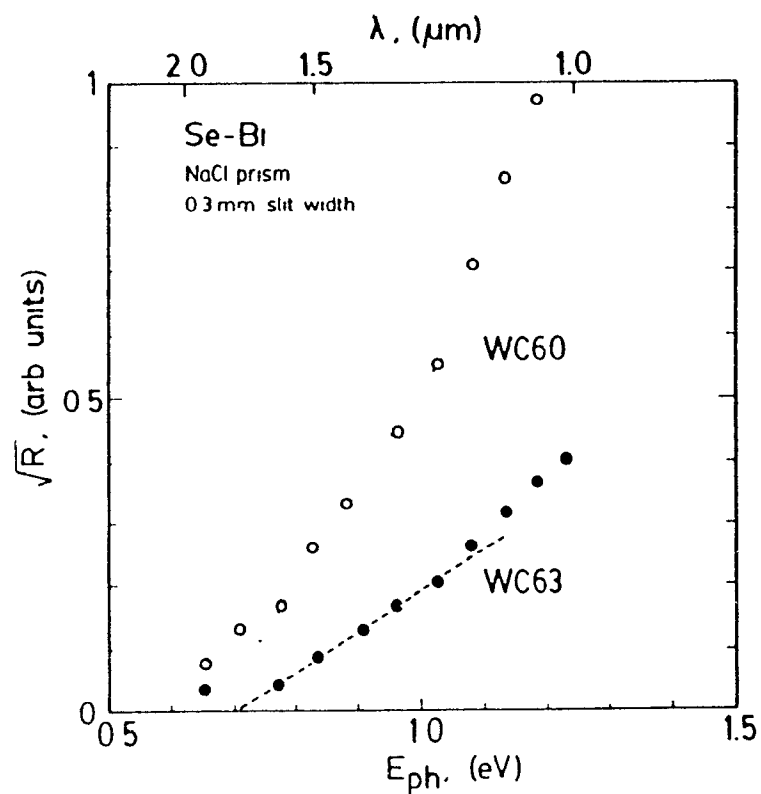


Fig.7.8. Fowler plot for Bi-Se-Bi samples WC60 and WC63 on day-0. The Littrow type monochromator had an SiO_2 prism and a 0.3 mm entrance and exit slit width.

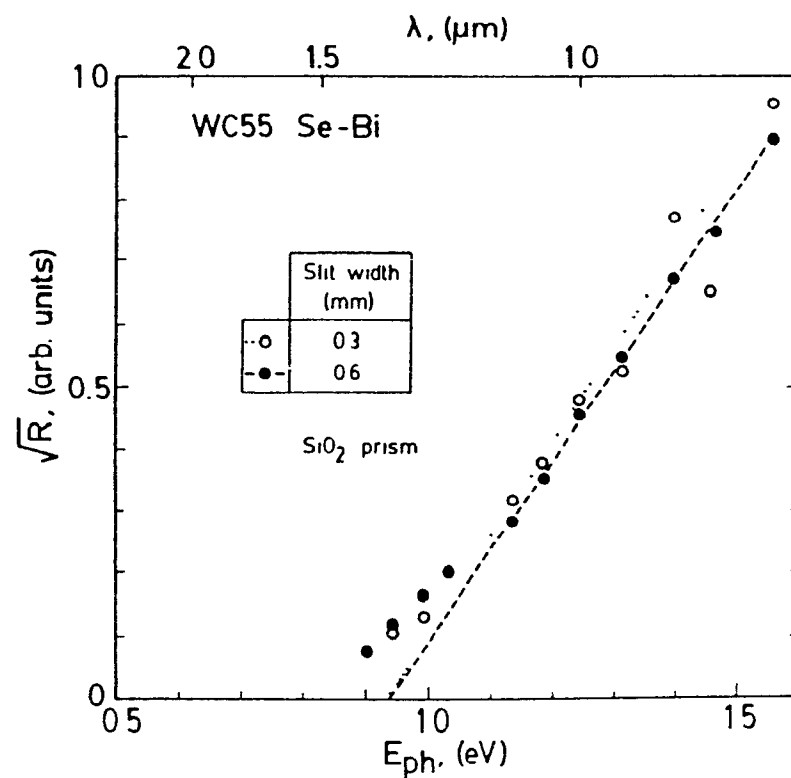


Fig.7.9. Fowler plot for Bi-Se-Bi sample WC55 on day-0 for the two monochromator slit widths of 0.3 and 0.6 mm. The Littrow type monochromator had an SiO_2 prism.

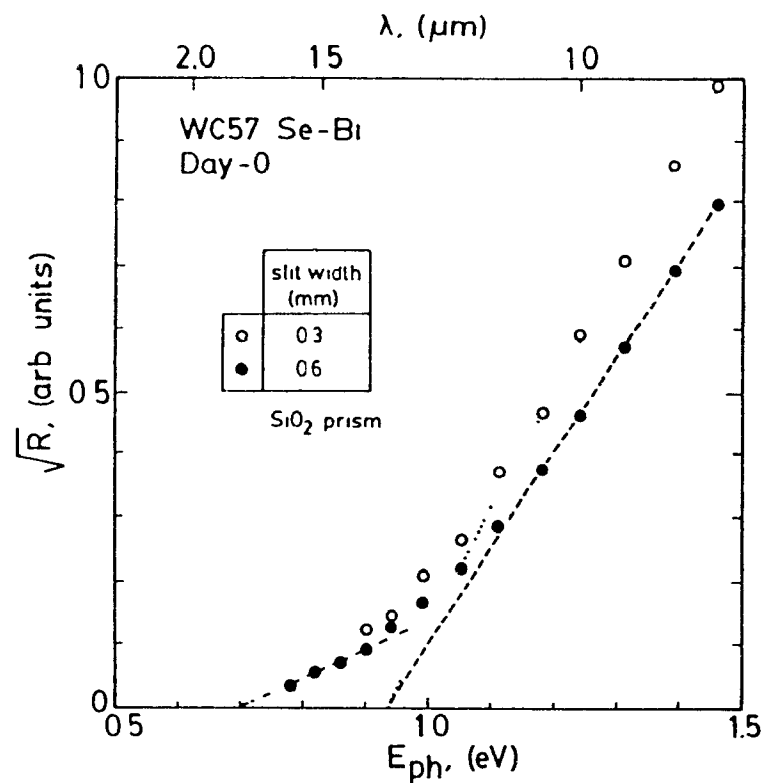


Fig.7.10. Fowler plot for Bi-Se-Bi sample WC57 on day-0 for the two monochromator slit widths of 0.3 and 0.6 mm. The Littrow type monochromator had an SiO₂ prism.

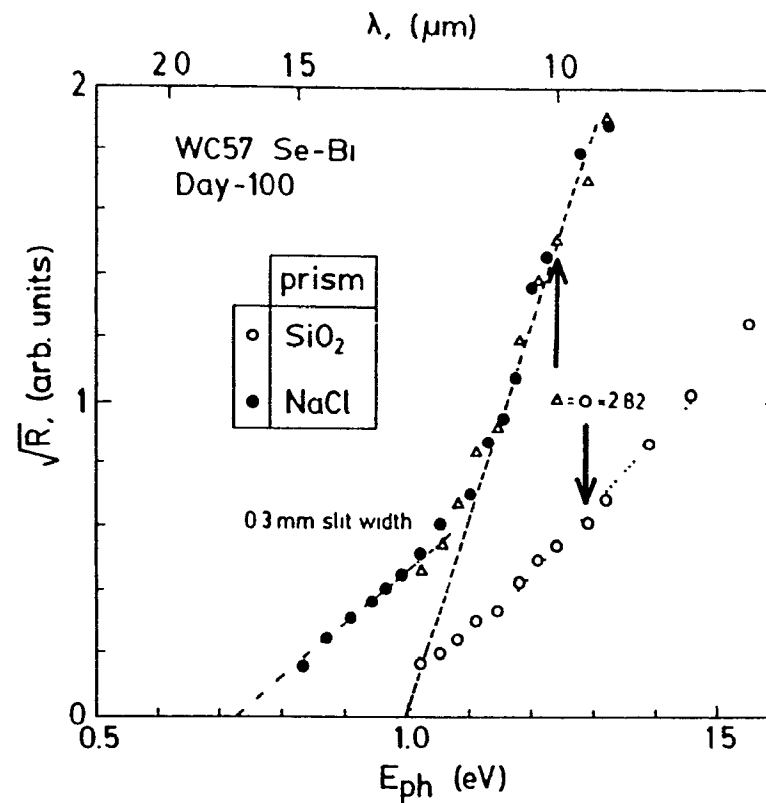


Fig.7.11. Fowler plot for Bi-Se-Bi sample WC57 on day-100 for the two monochromator prisms SiO₂ and NaCl and a slit width of 0.3.

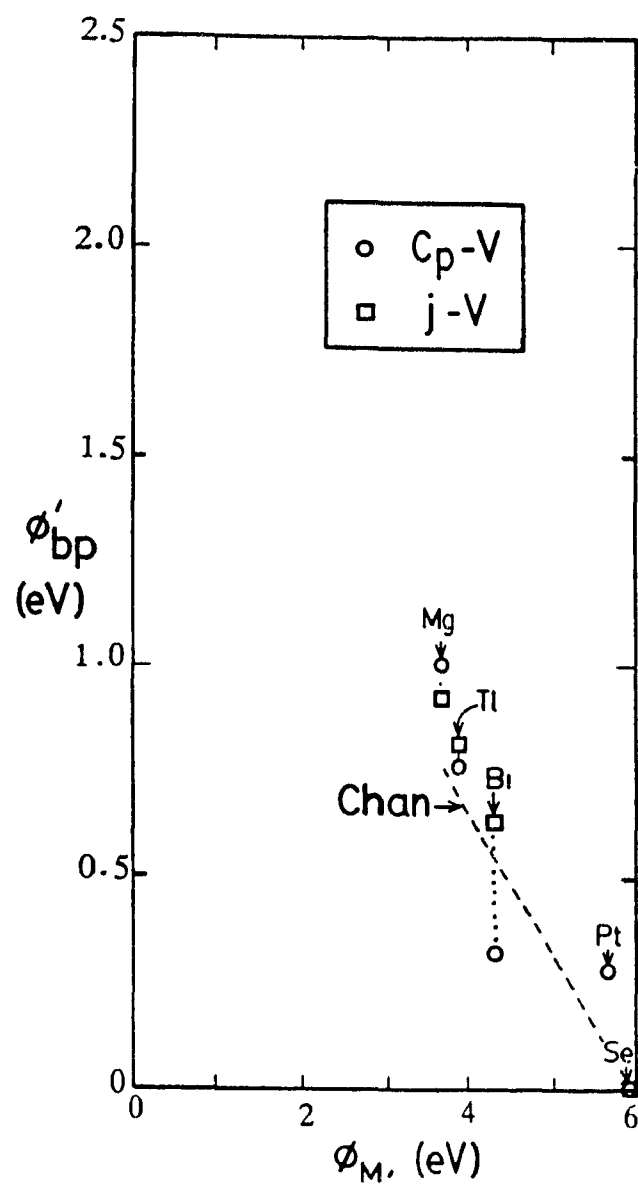


Fig.7.12. Plot of barrier height determined from j-V and C_p -V data against reported metal work function. Shown also is the dependency curve found from Chan's results [3]

8. GENERAL DISCUSSION

While brief discussions of the results were given at the end of each of the last three chapters, it is helpful in the present chapter to present a more comprehensive review of the results of the thesis as a whole. As is the case in many intensive research undertakings, the study provides some answers but also raises many more questions.

The most interesting result of this thesis is that diodes of this work showed non-Faraday inductive behaviour at low frequencies. This inductive effect, it is believed, was the result of high level injection into a thin semiconducting selenide layer that formed with storage time between the contact metal (i.e. the rectifying contact, which was the front contact for the Tl and Bi counterelectrode samples and the Pt back contact for the Pt-Se-Pt samples) and the selenium, as illustrated in Fig.8.1. It is suspected that the formation of this layer was accelerated in some cases by inadvertent heating of the sample during the fabrication process. This inductive effect was observed to be strongest and most consistent for samples made with a Tl counterelectrode where, indeed, TlSe was detected by x-ray diffraction but not confirmed to exist as a well defined thin layer from SEM photographs. The inductive effect was weakest for Pt contact samples. It is suspected further that this is due, in part, to the fact that Pt was the least reactive, while Tl was the most reactive element of the three metals. Therefore, while a substantial quantity of TlSe formed in the Tl samples in a relatively short time, this was not the case for the rectifying contacts of Bi and Pt, which had a much slower rate of reaction with the Se. With very long aging in the samples with a Tl counterelectrode the inductive effect was found to decrease. This can be explained, qualitatively, by a lessening of the injection of holes into the n-type TlSe layer as this layer

widens in comparison with the hole diffusion length. It should also be mentioned here that, a semiquantitative calculation [20] postulating an equivalent circuit model with an inductor present explains how the capacitance returned from a negative value to a positive value as the forward bias was increased. This model also explains, qualitatively, how the magnitude of the negative capacitance values decreased as the frequency increased.

Another very interesting result was the observation of minima in the C_p -V curves. This was despite the absence of any anomalies in the j -V and R_p -V characteristics. It is speculated that these capacitance minima were due to deep levels [21] in the Se. According to Roberts and Crowell [21] the energy of such a level above the valence band edge corresponds to the voltage at which an inflection point appears in the C_p -V characteristics. This energy is determined by subtracting the voltage at the inflection point from the barrier height potential. Now, it was observed that many of the Tl samples had such an inflection point at about 0.2 volt, while Bi counterelectrode samples showed an inflection point at about 0 volt. If the barrier heights are taken to be about 0.8 eV for Tl samples and about 0.6 eV for the Bi samples (i.e. the barrier heights corresponding to those found from j -V characteristics), then the deep level determined in both cases turns out to be at around 0.6 eV above the valence band edge. Multiple minima were also seen in samples, particularly those for aged Tl samples. This would suggest that there were multiple levels present. It is speculated in these cases that these extra levels were brought about by the diffusion of metal atoms from the counterelectrode into the Se layer. The minima seen at low voltages corresponded to levels deep in the gap, while the minima at higher voltages corresponded to levels which were not as deep. It was reported also, however, that a minimum in the C_p -V curves can occur as a result of a parallel combination of a capacitor and resistor in series

with a diode [18]. Since the minimum in this case would appear at a prescribed current, the voltage at which it occurs would also be dependent on the metal used at the counterelectrode, as each metal gives a different barrier height to Se. This voltage would increase as the barrier height of the diode increased. Thus, samples with low barriers would show a capacitance minimum at a lower voltage than samples with high barriers. This was, in fact, observed in this work, as the large barrier height Tl samples in general displayed minima at higher forward voltages than the low barrier height Bi and Pt samples. In the samples of this work, this extra capacitor and resistor, it is suspected, would arise from a non-ohmic back-contact.

Storage in air aging also had some interesting effects on the current-density versus voltage characteristics. The forward current-density decreased monotonically with storage time for Se-Tl samples in a similar manner to that reported by Pan [2] [12]. Pan attributed this decrease to the conversion of the Tl counterelectrode to Tl_2CO_3 , an insulator, which resulted in an overall increase in the resistance of the device. While this carbonate was also observed in several samples of the present work, in other samples, where the decrease in forward current-density was also very apparent, it was not likely to have formed, since their counterelectrodes were completely covered by a protective indium layer. Chan [3], on the other hand, suggested that the decrease in forward current-density was due to the formation of TlSe at the Tl/Se interface, which resulted in an n-type TlSe/p-type Se heterostructure. Thus, the forward current-density decreased because the n-type TlSe had far fewer carriers than Tl metal. The ideality factor and the reverse current density also changed with storage time, in that, they both increased. It is suggested that this effect was also due to the formation of the TlSe layer. The lattice mismatch between the TlSe and the Se [14]

resulted in a high density of recombination traps at the interface. As the TlSe grew the effect of recombination resulted in an increase of the ideality factor and the reverse current-density [9] [10]. In fact, even a freshly made Tl sample had an overall tendency to yield a larger ideality factor if its reverse current was large, as shown in Fig.8.2, where the 1 volt reverse current density j_{Rev} is plotted against $n-1$. Plotted also are the j_0 values of several Se-Tl samples. It is seen in this case also that the ideality factor increases as the j_0 increases. The emergence of this recombination may also have contributed to the decline in the negative capacitance effect mentioned earlier, since injection of carriers into the TlSe would have been lowered as well.

Chan [3] also suggested that the formation of a TlSe layer in the Se-Tl samples had an effect on the Mott-Schottky plots. In this case, he stated that the depletion region extended into the newly formed TlSe layer, where there was a carrier concentration lower than in the bulk Se. This resulted in Mott-Schottky curves that became steeper as the TlSe layer grew thicker with storage time. In this work too, such an aging effect was observed in the Mott-Schottky plots for several samples of this type and it is believed to be the result of the selenide layer formation as just described.

It was seen also in this work that, Pt counterelectrode contacts deposited on to the Se by evaporation were of low resistance. In fact, as mentioned previously, the evaporated Pt contact to Se in a sample was always of lower resistance than the Bi or Pt back-contact. This resulted in a rectification direction opposite to that usually found in Tl and Bi counterelectrode samples. Pt back-contacts, however, were not seen to have these low resistance properties and in fact showed rectifying characteristics. It is believed that the low gap energy semiconductor $PtSe_2$ ($E_g = 0.1$ eV [16]) formed at the Pt front-contact and was

responsible for the low resistance path to the Se. This compound would not normally form at the Pt back-contact because the temperatures involved in the formation of this interface during the Se deposition (Se melting point 217 °C; substrate temperature 130°C) are believed to be too low. Therefore, the back-contact, in this case, was essentially a Schottky junction between the Se and the Pt. On the other hand, the selenide is believed to have formed at the front contact since the evaporation of the Pt during the deposition involved a much higher temperature process, as the melting point of Pt is some 1769 °C. Some preliminary heat-treatment studies (not presented in this thesis) on a Pt-Se-Pt sample have, in fact, shown that the back-contact resistance decreased after heating in N₂ gas at 130°C for 98 hours. It is believed that, in this time PtSe₂ formed at the back Pt-Se interface to give a low resistance contact. In any case, it seems that Pt as the back-contact can give a low resistance path to the Se if the junction is heated for a period of time.

Barrier heights of Tl, Bi and Pt contacts to Se were determined from j-V and C_p-V data and in the case of Bi, also from photoelectric measurements. It was seen that the barrier height value did, in fact, show a decrease with increase in metal work function despite the presence of surface states. Thus, pinning of the Fermi level, due to surface states, in these structures did not appear to be very important. It was also seen that the barrier values determined from the capacitance data were frequently lower than the values obtained from the j-V characteristics. They were also lower than the values determined from the photoelectric measurements in the case of Bi samples. It is speculated that the value was low because of an overestimate of the free hole concentration in the Se. The free hole concentration is believed to be much lower than that obtained from the slope of the Mott-Schottky curves and it is suspected that a presence of a large concentration of immobile

centres is responsible. While such centres were probably relatively shallow, there may also have been many deeper-lying traps located near the middle of the gap of the Se. These latter traps could explain the second higher energy photoelectric threshold value observed in the Fowler plots of the photoelectric measurements. Of course, by the same reasoning, it can be argued that the 0.7 eV barrier height value determined with the Fowler curves was actually due to yet another shallower level and not due to the Se-Bi junction barrier height at all. Therefore, in this case the barrier height may be substantially smaller than 0.7 eV. In any event, it is clear that the barrier height value determined is different for each of the methods employed. It is therefore believed that the structures studied here were much more complicated than the simple Schottky model.

Although this is the first time photoelectric measurements have been made in this laboratory to determine barrier heights, it is nevertheless believed that the measurements themselves were quite accurate. However, it is also believed that the samples were not pure Schottky junctions and so the results obtained from these measurements were somewhat uncertain.

Fabrication parameters are believed to have had a strong effect on the electrical properties of the diodes. For instance, better rectifiers resulted from samples made with long Se deposition times (about an hour or more) as opposed to samples made with very short deposition times (2 minutes). It is thus believed that the morphology of the Se film was quite different for the two deposition rates and this resulted in very different electrical characteristics. Another very interesting parameter was the Bi back-contact layer thickness. Samples made with a thick (1 to 3 μm) Bi back-contact were seen to show a higher forward current density than samples made with thinner Bi back-contacts. Furthermore, Bi-Se-Bi

samples made with a thin Bi back-contact were seen to show semi-symmetrical Mott-Schottky plots similar to what is expected for a back-to-back diode structure. It is therefore speculated that thin Bi back-contact layers only partially covered the surface of the Al substrate. Thus, the Al substrate was exposed in certain areas to the Se, giving rise to high resistance Al-Se contact areas. Another possible explanation is that the thin Bi layer was completely consumed in the formation of Bi_2Se_3 at the back contact during the Se deposition. Thus, the back contact was actually a heterojunction of the form Al- Bi_2Se_3 -Se, which was rectifying, since the Al did not make an ohmic contact to the selenide. A thicker Bi layer would not have been completely consumed, so that the back-contact junction would be of the form Bi- Bi_2Se_3 -Se and in this case the Bi provided an ohmic contact to the selenide. The selenide here has such a low gap energy (0.35 eV) that it would make only a weakly rectifying contact to the Se. The effect of the Bi back-contact thickness was not so apparent in samples made with a Te counterelectrode because the barrier height of the front contact is so high that the current through the device is too low for this effect to be seen, even at 1 volt in the forward direction. Furthermore, it is believed that the back-contact also had a strong effect on the determination of barrier heights for the Bi counterelectrode samples. This would explain why the barrier values found from the Mott-Schottky curves for these samples was unusually low.

The question arises at this point as to why negative capacitance is not believed to have come from the Bi back-contact or the Pt front-contact. After all, the fabrication of these low resistance contacts, it is speculated, resulted in the formation of a selenide and such selenides are believed to have been responsible for negative capacitance. It should be clarified that the two effects here (low resistance and negative capacitance) are believed to

be dependent on the quantity of the selenide involved. The Bi back-contact and the Pt front-contact are believed to have had relatively thick layers of selenide present. Therefore, as discussed earlier, with such a large thickness, the negative capacitance effect from these contacts would have been virtually insignificant.

It was seen that most of the Mott-Schottky plots of this work displayed slopes corresponding to a nominal hole concentration of about 10^{16} cm^{-3} . However, several freshly made samples, particularly those where the back-contacts were rectifying, had Mott-Schottky plots with slopes of about 10 times larger than usual for voltages where the back-contact was reverse biased. This suggests that the nominal hole concentration in the Se layer at these back-contacts was about 1/10th that at the front-contacts. It is speculated that this concentration value was somewhat low for two reasons. First, out-diffusion of dopant Ce atoms from the Se layer may have occurred during the Se deposition process. This would be of greater extent at the back contact since the Se deposited here was at an elevated temperature (130°C) for a long time (virtually the entire deposition time), whereas that deposited at the top of the layer was at this temperature for a much shorter time. Second, during the Se deposition, the molten Se in the crucible would become more and more concentrated with dopant impurities as the Se evaporated. Therefore, as the deposition proceeded the Se evaporant and, hence, that deposited, would have had a higher and higher dopant concentration.

Measurements of R_p versus V at different frequencies showed that for reverse bias voltages in Tl and Bi samples and for back-negative voltages with Pt-Se-Pt samples, there was a large dispersion with frequency. In the opposite voltage polarity the dispersion was much smaller. It was also observed that both C_p and R_p tended to become less and less bias

dependent as the frequency was raised to above 10^6 Hz. In several Tl samples, the C_p -f characteristics showed a tendency to a plateau at frequencies above about 10^5 Hz for forward bias voltages. Similar characteristics were also observed by previous workers [2] [3] [15] and they explained them at least qualitatively with a simple circuit model involving a diode in series with a parallel combination of a capacitor and a resistor. In the samples, this extra resistor and capacitor combination, it is speculated, would arise from an imperfect back contact. This model, however, does not explain the appearance of inductance in the samples at low frequencies. The model also predicts an $R_p \propto 1/f^2$ dependence, whereas most of the samples in this work showed a dependence closer to $R_p \propto 1/f$. It also falls short of explaining the appearance of multiple minima in the C_p -V characteristics. In any case, more analysis of this nature is required, possibly involving a model incorporating an inductor similar to the one proposed previously [20].

In many of the Se-Tl samples it was observed that the current density showed a dependence of the form $j \propto V^p$, where p was somewhat high between 3 and 4. An ohmic j -V dependence would have p as being equal to 1 and a space-charge limited current would show a dependence where $p = 2$. It is speculated that the high p value in this work was due to high level injection as explained here. As the forward voltage was increased, injection became stronger and stronger and so the overall resistance of the device decreased more and more. Thus, the current through the device increased at a superlinear rate dependent on the injection level. With high-level injection the p value would have been quite large. Such a high p value was not found for the Bi and Pt samples because their injection levels are believed to have been much smaller, since their selenides did not form as readily at the rectifying contact as did TlSe in the Tl samples.

Though the barrier height values determined for Tl and Bi samples were similar to those obtained by Pan [2], other electrical characteristics were somewhat different. The most striking differences were the observation of negative C_p values at low frequency (even at 1 kHz) and the higher and more consistent forward current densities observed in the present work. It is believed that these differences were mainly the result of fabrication differences. Samples in the present work were made under cleaner conditions. Therefore, the interfaces between the Se and the metal films were more intimate and uniform in the present work and therefore, more conductive. This, it is believed, resulted in larger and more consistent current densities but also a higher chemical reaction rate between the Tl and the Se in the Se-Tl diode cases, which in turn resulted in a more immediate appearance of negative capacitance. With the cleaner systems a better Bi back-contact was also expected. According to Werner et. al. [8] a more ohmic back-contact would also result in a stronger inductive effect. Furthermore, the smaller resistance of this ohmic back-contact would not be as apparent in the high frequency portion of the resistance versus frequency curves. This may explain why in the present work a plateau in the R_p -f characteristics was not seen at high frequency, while it was seen in Pan's work.

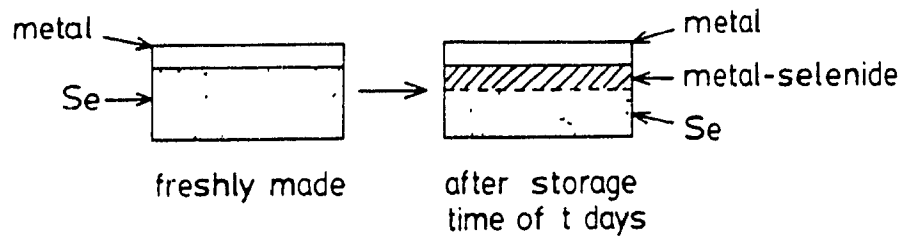


Fig 8.1. Cross-section of actual sample structure believed to be present when freshly made and after a time, t -days, in storage.

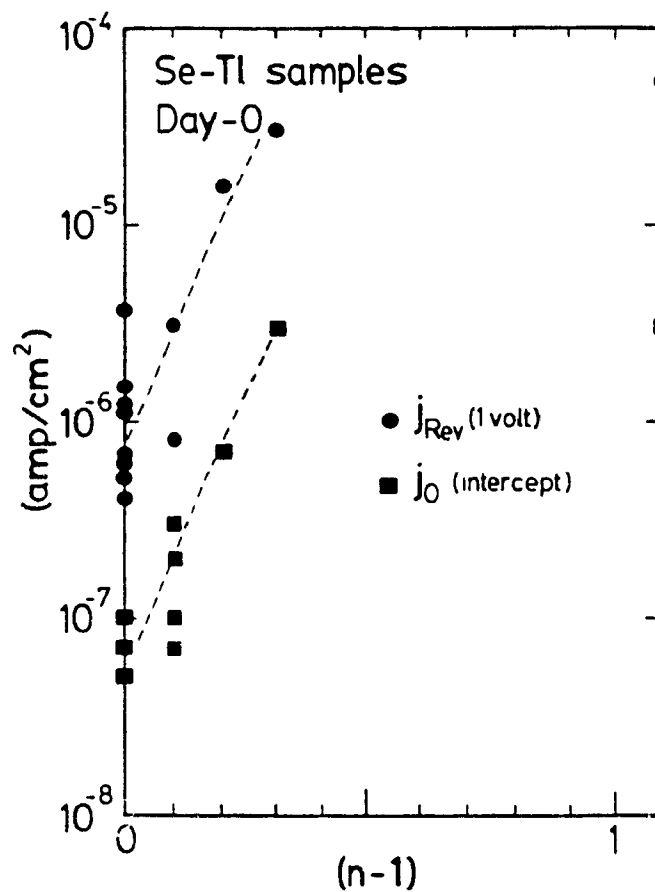


Fig 8.2. Plot of reverse current-density at 1 volt and j_0 value against $(n-1)$ for Se-Tl samples on day-0.

9. CONCLUSIONS AND FURTHER WORK

This chapter first presents some conclusions that can be made from the present work and then suggests some further studies to answer possibly some questions which arose from this and other studies.

9.1 Main Conclusions

The first conclusion is that non-Faraday inductance has been observed in structures of this work at low frequency, whether they were made with Tl, Bi or Pt contacts. The strength of this inductive effect was largest for the Tl samples and changed with storage time. It is believed that this effect was the result of hole injection from the p-type Se into a thin n-type selenide layer that formed at the rectifying metal-Se contact. The growth of this layer would account for the changes seen in the inductive effect over the storage time period. For the Tl-Se samples, it was the semiconductor TlSe that formed, as determined from x-ray diffraction analysis.

The next major conclusion is that a low resistance contact to Se can be obtained with either a Bi back-contact, where the Se is deposited on to a Bi layer, or with a Pt front contact, where the Pt is evaporated on to the Se. It is believed that a low resistance contact resulted because of the formation of low gap energy semiconducting selenides of Bi (Bi_2Se_3) and of Pt (PtSe_2) at the interface.

Another major conclusion that can be made from this work is that the barrier heights of

the samples do depend on the metal used as the rectifying contact. It was seen, in fact, that the barrier height decreased as the work function of the metal increased in agreement with what is expected for Schottky diodes with few surface states. However, the barrier height values found from the current-voltage, capacitance-voltage and photoelectric measurements were different from each other.

Consistent phototreshold values for Bi samples of this work were determined in this laboratory for the first time using the photoelectric measurements technique described. This technique should provide an additional and important means of further characterizing more samples made in this laboratory.

9.2 Further Work and Recommendations

It is clear that a great amount of work is still required to answer the questions raised in this work. This section describes what the candidate thinks ought to be the immediate set of experiments in the on-going study.

9.2.1 Negative Capacitance Studies

Studies should be undertaken to determine if, in fact, a selenide layer is responsible for the inductive effect. This would involve more aging studies and even heat-treatment of Tl, Bi and Pt samples. It is recommended that these heat-treatments be done in an inert atmosphere and at a relatively high pressure (i.e. 1 atm) to avoid atmospheric attack and

reevaporation of the films. Along with the electrical measurements, more x-ray diffraction (XRD) and scanning electron microscopy (SEM) analyses would be in order. It is recommended that x-ray photo-spectroscopy (XPS or ESCA) also be performed. This analysis technique would provide information as to the exact structure of the samples by determining what compounds are present and in what regions. In essence, ESCA would determine whether a selenide layer really was located between the metal and the selenium and also how thick this layer was.

The effect of a selenide at the interface could also be examined by intentionally depositing the selenide on to a Se layer to form a heterostructure. Such a sample it is expected would be more stable chemically and so measurements from day to day would be more consistent.

Experiments ought to be carried out to determine whether or not heating of the sample is, in fact, taking place during the counterelectrode deposition step and if this heating results in negative capacitance values in the samples on day-0. If this does turn out to be the case, a sample cooling apparatus for the counterelectrode deposition step would be helpful in reducing this effect.

9.2.2 C_p -V Minima Studies

Efforts to determine the cause of the minima in the C_p -V characteristics ought also to be undertaken. Making capacitance measurements at different temperatures would provide useful information, since any deep levels present would become slower as the temperature

would drop so that the minima would become less apparent. Of course deep level transient spectroscopy (DLTS) would also be helpful in this study, provided it is carried out at a sufficiently low frequency. In either case, care will have to be taken to ensure that the samples are not irreversibly changed by temperature cycling.

It was suggested that atoms diffusing into the Se layer may be responsible in part for these minima, as these atoms may introduce deep levels. Secondary ion mass spectroscopy (SIMS) would be quite helpful in determining the identity of such atoms, as well as, their distribution in the Se.

9.2.3 Bi and Pt Contact Studies

It is believed that the low resistance nature of the Bi and Pt contacts to Se was actually due to the formation of a small gap energy semiconductor, either Bi_2Se_3 or PtSe_2 , at the interface. Further efforts in heat-treatment, as well as, more materials analysis studies of the structures, like those mentioned above (XRD, SEM, ESCA), would provide useful information as to whether this, in fact, is the case.

It would also be useful to fabricate samples with varying Bi back-contact thicknesses to confirm the belief that thick (1 to 3 μm) Bi films result in low resistance contacts to Se, whereas thinner Bi films are rectifying. A good choice of front contact would be Pt, as it would be of low resistance.

Depositing a Pt front contact by sputtering may prove to be a useful technique for getting a Schottky Se-Pt interface. By sputtering, the energy of the free Pt atoms could be much less

than that when the Pt is evaporated. This would result in virtually no chemical reaction between the Se and the Pt, so that no PtSe_2 is formed at the front contact.

While Bi and Pt metals have been seen to give low resistance contacts to Se other materials might also. The metal Ni was employed in commercial Se rectifiers as the back-contact. Therefore, studies should be carried out in this laboratory to see if Ni makes a good low resistance contact to Se. Tellurium, Te, has previously been used in this laboratory as the back-contact material [3] and it would be of interest to perform experiments to compare this type of back-contact against Bi, Pt or even Ni contacts.

9.2.4 Barrier Height Studies

Barrier heights determined for samples with metals of even lower work function than Tl or Mg (e.g. Ba, Ca, Y) would give more insight into the dependence of barrier height and work function. Such low work function metals ought to have very large barrier heights. The rectification ratio of such samples might be even larger than the 5 orders of magnitude found for the Tl samples. Of course difficulties will arise due to the reactive nature of the metals mentioned here. A metal protective layer, like the In layer used for the Tl samples of the present work, might be sufficient to inhibit atmospheric attack.

It would also be very interesting to determine the barrier height values with the photoelectric technique for samples with Tl and Pt contacts to see if these values correspond to those found from the j -V or C_p -V measurements. Such a study would give more insight into the question of which technique is the most reliable for determining

barrier heights.

Finally, it is recommended that some samples be made with single crystal Se instead of its polycrystalline form. The results obtained from such samples would be more consistent and, therefore, more easily analyzed and understandable. Furthermore, materials analyses would be greatly facilitated, since the layers in these structures would be expected to be better defined, at least when freshly made.

BIBLIOGRAPHY

1. H.B. Michaelson, "Relation between an Atomic Electronegativity Scale and the Work Function," IBM J. Res. Dev. **22**, 72 (1978).
2. J. Pan, "Characteristics of Selenium Diode Structures," M.Eng. thesis, McGill University (1988).
3. A.C.L. Chan, "Fabrication and Measurements on Metal-Semiconductor Diodes," M.Eng. thesis, McGill University (1987).
4. Y. Kanai, "On the Inductive Part of the ac Characteristics of the Semiconductor Diodes," J. Phys. Soc. Japan **10**, 718 (1955).
5. T. Misawa, "Impedance of Bulk Semiconductor in Junction Diode," J. Phys. Soc. Japan **12**, 882 (1957).
6. H. Melchior and M.J.O. Strutt, "Small Signal Equivalent Circuit of Unsymmetrical Junction Diodes at High Current Densities," IEEE Trans. Electron Devices **ED12**, 47 (1965).
7. M.A. Green and J. Shewchun, "Minority Carrier Effects Upon the Small Signal and Steady-State Properties of Schottky Diodes," Solid-State Electron. **16**, 1141 (1973).

8. J. Werner, A.F.J. Levi, R.T. Tung, M. Anzlowar and M. Pinto, "Origin of the Excess Capacitance at Intimate Schottky Contacts," *Phys. Rev. Lett.* **60**, 53 (1988).
9. S.M. Sze, *Physics of Semiconductor Devices* (John Wiley & Sons, Inc., Toronto, 1981), 2nd ed.
10. L.H. Rhoderick, *Metal-Semiconductor Contacts* (Clarendon Press, Oxford, 1980).
11. R.H. Fowler, "Photoelectric Sensitivity Curves for Clean Metal at Various Temperatures," *Phys. Rev.* **38**, 45 (1931).
12. C.H. Champness and J. Pan, "Stability of Se-Tl Schottky Junctions," *Phosphorus and Sulfur* **38**, 399 (1988).
13. Private communication with M. Blostein, Dept. of Elect. Eng., McGill University.
14. R.W.G. Wyckoff, *Crystal Structures* (John Wiley & Sons, New York, 1963) 2nd ed.
15. C.H. Champness and J. Pan, "Anomalous Capacitance in Selenium Schottky Diodes," *J. Appl. Phys.* **65**, 2321 (1989).

16. J. Guggenheim, F. Hulliger and J. Muller, "PdTe₂, A Superconductor with CdI₂-Structure," *Helv. Phys. Acta.* **34**, 408 (1961).
17. V.V. Sobolev, "Structure of the Energy Bands of Semiconductors of the A₂B₃ type," *Inorg. Mater.* **2**, 47 (1966).
18. C. van Opdorp and H.K.J. Kanerva, " Current-Voltage Characteristics and Capacitance of Isotype Heterojunctions," *Solid-State Electron.* **10**, 401 (1967).
19. Y.F. Go, "Variations in the Fabrication of a Se-CdO Photovoltaic Cell," M.F.Eng. thesis McGill University (1989).
20. C.H. Champness and W.R. Clark, "Anomalous Inductive Effect in Selenium Schottky Diodes," *Appl. Phys. Lett.* **56**, 1104 (1990).
21. G.I. Roberts and C.R. Crowell, "Capacitance Spectroscopy of Deep-Lying Semiconductor Impurities Using Schottky Barriers," *J Appl Phys* **41** 1767 (1970)

APPENDIX

This appendix shows the results of some SEM x-ray fluorescence (XRF) analyses that were made on Se-Tl samples WC49 and WC54. A typical analysis run consisted of scanning the electron beam of the SEM across the cross section of the sample and measuring the resultant x-rays emitted. Each element has its own characteristic x-rays, so that the elements encountered by the beam could be identified. With the beam scanning across the cross-section of the sample a **qualitative** distribution of the elements in the structure was obtained.

Fig.A.1 shows the result of such a scan on sample WC49. Here, distributions of Tl, Se and Bi are seen as plots of x-ray detector counts against position across the sample cross-section. The counts value on the vertical scale is proportional to the amount of the element present. Note that these are only qualitative distributions and do not represent the relative proportions of the elements compared to one another. Nevertheless, it is seen that there is a large amount of Bi indicated on the left hand side of the figure, corresponding to the Bi back-contact layer. A large amount of Se is indicated in the middle portion of the plot, corresponding to the Se layer in the sample. A large amount of Tl is present at the extreme right of the scan, which corresponds to the Tl counterelectrode layer. Note in this figure that while the Bi/Se interface appears to be relatively abrupt, the Se/Tl interface is not so well defined. In fact it seems that some Tl has diffused into the Se layer as far as about 15% of the way through the Se layer. Evidence of such diffusion was also seen from the SEM photographs of the back-scattered electron images of Fig 5.31 presented in chapter 5 section 5.3.6. Fig.A.2 is the same type of scan but on sample WC54. This figure shows much

better definition of the Se/T ℓ boundary than for WC49. The SEM photograph of sample WC54 in cross-section, also in Fig 5.31, showed a well defined Se/T ℓ interface as well.

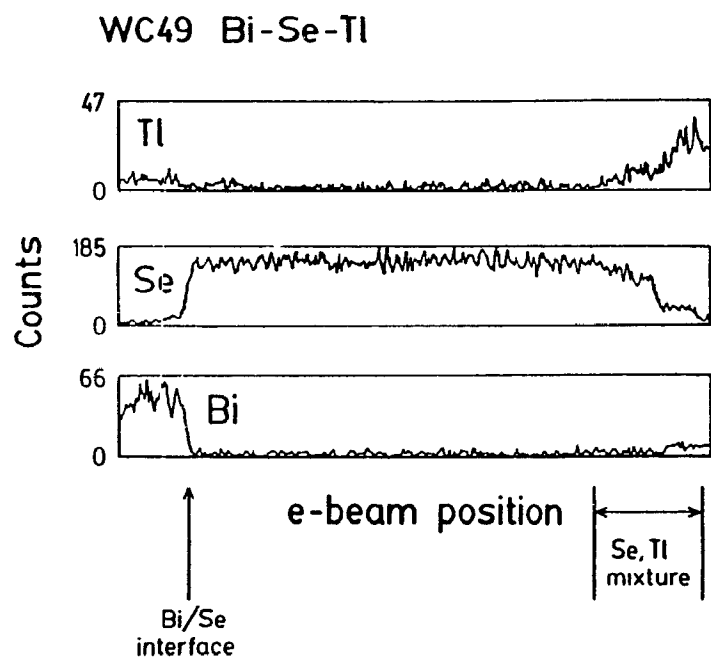


Fig.A.1. Results of XRF linescan on cross-section of Bi-Se-Tl sample WC49.

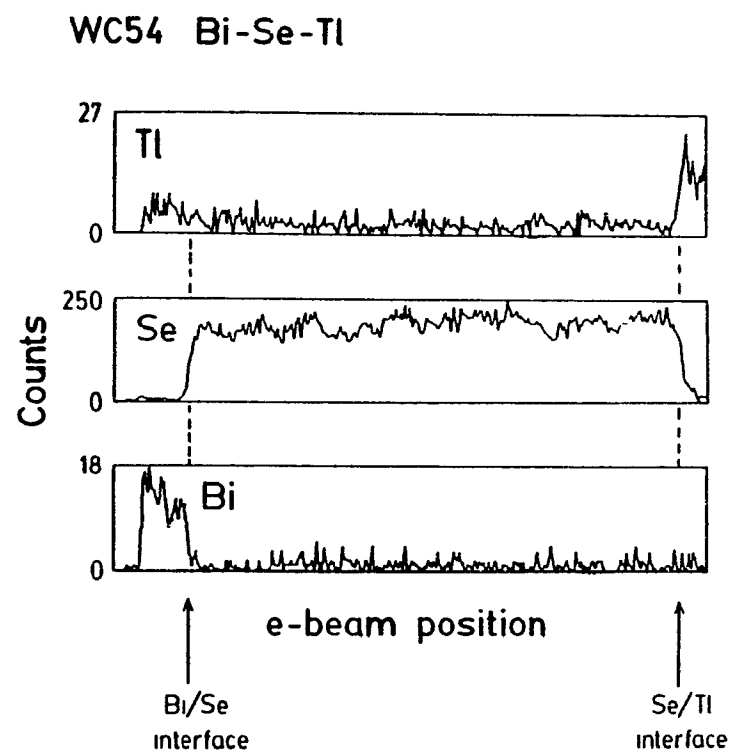


Fig.A.2. Results of XRF linescan on cross-section of Bi-Se-Tl sample WC54.